공학박사학위논문

A study on the preparation of organogel based functional polymers

유기젤을 기반으로한 기능성 고분자의 제조에 관한 연구

2016년 8월

서울대학교 대학원

재료공학부

최 태 진

A study on the preparation of organogel based functional polymers

유기젤을 기반으로한 기능성 고분자의 제조에 관한 연구

지도교수 장 지 영

이 논문을 공학박사 학위논문으로 제출함
2016년 4월

서울대학교 대학원
재료공학부
최 태 진

최태진의 공학박사 학위논문을 인준함
2016년 6월

위 원 장 박 종 래 (인)
부위원장 장 지 영 (인)
위 원 곽 승 엽 (인)
위 원 안 철 희 (인)
위 원 김 종 표 (인)

Abstract

A study on the preparation of organogel based functional polymers

Tae Jin Choi

Department of Materials Science and Engineering

Seoul National University

An organogel generally has a three dimensional network structures caused by physical or chemical cross-linking and contains a large amount of organic solvent molecules. A physically cross-linked network structure is produced by the self-assembly of small molecules promotes whereas a chemically cross-linked network structure forms by the polymerization of bi-, tri- or multifunctional monomers or the cross-linking reaction between polymer chains. In this study, functional polymers were prepared using reactive organogels and their properties and application possibilities were investigated.

Firstly, thermochromic polymer nanocomposite films were prepared from polymerizable organogels. Organogelator **1** had a structure within which 3,4,5-

tris(*ω*-decenyl)benzamide groups were attached to a quarterthiophene core through amide bonds. Organogelator **2** had the same structure except that tris(*ω*-decenyl) groups were replaced by tris(*n*-decanyl) groups. The PMMA nanocomposite films were prepared by the photopolymerization of the organogels formed in MMA. The film containing **1** (0.5 wt%) showed reversible thermochromism. The emission under 365 nm irradiation was changed from orange to bright green by heating up to 120 ^{o}C and returned to its initial orange by cooling. To the contrary, the PMMA composite film prepared from the organogel of **2** (0.5 wt%) didn't show a reversible thermochromic property. Organogelator **1** with polymerizable terminal vinyl groups was covalently embedded in the PMMA matrix, but **2** didn't. The reversible thermochromism was likely caused by the thermally reversible conformational change of quarterthiophene units in the polymer fibers.

Secondly, a chemical gel prepared from the Sonogashira-Hagihara reaction between 1,4-diiodobenzene and 1,3,5-triethynylbenzene was used to preparing a compressible and monolithic hierarchical porous polymer (HM). The polymers with an acid (HM-A) and base functionality (HM-B) were prepared by sulfonation of HM and by an additional Sonogashira-Hagihara reaction with a monomer bearing an amine group in the presence of HM, respectively. HM-A having sulfonic acid group and HM-B with amine group

also showed compressibility, monolithic properties, and hierarchically porous structures. They were cut and fitted into a syringe sequentially and the syringe was used as a semi-continuous flow reactor. The acid catalyzed deacetalization reaction of benzaldehyde dimethyl acetal and base catalyzed Knoevenagel condensation reaction between benzaldehyde and maloronitrile were carried out in the semi-continuous flow reactor. The tandem reaction in the semi-continuous flow reactor required less solvent and time than in a conventional batch type reactor. The reactor could be recycled several times without a significant decrease in the reaction efficiency.

Thirdly, a chemical gel was formed with a commercial polyurethane sponge. A compressible and hierarchically porous polymer composite (PUS-MOP-A) was prepared by Sonogashira-Hagihara coupling reaction of 1,3,5-triethynylbenzene, 1.4-diiodobenzene and 2,5-diiodobenzoic acid in a polyurethane sponge (PUS). 2,5-Diiodobenzoic acid was used as a co-monomer to provide acidic functionality to the pore surface. The microporous organic polymer (MOP-A) formed inside the PUS network showed fibrous morphology when 1,4-diiodobenzene was used as a major aryl halide. For the synthesis of PUS-MOP-A, the molar ratio between 1,4-diiodobenzene and 2,5-diiodobenzoic acid was chosen as 4:1. The Brunauer-Emmett-Teller (BET) surface area of PUS-MOP-A was 306 m^2g^{-1}. PUS-MOP-A was treated with

KOH, which converted the carboxyl groups on the MOP-A backbone to the carboxylate anions. The resulting polymer composite (PUS-MOP-Aa) absorbed water quickly, showing a water contact angle of 0^{o}. PUS-MOP-Aa to remove chemical pollutants in an aqueous solution was studied using a cationic dye, Methylene Blue (MB) and an anionic dye, Methylene Orange (MO) as a model chemical. PUS-MOP-Aa could be manually compressed and released in an aqueous solution of MB, resulting in the fast dye removal. When an aqueous solution contained both the anionic and the cationic dye, PUS-MOP-Aa preferentially removed the cationic dye. PUS-MOP-Aa was recyclable after removing the absorbed dyes by treating with an acid and washing.

Lastly, a compressible heterogeneous catalyst containing a Pd nanoparticles encapsulated microporous polymer (S-M-Pd) that sharing the same hierarchical porous polymer (PUS-MOP-A) was studied. Pd catalysts, used for the Sonogashira-Hagihara reaction, were exploited as the precursors for the generation of Pd NPs. 2,5-Diiodobenzoic acid was introduced to adjust wettability to aqueous environment. S-M-Pd has a hierarchical pore structure and Brunauer-Emmett-Teller (BET) surface area of 270 m^2g^{-1}. It showed good mechanical stability against compressive stress. S-M-Pd was successfully used for the 4-nitrophenol reduction reaction and the Suzuki-Miyaura coupling reaction. A compression and release of the S-M-Pd in the reaction mixture

allowed the reactants to access the catalyst more easily. The 4-nitrophenol reduction reaction with repeated compression and release was 6 times faster than in static conditions. The cylindrical S-M-Pd was fitted into the syringe, and was used as a semi-continuous flow reactor for the methylene blue reduction. The reactor showed no undesirable leakage and was used for several successive reactions without further purification.

Keywords: organogel, thermochromism, hierarchically porous polymer, sponge, catalyst.

Student Number: 2010-20642

Contents

List of Schemes

List of Tables

List of Figures

Figure V-15. Sequential photographs taken during a methylene blue solution (0.2 mM) without $NaBH_4$ passed through a semi-continuous flow reactor.

Figure V-16. UV-Vis absorption spectra of methylene blue without $NaBH_4$ before and after passing through the S-M-Pd. The methylene blue solution before and after passing through the S-M-Pd were diluted 10 times.

Chapter I.

Introduction

I-1. Introduction to Organogel

I-1-1. Definition of Organogel

The concept of a gel has been evolving since the introduction of gel theory by Thomas Graham in 1861.[1-6] Even though there are still many different definition of a gel, a substance can be classified as a gel if (i) the material has a continuous microscopic structure with macroscopic dimensions during the whole process of analytical experiment and (ii) it shows solid-like rheological behavior even though it is mostly liquid.[7]

Depending on types of the liquid, a gel can be classified into two groups: hydrogel and organogel which are water and organic solvent, respectively.[8] In general, gelation occurs by crosslinking of polymeric strands. The polymeric strands can be a conventional polymer or a supramolecular polymer. Depending on the type of crosslinking, a gel can be classified into two groups: chemical and physical gel. Chemical gels involved the formation of covalently cross-linked networks, which fixes the gel to be thermally irreversible. In physical gels, the formation of cross-linked networks was attributed to non-covalent interactions including hydrogen bonding, π-π stacking, electrostatic interactions, van der Waals interactions and so on.

I-1-2. Physical Gels

Physical gels are usually molecular gels, which consists of low molecular weight gelators (LMOGs) (arbitrarily limited to <3000 Da).[7] The molecular self-assembly via non-covalent interactions leads to formation of one-dimensional fiber-like structures. The fibrous strands, or supramolecular polymer, are entangled physically to form three-dimensional networks and solvent molecules are immobilized in the networks. The formation of physical gels commonly follows these steps: (i) Dissolve low molecular weight gelators usually at high temperature to obtain a solution or sol (ii) During the cooling process, the stochastic nucleation and aggregation of LMOGs appear below its characteristic gelation temperature (T_g) in adequate solvent (iii) Microscopic phase separation occurs rather than macroscopic phase separation common to crystallization processes. Figure I-1 described the gelation processes from LMOGs. The physical gels from this gelation processes are thermally reversible.

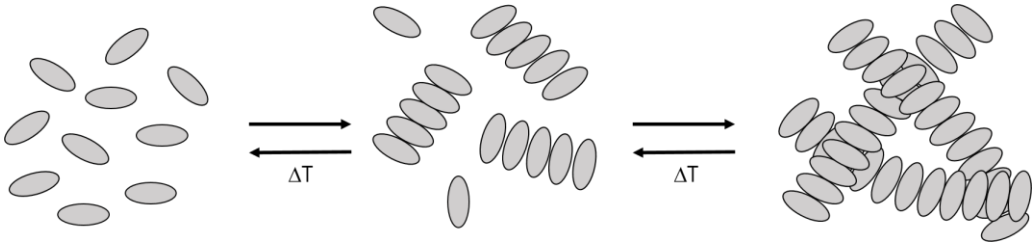

Figure I-1. Schematic descriptions of the gelation processes from LMOGs.

To figure out formation of gel, the inverted tube method is widely used. Specifically, a mixture of LMOGs and solvent in a tube were heated above the sol-gel transition temperature (T_g) where all of solid was dissolved. After being cooled down to room temperature for fixed time usually less than 24 h, the tube was inverted for 1 h to observe flow. If no flow was observed, it can be called a gel.[7]

To promote one-dimensional growth of LMOGs, highly specific interaction such as hydrogen bonding, π-π stacking, electrostatic interactions, van der Waals interactions are required. General structural requirements for gelators can be gained from a variety of gelators. Figure I-2 described the functional groups which have been proved to be important for gelation.[9] At first, hydrogen bond formation from the functional groups such as hydroxyl, amide, urea, carboxylic acid peptides, cholesterol, sugar and cyclohexyl amine helps to promote gelation. Strong π-π stacking of aromatic core also has been found to facilitate

gelation effectively. It has been known that the alkoxy chains maintain subtle balance between solvation and precipitation of the gelators. The balance between gelator-solvent and gelator-gelator is a deciding factor for gelation. If the balance is not appropriate, a supramolecular polymer can be precipitated or crystallized. The nature of solvent such as dipole moment, dielectric constant and refractive index is important factor for formation of gel.

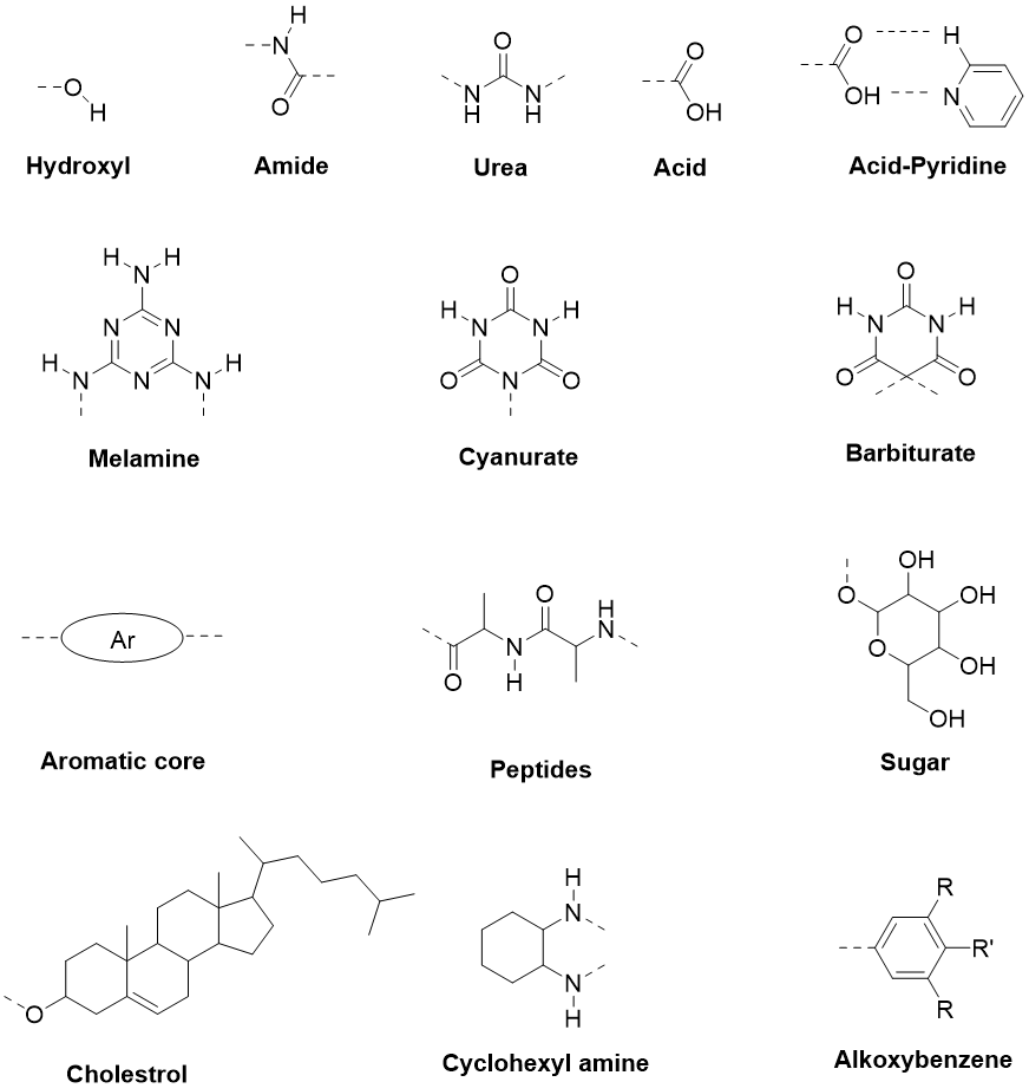

Figure I-2. Structural requirements for LMOGs.

Luminescent π-gelators

As mentioned above, π-π stacking is one of highly specific non-covalent interactions to lead formation of gel. Among the organogelators, π-systems based organogelators are called π-gelators. A gelator with more than one aromatic π-units which are fused or conjugated are included. Because of the conjugation of π-systems, π-gelators have optical properties in visible region. A number of π-gelators with luminescent properties have been explored.[9]

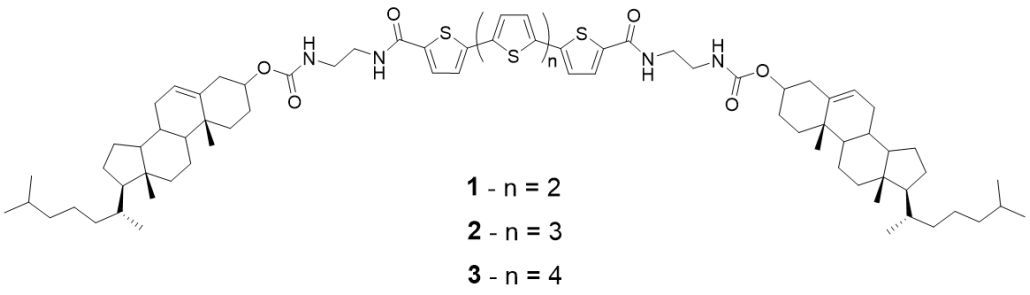

Figure I-3. Structures of oligothiophene based organogelators with the different number of thiophene units (**1** – quarterthiophene, **2** – quinquethiophene and **3** – sexithiophene).

Basically the optical properties of π-conjugated systems can be varied according to the number of repeating units.[10,11] The excitation energy of the lowest excited state generally decreases when the number of repeating units

increases. Shinkai group reported the oligothiophene based organogelators with the different number of thiophene units.[12] As presented in Figure I-3, quarter-, quinque- and sexi-thiophenes bearing cholesteryl groups were prepared. The effective conjugation length increases when the number of thiophene units increases. As expected, a sexi-thiophene gelator showed the lowest excitation energy with the longest wavelength absorption. Those gelators commonly gelated diphenyl ether, anisole, benzonitrile and tetrachloroethane. The colors of quarter- (**1**), quinque- (**2**), and sexi-thiophenes (**3**) gels under visible light were yellow, orange, and red, respectively.

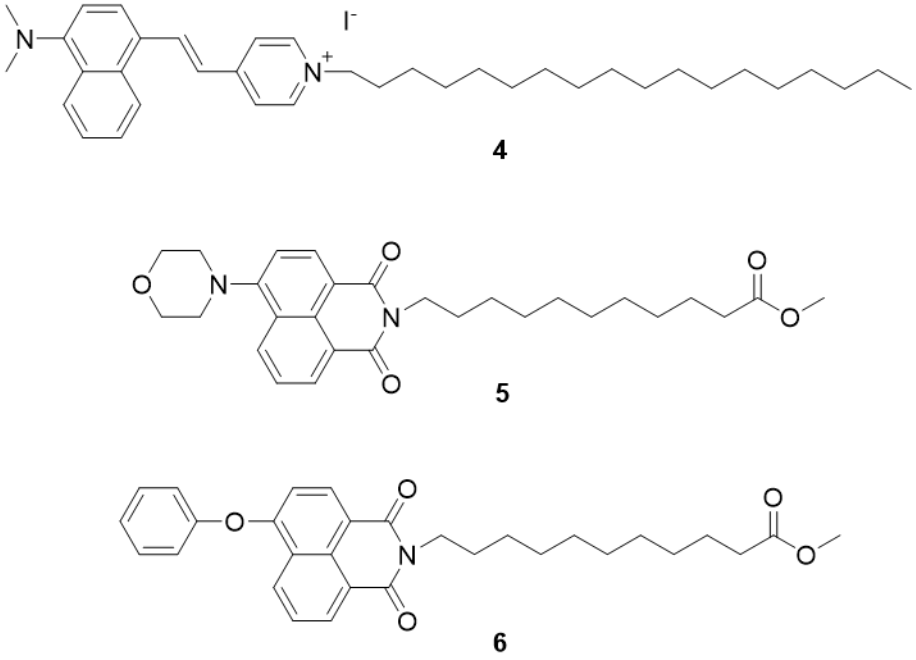

Figure I-4. Structures of hemicyanine dye (**4**) and 1,8-naphthalimide derivatives (**5** and **6**) gelators.

Shu group explored the luminescent properties of hemicyanine dyes gelator and 1,8-naphthalimide derivatives gelators (Figure I-4).[13] The organogelator **4**, **5**, and **6** formed a gel in *n*-octanol or *n*-dodecanol. In a gel state, **4**, **5**, and **6** showed strong red, green and blue emission properties under 365 nm irradation, respectively.

On the other hands, the absorption band of **4** overlapped with the emission of **5** and **6**. The Förster resonance energy transfer from **5** and **6** to **4** was observed. Thus, six different emission colors when under 365 nm irradiation

were obtained from the mixed gels. Although the organogelators have their own optical properties, the optical properties of mixed gels are changed by energy transfer.

Besides the energy transfer, the optical properties can be controlled by aggregation mode of molecules. When molecules are aggregated, there are two types of aggregation mode: H-aggregation and J-aggregation.[14-23] The Figure I-5 described the possible transition depending on the aggregation mode of dimer.[14] H-aggregation denotes the aggregation showing a blue-shifted band (hypsochromic shift) to molecular absorption band, whereas J-aggregation exhibit a red-shift (bathochromic shift). Specifically, due to the π-π interaction of two conjugated chromophoric groups, there are two energy levels for dimer, the upper level and the lower level. In the case of H-aggregation, only the upper level is allowed while only the lower level transition is allowed in J-aggregation. In McRae's theory, the align angle between transitional moments and the center-to-center axis of the two chromophores determines the formation of H- or J-aggregation. The criterion to determine aggregation mode is 54.7°. H-aggregation refers to a degree larger than 54.7° whereas J-aggregation has an angle smaller than 54.7°. In addition, the H-aggregation is represented by face to face arrangement in chromophore and parallel alignment of transition dipole moments. J-aggregation is referred to edge to edge arrangement in chromophore

and head to tail alignment of transition dipole moments.

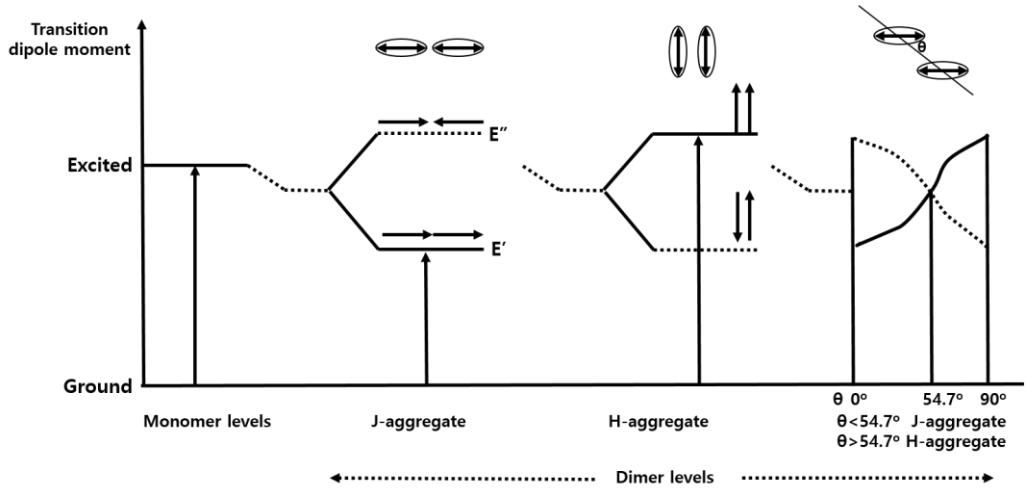

Figure I-5. Classification of possible transitions for dimer: H-aggregation and J-aggregation.

Würthner group studied the aggregation mode of perylene bisimide group based organogelators depending on the peripheral alkyl side chains.[20] The gelator **7** and **8** have linear alkyl chains while **9** and **10** have branched alkyl chains. In the case of **9,** the side chain has a chirality but **10** has no chirality. All gelators could form stable gels in aromatic solvent such as toluene and benzene, but could not form gels in hydrogen-bond acceptor solvent such as DMF and DMSO. It was found that those with linear alkyl chains formed H-type aggregates and those with branched side chains formed J-type aggregates.

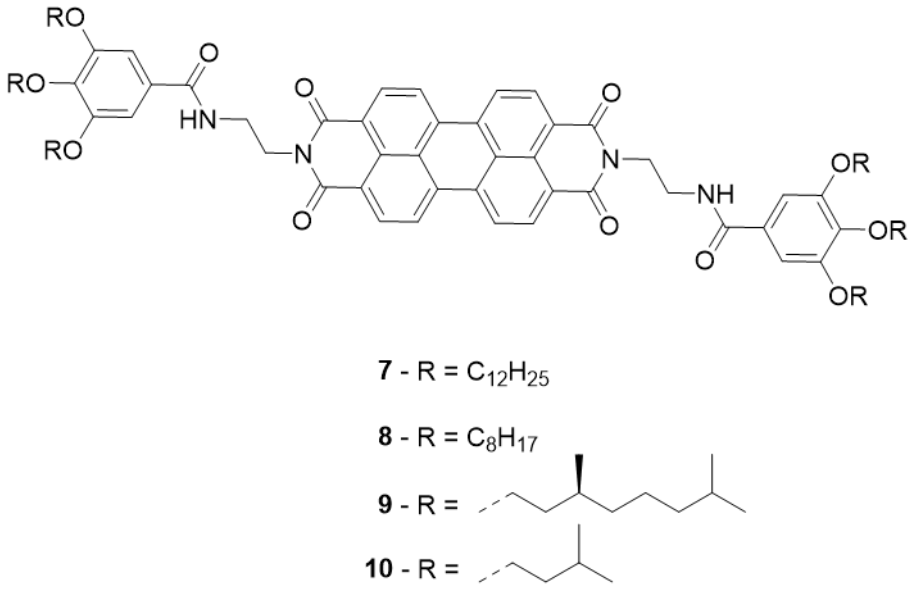

Figure I-6. Structures of perylene bisimide group based organogelators with linear alkyl chains (**7** and **8**) and side branched alkyl chains (**9** and **10**).

Comparison between **7** and **8**, the alkyl chain length had no critical effect to the aggregation mode. A chirality also did not have any specific role because **9** and **10** both showed a J-aggregation. The bulky side chains destabilized the more densely packed face to face H-type π-stacking, which induced the J-type π-stacking. Therefore, even if their aromatic core structures were same, the H-type aggregate gels of **7** and **8** showed red color and the J-type gels exhibit black, respectively.

Polymerizable gelator

Physical gels can suffer from the lack of mechanical and chemical stability due to the nature of soft materials. To form highly stable organogels, the polymerizable groups can be introduced to the gelators. A number of studies nicely demonstrated the polymerizable orgnogelators bearing vinyl, methacrylate, acrylate or diacetylene units.[24-31]

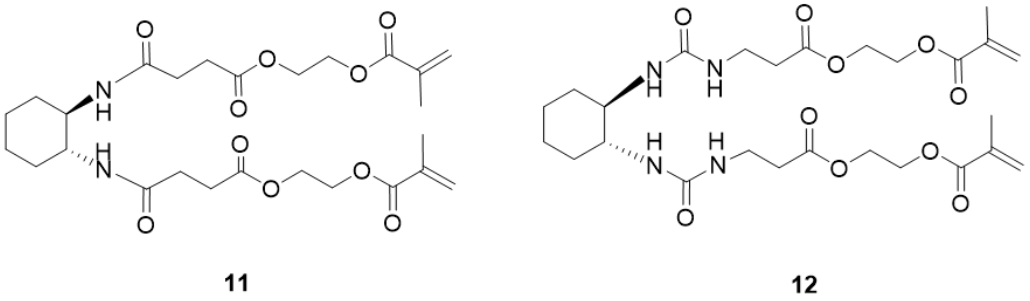

11 **12**

Figure I-7. Structures of polymerizable organogelators bearing two methacrylate groups (**11** and **12**).

Feringa group reported bis(amido)cyclohexane and bis(ureido)cychlohexane derivatives **11** and **12** which contain two methacrylate groups (Figure I-7).[24] In the case of **12**, it formed a gel in 1,2-dichloroethane and subsequent photopolymerization was achieved. While nonpolymerized gel of **12** in 1,2-dichloroethane started to crystallize after 1 h, the polymerized gel could be

stored for months without significant change. The polymerized gels showed high thermal stability showing stable gel up to at least 135 ºC which was above melting point of nonpolymerized gel.

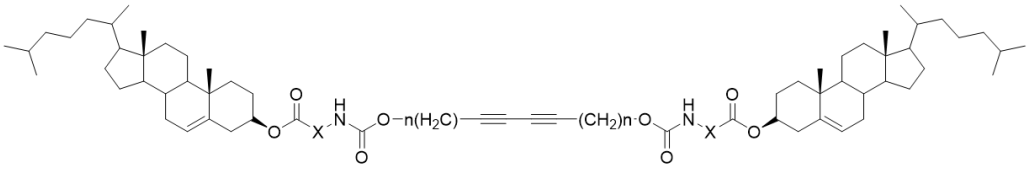

13: n = 1, X = $(CH_2)_2$ **20**: n = 3, X = $CHCH_3$ (L-Ala)

14: n = 1, X = $(CH_2)_3$ **21**: n = 3, X = $CHCH_3$ (D-Ala)

15: n = 2, X = CH_2 **22**: n = 4, X = CH_2

16: n = 2, X = $(CH_2)_3$ **23**: n = 4, X = $(CH_2)_2$

17: n = 3, X = CH_2 **24**: n = 4, X = $(CH_2)_3$

18: n = 3, X = $(CH_2)_2$ **25**: n = 4, X = $CHCH_3$ (L-Ala)

19: n = 3, X = $(CH_2)_3$ **26**: n = 4, X = $CHCH_3$ (D-Ala)

Figure I-8. Structures of polymerizable organogelators bearing diacetylene groups (**13 - 26**).

Nagasawa and coworkers explored diacetylene dicholesteryl ester derivatives (**13** – **26**) (Figure I-8).[27] The photopolymerization of diacetylene units of various gelators in organogel state was successful, and the fibrous structure in the gel was not significantly changed after polymerization. The polymerized gels shrank but maintained its overall shape after heated above sol-

gel transition temperature.

A gelator with two different polymerizable groups that form a gel in monomeric solvent was investigated by Chang et al.[32] As presented in Figure I-9, it consisted of acryl and diacetylene groups, which formed a gel in monomeric solvents such as methyl methacrylate and hexyl methacrylate. An acryl group of gelators could participate in the photopolymerization of monomeric solvents in gel state resulting in formation of gel fiber embedded polymer matrix. At the same time, the polydiacetylene chains exhibited more strong emission allowing visualization of nonofibrillar structures in confocal laser scanning microscopy.

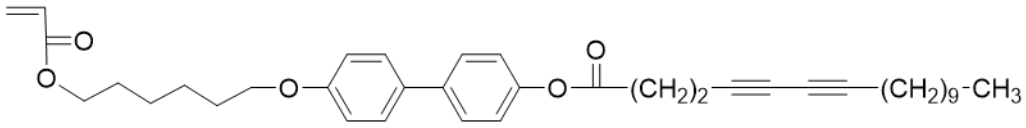

27

Figure I-9. Structures of polymerizable organogelators bearing two different polymerizable groups (**27**).

I-1-3. Chemical Gels

Chemical gels are covalently crosslinked three-dimensional networks polymers swollen in a large amount of solvent.[8,33] Due to irreversible covalent bond, this type of gel is thermodynamically irreversible. They can be prepared by the swelling of a preliminarily crosslinked polymer[34,35] or by the crosslinking of monomers or oligomers at the reactive terminal groups in a solvent medium. Figure I-10 shows schematic descriptions of chemical gelation from two different ways.

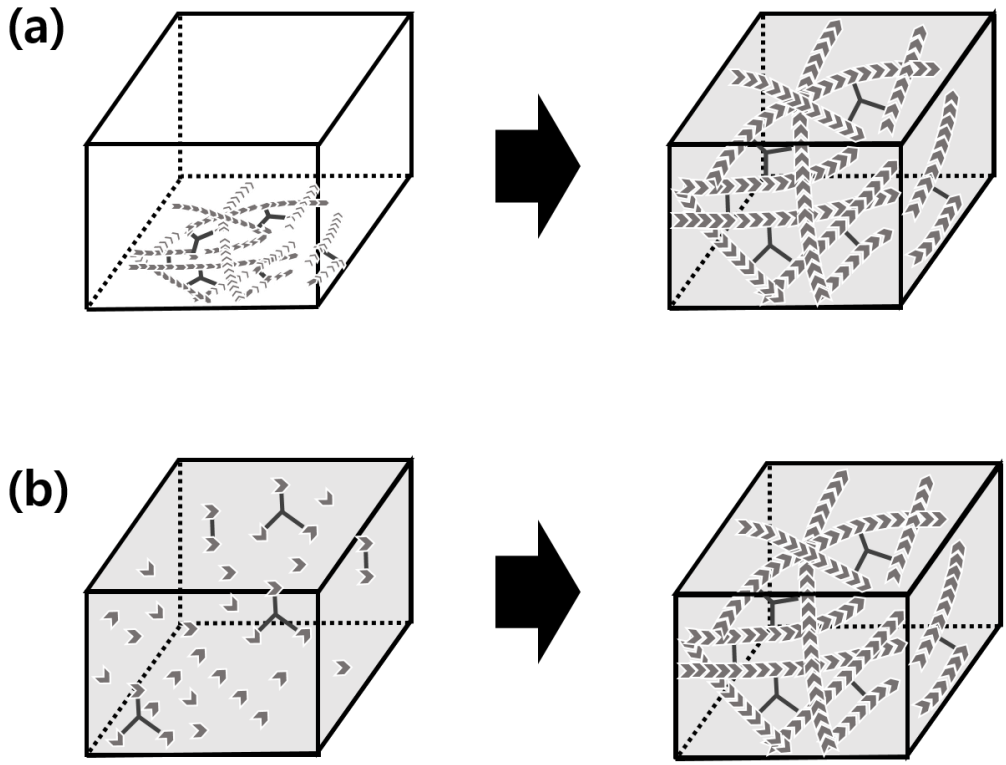

Figure I-10. Schematic descriptions of formation of chemical gels by (a) swelling of preliminarily crosslinked polymer and (b) crosslinking of monomers or oligomers in a solvent medium.

In the case of chemical gels, they can be stable after removing of solvents due to its thermodynamically irreversibility and mechanical stability. Therefore, chemical gels can be further studied as a method for the preparation of porous monolithic polymers, which have been widely used as a stationary phases for different types of chromatography, high-throughput bioreactors and in

microfluidic chip applications.[36]

For instance, as a simple case of chemical gels, Storey group early developed gelation process using styrene and p-divinylbenzene.[37] They controlled the amount of crosslinking agent, p-divinylbenzene, and investigated gelation time and swelling ratio. Moad group reported the styrene-co-divinylbene benzene copolymer gel based monolith system, which was synthesized by reversible addition-fragmentation chain transfer (RAFT) method.[38] They studied kinetic of monolithic formation and the morphology of the materials obtained.

Various monomers and cross-linkers for chemical gels were described in Figure I-11 and Figure I-12, respectively.[36] The various monomers are hydrophobic monomers such as styrene (**28**) and butylmethacrylate (**29**) and monomers bearing reactive functional group such as chloromethyl styrene (**30**), glycidyl methacrylate (**31**) and 2-vinyl-4,4-dimethylazolactone (**32**). There were also protected functionality monomer such as 4-acetoxystyrene (**33**) and water soluble hydrophilic monomer such as acrylamide (**34**) and 2-acrylamido-2-methyl-1-propanesulfonic acid (**35**). A monomer with zwitterionic charcters such as 2-(N-3-sulfopropyl-N,N-dimethyl ammonium)ethyl methacrylate (**36**) was also used.

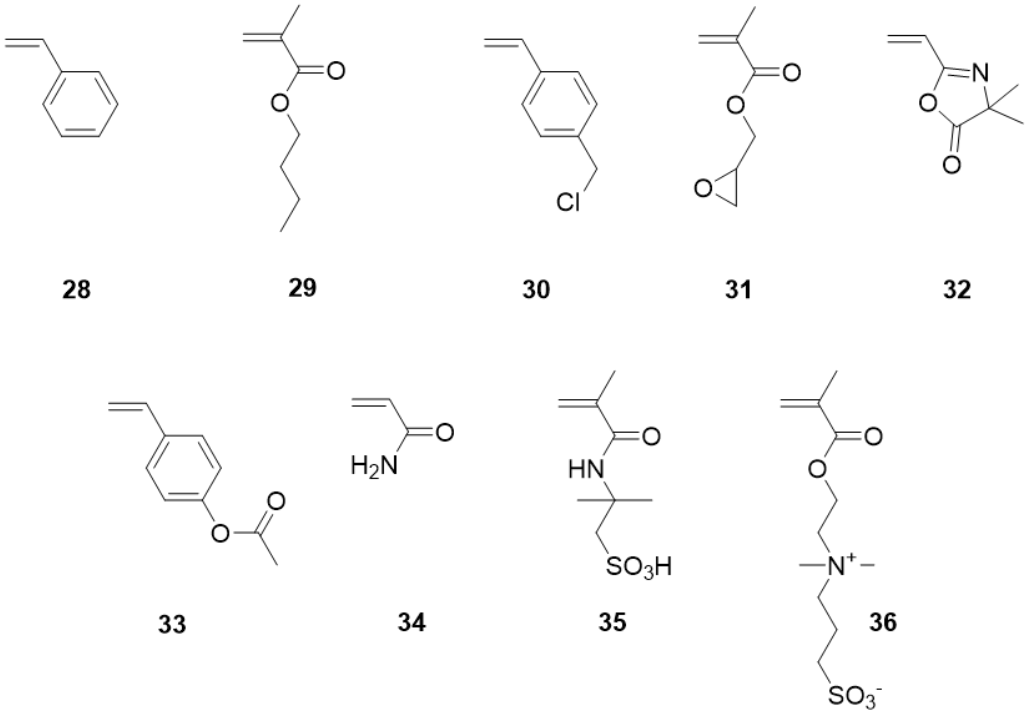

Figure I-11. Structures of monomers for chemical gels (**28** – **36**).

In the case of cross-linking agent, bifunctional monomers such as divinylbenzene (DVB) (**37**), N,N'-methylenebis(acrylamide) (BIS) (**38**), and ethylene gylcol dimethacrylate (EGDMA) (**39**) and trifunctional monomer such as trimethylolpropane trimethacrylate (TRIM) (**40**) were have been utilized intensively.

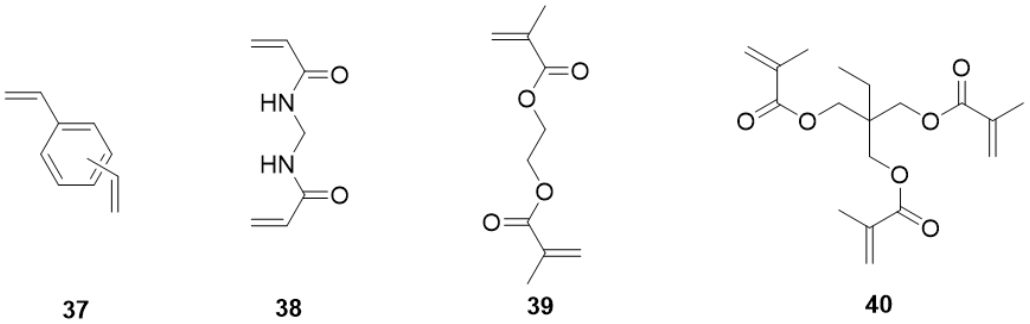

Figure I-12. Structures of cross-linkers for chemical gels (**37** – **40**).

I-2. Introduction to Thermochromism

I-2-1. Definition of Thermochromism

Thermochromism refers to the phenomenon of a color changes in materials with change of temperature.[39] The origin of color change is related to the interaction of a matter with visible light such as scattering, reflection, absorption and emission. In general, there are two possible systems for polymers to achieve thermochromic properties: Inherent and doped system. The former is that polymers have its own thermochromic properties inherently. The latter is that polymers have dopants able to interact with a polymer matrix. When it comes to inherent thermochromic polymers, the origin of thermochromism is usually from the morphological change of conjugated polymers. In the case of doped system, dye-dye aggregation-disaggregation in a

polymer matrix or a change of chemical structure of dyes in a polymer matrix have been widely investigated.

I-2-2. Chemical Structural Change System

Thermochormic properties can be achieved by chemical structure change according to temperature. Some dye molecules possessing a phenol group can show structural change, which results in thermocrhomism. Seeboth group intensively investigated this concept of thermochromism. They used Reichardt betain dye 2,6-diphenyl-4-(2,4,6-triphenylpyridinio)phenolate (DTPP) and Cresol Red dye (Figure I-13).[40]

Dye molecules were embedded in an aqueous polyviniyl alcohol-borax-surfactant gel network. In the case of DTPP, the color of gel was gradually changed from colorless at 10 ^{o}C to a deep violet at 80 ^{o}C. When it comes to the Cresol Red system, the color was changed from yellow to wine-red. The equilibrium between the phenol and phenolate form of those dyes was shifted due to temperature-induced shifts of the proton transfer equilibrium. The color changes were reversible and the closed hydrogel networks were essential.

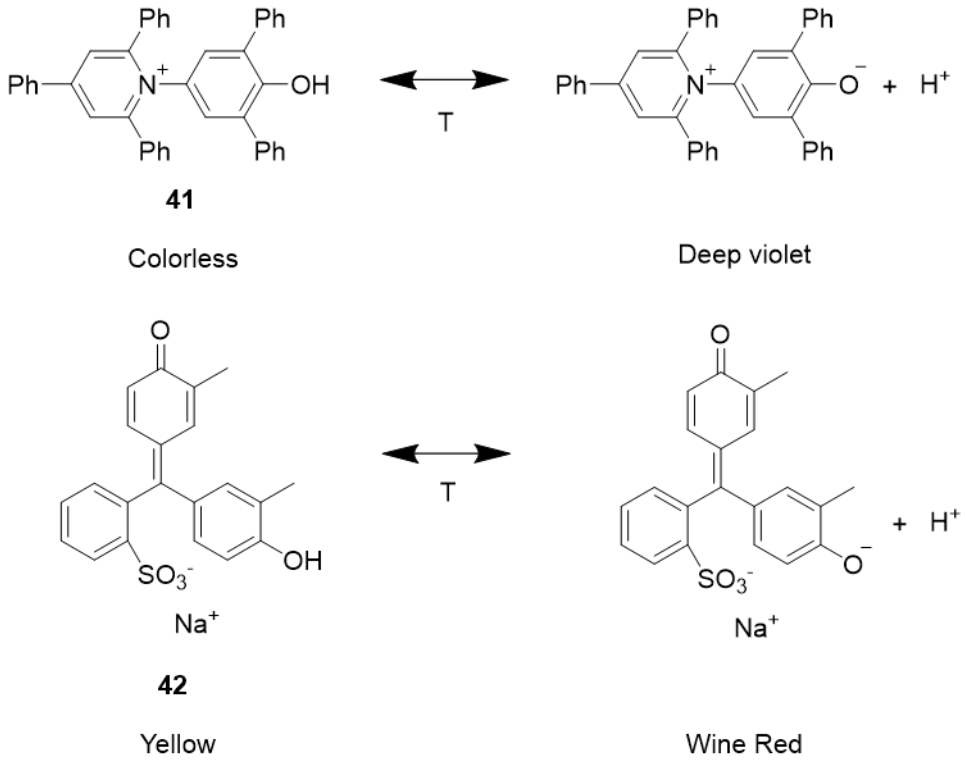

Figure I-13. Structures of temperature dependent structural change molecules Reichardt betaine dye (**41**) and Cresol Red dye (**42**).

A structural change induced thermochromism based on the polymer-dye complex formation have been investigated by Seeboth group.[41] The thermochromic polymer consisted of poly(lactic acid), cyanidin chloride, dodecylgallate and hexadecanoic acid. The color of anthocyanidin dye, cyaniding chloride, was changed from red in neutral state to violet at anionic anhydrobased form (Figure I-14). The proposed mechanism of this

phenomenon was as follows. In the molten state, or the mobile amorphous phase, the polymer-dye complex which had phenolate form was expected due to the stabilization by multiple hydrogen bond. However, the conformational change of the PLA backbone at room temperature induced destabilization of polymer-dye complex leading to disaggregation and change the equilibrium into neutral anhydrobase form. Therefore, a color change between a red at low temperature and violet at high temperature was observed.

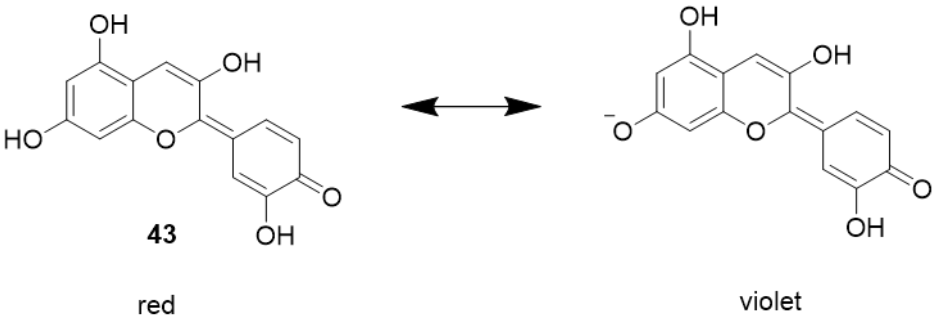

Figure I-14. Structures of temperature dependent structural change molecules anthocyanidin dye (**43**).

I-2-3. Morphological Change System

This type of thermochromism is not accompanied with chemical structural change. A conformational change of polymer backbone or variable

intermolecular interactions between polymer chains depending on a thermal energy induce color change of polymers. Dye-dye aggregation-disaggregation in polymer matrix provides color change as well.

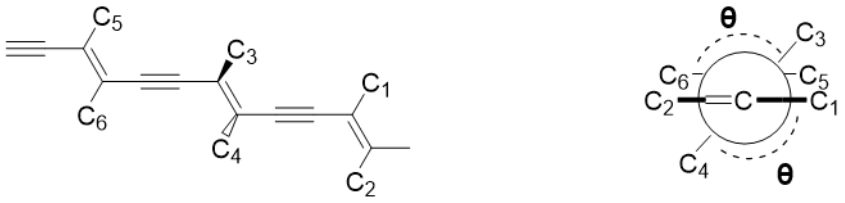

Figure I-15. Schematic representation of polydiacetylene and torsional angle (θ) of polymer backbone.

Schott et al studied principles of color change of polydiacethylenes (PDA).[42] The origin was explained by the torsion of polymer backbone (Figure I-15). The substituents, depending on the interactions with their surroundings, could induce some torsion of the main chain. The electronic structure of the polymer chain is changed due to the torsion of the backbone. And it induced a shift of the absorption peaks from the red part of the spectrum, as it is shown in the planar conformation, to the blue region, as it is shown in the twisted conformation. Its reversible change of planarity of backbone could be caused by thermal energy.

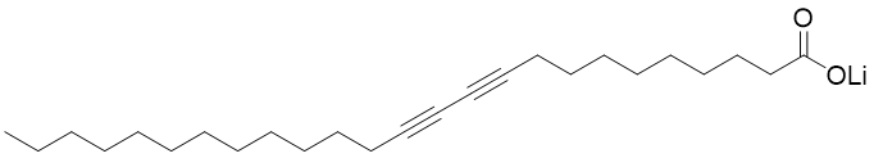

44

Figure I-16. Structures of lithium salt of 10,12-pentacosadiynoic acid (**44**).

Polydiacethylene based thermochromism was also intensively explored by Kim et al.[43] They prepared lithium salt of 10,12-pentacosadiynoic acid (Li-PDCA) embedded in polyvinyl alcohol (PVA) films (Figure I-16). After short irradiation of UV light, Li-PDCA embedded film showed navy blue color as a result of photopolymerization of diacetylene group. The film exhibited reversible thermochromism showing color change of the film from navy blue at room temperature to red at 140 ^{o}C. The colorimetric transition of polydiacethylene units was resulted from the change of effective conjugation length of polymer backbone which was triggered by conformational changes in backbone of polymers.

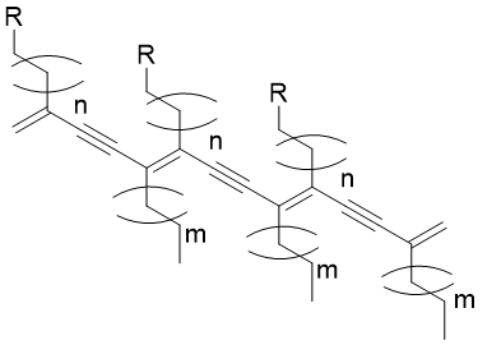

45 - n = 11, m = 8, R = COOH
46 - n = 11, m = 4, R = COOH
47 - n = 4, m = 8, R = COOH
48 - n = 9, m = 3, R = COOH
49 - n = 11, m = 8, R = COONa
50 - n = 11, m = 4, R = COONa

Figure I-17. Model structures of various side chain length and head group (**45** – **50**)

The effects of side chain and head group (R) of polydiacethylene were investigated by Hsu et al (Figure I-17).[44] Various type of PDA was prepared and the color change depending on the temperature was characterized. Overall, the colors of PDA were changed from blue to red with increase of temperature. The transition temperatures (T_t) were largely affected by length of alkyl chains. T_t of **45**, **46** and **47** were 65, 60 and 40 ^oC, which indicated that T_t would be increased as length of alkyl chain increases. The alkyl chains on the head group side were more effective to determine transition temperature, because **48** showed higher T_t than **47** even though they have same n + m value. All side chains involving strong hydrogen bond interactions (**45** – **48**) showed irreversible transition, but **49** and **50** with electrostatic interactions showed reversible thermochromism. Because long-range and nonspecific electrostatic

interactions could easily accommodate the morphological changes corresponding to the temperatures, they exhibited reversible thermochromism.

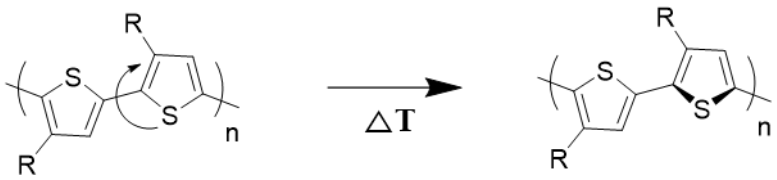

Figure I-18. Schematic representation of polythiophene conformational change

Thermochromism in polythiophene generally has been explained by the conformational change of polymer backbone (Figure I-18).[45] A blue shift of absorption spectra was observed as the temperature increased. The backbone of polymer has coplanar or nearly planar conformation at low temperature whereas the backbone of twisted conformation at high temperature results in change of effective conjugation length. A lot of studied have been elucidated this thermochromic phenomenon. [45-55]

Leclerc group investigated polythiophene with different side chains and various stimuli sensitive optical properties including thermal stimulus. In UV-Vis absorption spectra of poly(3-octylthiophene) in solid state, the absorption maximum was shifted to higher energy region by heating. Thermally-induced disordering of the side chains in polythiophene leaded to twisting of conjugated

polymer backbone resulting in strong hypsochromic shift in the absorption maximum.[50] The thermochromism operated by conformational change of backbone was controlled by delicated balance between repulsive side-chain steric interactions and attractive interchain interactions.[55]

Aggregation of dye molecules can affect the absorption properties as mentioned above (Figure I-4). The dye molecules in polymer matrix can exhibit different color depending on temperature. There can be two different ways for controlling dye aggregation-disaggregation. One is kinetically immobilized dye molecules by high viscous matrix, which prevents the formation of thermodynamically stable aggregated form. When the temperature is above glass transition temperature of polymers (T_g), the mobility of dyes increases and aggregates can be formed irreversibly. Another approach is that an aggregation-disaggregation of dye molecules is carried out in the cross-linked polymer matrix, which frustrates dyes to diffuse into the polymer matrix.

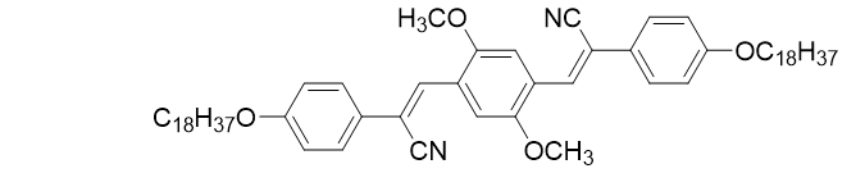

51

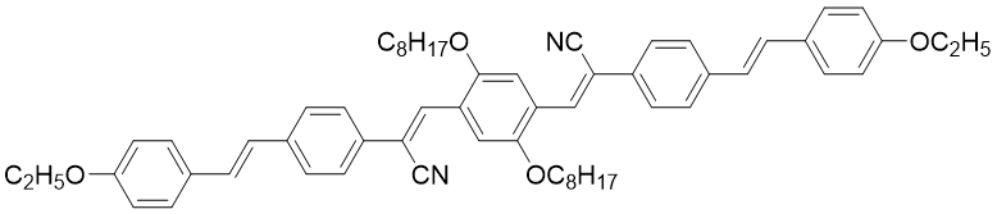

52

Figure I-19. Structures of oligo(p-phenylene vinylene) dyes (**51** and **52**).

As an example of the first approach, Weder and coworkers investigated thermochromic cyano oligo(p-phenylene vinylene) polymer blends (Figure I-19).[56,57] Those dye molecules were dissolved in melt polymer and rapidly quenched to room temperature to reduce mobility of dye molecules, thereby thermodynamically unstable monomeric forms still existed in the polymer matrix. When heated above the respective T_g, the viscosity of polymer matrix was reduced. Thus the mobility of dye molecules increased. As a result, thermodynamically favored aggregated forms were generated with a change of the perceived color. There was an upper temperature limit where all dye molecules were disaggregated. Within this temperature region, the polymer

blends could act as a time-temperature indicator. In the case of **51** with poly(ethylene terephthalate glycol) blend, annealing at 90 ºC leaded to an irreversible color change from yellow to orange within 1 h. While annealing at 120 ºC, same color change was generated in less than 5 min. In the case of the polymer blend with **52**, the color change was much slower than **51** due to reduced mobility.

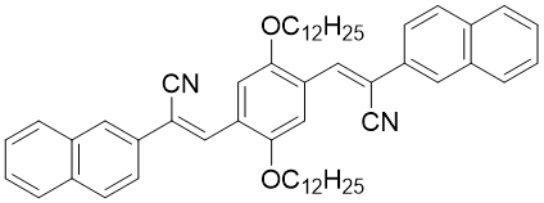

53

Figure I-20. Structures of oligo(p-phenylene vinylene) dyes **53**.

The thermochromism from the approach mentioned above was irreversible. On the other hand, reversible thermochromism was possible with the help of cross-linked polymer matrix. The fluorescent organogelator **53** formed a gel in ethyelen glycol dimethacrylate which was a cross-linkable monomeric solvent (Figure I-20).[58] A nanocomposite polymer film was prepared by photopolymerization of the organogel for not disrupting the self-assembled structure. This polymer film showed reversible thermochromism showing color

change from orange at room temperature to yellowish green at 120 ºC under 365 nm irradiation. The reversible aggregation-disaggregation of dye molecules in a cross-linked polymer matrix was in charge of the color change. The reversibility might be originated from the poor interactions of molecules with the polymer matrix which restrict the diffusion of dye molecules into polymer matrix.

I-3. Introduction to Hierarchical Porous Polymer

I-3-1. Definition of Hierarchical Porous Polymer

In general, porous materials are classified into three types by pore size: micro-, meso- and macroporous. According to the IUPAC (International Union of Pure and Applied Chemistry) notation, micropores are less than 2 nm, mesopores are between 2 nm and 50 nm, and macropores are larger than 50 nm in pore diameter.[59] A hierarchical porous structure indicates having all kinds of pores (micro-, meso- and macropores).[60-63] A large surface generated by micro- and mesopores is one of the important parameters in various applications such as gas storage, separation, catalysis and biomedical applications whereas macropores provide pathways to micro- and mesopores. Pore characters such as

pore size distributions and Brunauer-Emmitt-Teller surface area are determined by nitrogen adsorption-desorption isotherms. There are generally accepted six type of adsorption isotherms.[64]

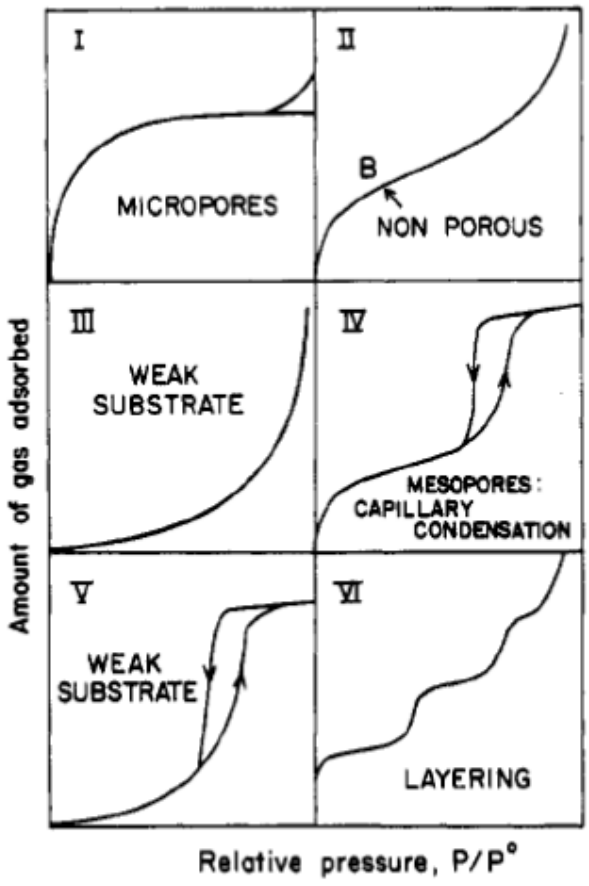

Figure I-21. The six types of adsorption isotherms according to the IUPAC classification.

Type I (the Langmuir isotherm) is usually obtained from microporous polymers. Type II and Type III are can be observed from typical nonporous

materials with strong (type II) or weak (type III) interaction between fluid and pore wall. Type IV and type V occur in strong (type IV) or weak (V) interaction between fluid and pore wall, respectively, showing hysteresis loops. The hysteresis loops came from the capillary condensation.[65] Type VI is not typical isotherms but occurs when the temperature is near the melting point for the adsorbed gas. In general, Non-Local Density Function Theroy (NLDFT) method based on statistical mechanics is widely used to estimate pore size distribution from the isotherm curves.[66]

I-3-2. Preparation of Hierarchical Porous Polymer

To pursue hierarchical porous structures, post modifications for developing of micropores to materials having meso- and macroporous have been investigated. Variety sacrificial templates such as solvent,[67] surfactant,[68,69] polymer,[61,62,63] silica and metal oxides[70] that are removed after completion of the reaction have been used for formation of meso- and macropores. The activation processes including carbonization[71] and gas developing activation[72,73] or post modification reactions[74,75] such as hyper-crosslinking have been widely used for formation of micropores. In other words, meso- and macropores are created first and micropores are formed later.

On the other hand, creating micro- and mesopores and then creating macropores can be another approach. Microporous organic polymers (MOPs) which generally have micro- and mesopores have been intensively investigated due to its high surface areas and physicochemical stability.[76-78] MOPs were usually prepared by various types of condensation reactions and metal-catalyzed reactions, which generate permanent porosity.[77] Therefore, formation of microporous polymer with macroscopic sacrificial porogen such as silica and solvent and removal of them after polymerization can construct hierarchical porous structures.

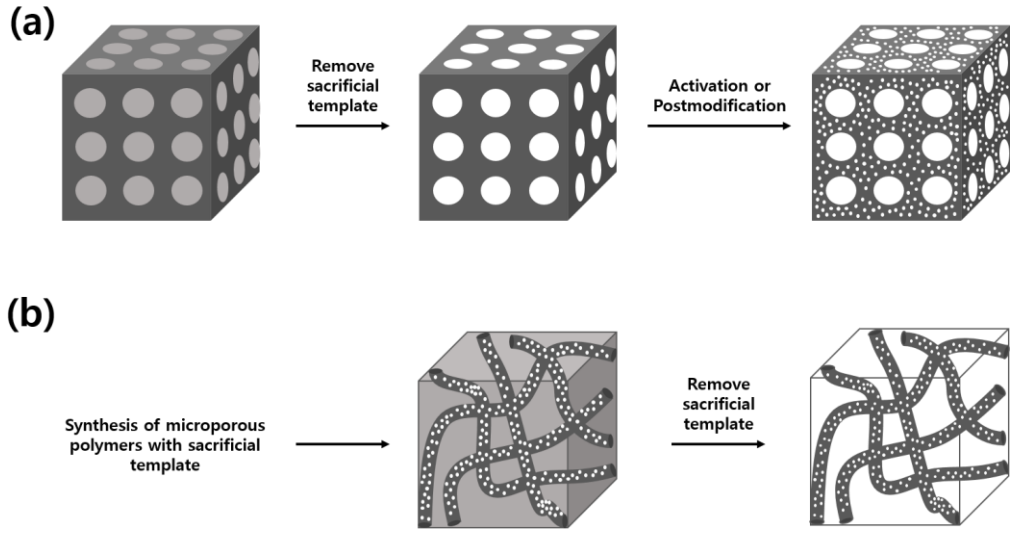

Figure I-22. Schematic descriptions of constructing hierarchical porous structures by (a) formation of meso- and macropore followed by micropores, or (b) formation of micro- and mesopore followed by macropores.

Nguyen group reported hierarchically porous organic polymers from conventional porous polymers with sacrificial mesoporous silica aerogel.[79] The cobalt-catalyzed trimerization of 1,4-diethynylbenzene reaction[80] was carried out in the mesoporous silica aerogel. After forming stable aromatic networks, silica aerogel was etched by HF. Micro- and mesopores were developed by aromatic networks generated by trimerization of 1,4-diethynylbenzene, and larger meso- and macropores were produced presumably from the interstitial spaces between the silica particles that made up the aerogel template.

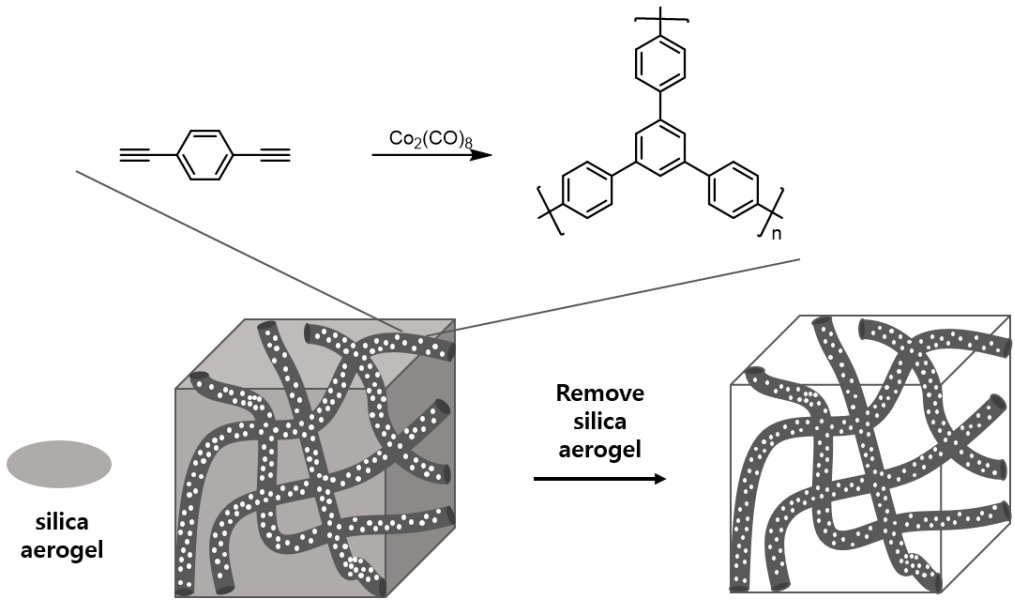

Figure I-23. Schematic description for preparing hierarchical porous polymers with sacrificial silica aerogel.

Conjugated Microporous Polymers (CMPs) aerogels were designed by Zhang et al. Poly(1,3,5-triethynylbezene) aerogel (**54**) was prepared by the Glaser coupling reaction (Figure I-24).[81] During polymerization, the 3D network was constructed in the same manner as formation of chemical gel. After purification and a solvent-exchange process with water, the monolithic poly(1,3,5-triethynylbenzene) aerogels were obtained by a freeze drying. The sublimation of a pre-frozen solvent was utilized to avoid pore shrinkage and internal structure collapse resulting in about 70% higher surface area (1701 m^2g^{-1}) than vacuum-dried (1085 m^2g^{-1}).

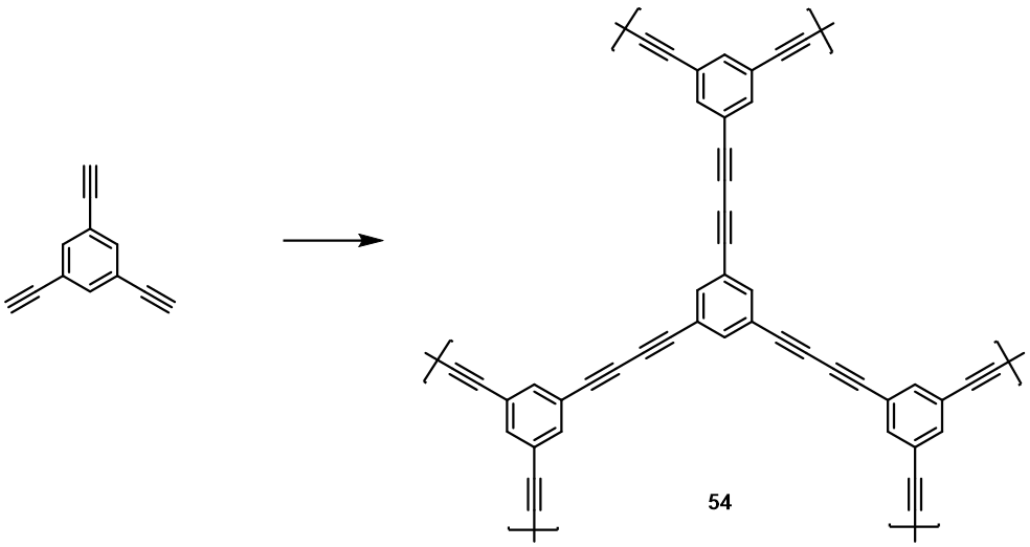

Figure I-24. Structures of conjugated microporous aerogels (**54**).

.

The hierarchical porous polymers without freeze-drying process reported by Chang and coworkers.[82] During the Sonogashira-Hagihara coupling reactions, a chemical gel was formed (Figure I-25). The 3D network of monolithic microporous polymer was stable even after drying process in vacuum at 120 ^{o}C. The BET surface areas of **55** was 463 m^2g^{-1} with hierarchical pore structures. Strikingly, the monolithic microporous polymers (**55**) had a mechanical stability against compressible stress showing reversible compression and release cycles without significant change.

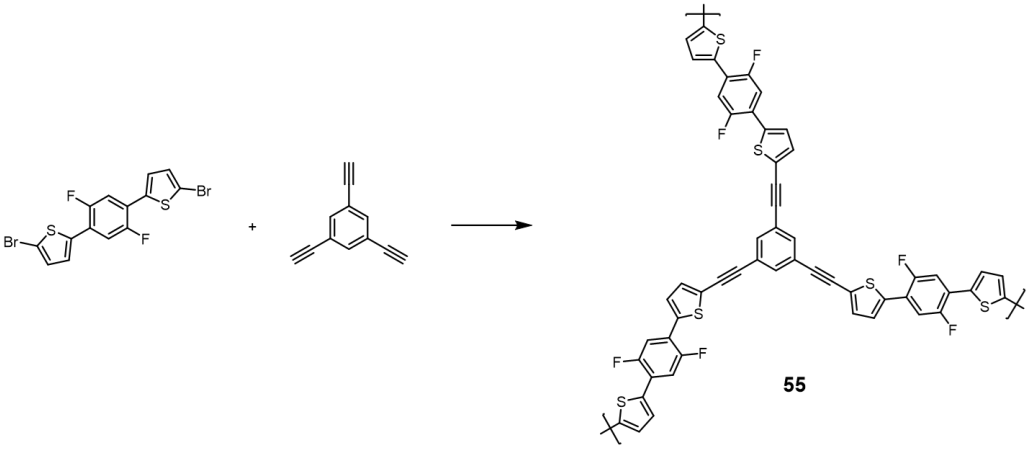

Figure I-25. Synthetic description of a microporous organic polymer (**55**) for hierarchical porous polymer.

In this study, the physical gels from self-assembly of low molecular weight gelators bearing oligothiophene core were utilized to prepare reversible

thermochromic polymer film. And the chemical gels prepared from the Sonogahira reaction between trifunctional monomers and bifunctional monomers were used for preparing hierarchical porous polymers.

I-4. References

1. Weiss, R. G.; Terech, P. *Molecular gels: materials with self-assembled fibrillary networks*, Springer, Dordrecht, **2006**.
2. Terech, P.; Weiss, R. G. *Chem. Rev.* **1997**, *97*, 3133-3159.
3. Abdallah, D. J.; Weiss, R. G. *Adv. Mater.* **2000**, *12*, 1237-1247.
4. Sangeetah, N. M.; Maitra, U. *Chem. Soc. Rev.* **2005**, *34*, 821-836.
5. Murdan, S. *Expert Opin. Drug Deliv.* **2005**, *2*, 489-505.
6. Sahoo, S.; Kumar, N; Bhattacharya, C.; Sagiri, S. S.; Jain, K.; Pal, K.; Ray, S. S.; Nayak, B *Des. Monomers Polym.* **2011**, *14*, 95-108.
7. Lan, Y.; Corradini, M. G.; Weiss, R. G.; Raghavan, S. R.; Rogers, M. A. *Chem. Soc. Rev.* **2015**, *44*, 6035.
8. Osada, Y.; Gong, J. P.; Tanaka, Y. *J. Macromol. Sci. Par C Polym. Rev.* **2004**, *44*, 87-112.
9. Babu, S. S.; Praveen, V. K.; Ajayaghosh, A. *Chem. Rev.* **2014**, *114*, 1973-2129.
10. Izumi, T.; Kobashi, S.; Takimiya, K.; Aso, Y.; Otsubo, T. *J. Am. Chem. Soc.* **2003**, *125*, 5286-5287.
11. Rissler, J. *Chem. Phys. Lett.* **2004**, *395*, 92-96.
12. Kawano, S. I.; Fujita, N.; Shinkai, S. *Chem. Eur. J.* **2005**, *11*, 4735-4742.

13. Shu, T.; Wu, J.; Lu, M.; Chen, L.; Yi, T.; Li, F.; Huang, C. *J. Mater. Chem.* **2008**, *18*, 886-893.

14. Deng, Y.; Yuan, W.; Jia, Z.; Liu, G. *J. Phys. Chem. B* **2014**, *118*, 14536-14545.

15. Bore, S. D.; Wiersma, D. A. *Chem. Phys. Lett.* **1990**, *165*, 45-53.

16. Whitten, D. G. *Acc. Chem. Res.* **1993**, *26*, 502-509.

17. Nüesch, F.; Grätzel, M. *Chem. Phys.* **1995**, *193*, 1-17.

18. Siddiqui, S.; Spano, F. C. *Chem. Phys. Lett.* **1999**, *308*, 99-105.

19. Mandal, A. K.; Pal, M. K. *Chem. Phys.* **2000**, *253*, 115-124.

20. Eisfeld, A; Briggs, J. S. *Chem. Phys.* **2006**, *324*, 376-384.

21. Ghosh, S.; Li, X. Q.; Stepanenko, V.; Würthner, F *Chem. Eur. J.* **2008**, *14*, 11343-11357.

22. Wu, H.; Xue, L.; Shi, Y.; Chen, Y.; Li, X. *Langmuir* **2011**, *27*, 3074.

23. Gierschner, J.; Luer, L.; Milian-Medina, B.; Oelkrug, D.; Egelhaaf, H. *J. Phys. Chem. Lett.* **2013**, *4*, 2686-2697.

24. de Loos, M.; van Esch, J.; Stokroos, I.; Kellogg, R. M.; Feringa, B. L *J. Am. Chem. Soc.* **1997**, *119*, 12675-12676.

25. Wang, G.; Hamilton, A. D. *Chem. Eur. J.* **2002**, *8*, 1954-1961.

26. George, M.; Weiss, R. G. *Chem. Mater.* **2003**, *15*, 2879-2888.

27. Nagasawa, J.; Kudo, M.; hayashi, S.; Tamaoki, M *Langmuir* **2004**, *20*,

7907-7916.

28. Shirakawa, M.; Fujita, N.; Shinkai, S. *J. Am. Chem. Soc.* **2005**, *127*, 4164-4165.
29. Dautel, O. J.; Robitzer, M.; Lère-Porte, J. P.; Serein-Spirau, F.; Moreau, J. J. E. *J. Am. Chem. Soc.* **2006**, *128*, 16213-16223.
30. Nie, X.; Wang, G. *J. Org. Chem.* **2006**, *71*, 4734-4741.
31. Jahnke, E.; Lieberwirth, I.; Severin, N.; Rabe, J. P.; Frauenrath, H. *Angew. Chem. Int. Ed.* **2006**, *45*, 5383-5386.
32. Kang, S. H.; Jung, B. M.; Chang J. Y. *Adv. Mater.* **2007**, *19*, 2780-2784.
33. Rogovina, L. Z.; Vasil'ev, V. G.; Braudo, E. E. *Poly. Sci. Ser. C* **2008**, *50*, 1397-1406.
34. Daoud, M.; Bouchaud, E.; Jannink, G. *Macromolecules* **1986**, *19*, 1955-1960.
35. Kudo, S.; Otsuka, E.; Suzuki, A. *J. Polym. Sci. Part B Polym. Phys.* **2010**, *48*, 1978-1986.
36. Arrua, R. D.; Strumia, M. C.; Igarzabal, C. I. A. *Materials* **2009**, *2*, 2429-2466.
37. Storey, B. J. *J. Polym. Sci. Part A Gen. Pap.* **1965**, *3*, 265-282.
38. Barlow (née Tan), K. J.; Hao, X.; Hughes, T. C.; Hutt, O. E.; Polyzos, A.; Turner, K. A.; Moad, G. *Polym. Chem.* **2014**, *5*, 722-732.

39. Seeboth, A.; Lötzsch, D.; Ruhmann, R.; Muehling, O. *Chem. Rev.* **2014**, *114*, 3037-3068.

40. Seeboth, A. Kriwanek, J.; Vetter, R. *J. Mater. Chem.* **1999**, *9*, 2277-2278.

41. Seeboth, A.; Lötzsch, D.; Ruhmann, R. *J. Mater. Chem. C* **2013**, *1*, 2811-2816.

42. Filhol, J. S.; Deschamps, J.; Dutremez, S. G.; Boury, B.; Barisien, T.; Legrand, L.; Schott, M. *J. Am. Chem. Soc.* **2009**, *131*, 6976-6988.

43. Balakrishnan, S.; Lee, S.; Kim, J. M. *J. Mater. Chem.* **2010**, *20*, 2302-2304.

44. Yu, L.; Hsu, S. L. *Macromolecules* **2012**, *45*, 420-429.

45. Lucht, B. L.; Euler, W. B.; Gregory, O. J. *Polym. Prepr.* **2002**, *43*, 59-60.

46. Faïd, K.; Leclerc, M. *J. Chem. Soc., Chem. Commun.* **1993**, *11*, 962-963.

47. Roux, C.; Leclerc, M. *Chem. Mater.* **1994**, *6*, 620-624.

48. Yang, C.; Orfino, F. P.; Holdcroft, S. *Macromolecules* **1996**, *29*, 6510-6517.

49. Hirota, N.; Hisamatsu, N.; Maeda, S.; Tsukahara, H.; Hyodo, K. *Synt. Met.* **1996**, *80*, 67-72.

50. Leclerc, M; Faïd, K. *Adv. Mater.* **1997**, *9*, 1087-1094.

51. DiCésare, N.; Belletête, M.; Marrano, C.; Leclerc, M.; Durocher, G. *J. Phys. Chem. A* **1998**, *102*, 5142-5149.

52. Elmacı, N.; Yurtsever, E. *J. Phys. Chem. A* **2002**, *106*, 11981-11986.

53. Brown, P. J.; Thomas, D. S.; Köhler, A.; Wilson, J. S.; Kim, J. S.; Ramsdale, C. M.; Sirringhaus, H.; Friend, R. H. *Phys. Rev. B* **2003**, *67*, 064203.

54. Zhao, X. *J. Mater. Sci.* **2005**, *40*, 3423-3428.

55. Lukeš, V.; Breza, M. *J. Mol. Struct. THEOCHEM* **2007**, *820*, 35-39.

56. Crenshaw, B. R.; Kunzelman, J.; Sing, C. E.; Ander, C.; Weder, C. Macromol. *Chem. Phys.* **2007**, *208*, 572-580.

57. Sing, C. E.; Kunzelman, J.; Weder, C. *J. Mater. Chem.* **2009**, *19*, 104-110.

58. Sing, K. S. W.; Everett, D. H.; Haul, R. A. W.; Moscou, L.; Pierotti, R. A.; Rouquerol, J.; Siemieniewska, T. *Pure Appl. Chem.* **1985**, *57*, 603–619.

59. Sing, K. S. W.; Everett, D. H.; Haul, R. A. W.; Moscou, L.; Pierotti, R. A.; Rouquerol, J.; Siemieniewska, T. *Pure Appl. Chem.* **1985**, *57*, 603-619.

60. Liang, Y.; Wu, B.; Wu, D.; Xu, F.; Li, Z.; Luo, J.; Zhong, H.; Fu, R.; Matyjaszewski, K. *J. Mater. Chem.* **2011**, *21*, 14424-14427.

61. Seo, M.; Hillmyer, M. A. *Science* **2012**, *336*, 1422-1425.

62. Seo, M.; Kim, S.; Oh, J.; Kim, S. J.; Hillmyer, M. A. *J. Am. Chem. Soc.*

2015, *137*, 600-603.

63. Saba, S. A.; Mousavi, M. P. S.; Bühlmann, P.; Hillmyer, M. A. *J. Am. Chem. Soc.* **2015**, *137*, 8896-8899.
64. Balbuena, P. B.; Gubbins, K. E. *Langmuir* **1993**, *9*, 1801-1814.
65. Ball, P. C.; Evans, R. *Langmuir* **1989**, *5*, 714-723.
66. Ravikovitch, P. I.; Vishnyakov, A.; Russo, R.; Neimark, A. V. *Langmuir* **2000**, *16*, 2311-2320.
67. Muñoz-Bonilla, A.; Fernández-García, M.; Rodríguez-Hernández, J. *Prog. Polym. Sci.* **2014**, *39*, 510-554.
68. Chalal, N.; Bouhali, H.; Hamaizi, H.; Lebeau, B.; Bengueddach, A. *Microporous Mesoporous Mater.* **2015**, *210*, 32-38.
69. Riachy, P.; Stébé, M. J.; Lebeau, B.; Pasc, A.; Vidal, L.; Blin, J. L. *Microporous Mesoporous Mater.* **2016**, *221*, 228-237.
70. Thomas, A.; Goettmann, F.; Antonietti, M. *Chem. Mater.* **2008**, *20*, 738-755.
71. Cagnon, B.; Py, X.; Guillot, A.; Stoeckli, F. *Microporous Mesoporous Mater.* **2003**, *57*, 273-282.
72. Zhao, C.; Wang, W.; Yu, Z.; Zhang, H.; Wang, A.; Yang, Y. *J. Mater. Chem.* **2010**, *20*, 976-980.
73. He, X.; Zhao, N.; Qiu, J.; Xia, N.; Yu, M.; Yu, C.; Zhang, X.; Zheng, M.

J. Mater. Chem. A **2013**, *1*, 9440-9448.

74. Xu, S.; Luo, Y.; Tan, B. *Macromol. Rapid Commun.* **2013**, *34*, 471-484.
75. Abbott, L. J.; Colina, C. M. *Macromolecules* **2014**, *47*, 5409-5415.
76. He, Y.; Zhu, X.; Li, Y.; Peng, C.; Hu, J.; Liu, H. *Microporous Mesoporous Mater.* **2015**, *214*, 181-187.
77. Xu, Y.; Jin, S.; Xu, H.; Nagai, A.; Jiang, D. *Chem. Soc. Rev.* **2013**, *42*, 8012-8031.
78. Jiang, J. X.; Cooper, A. I. *Top. Curr. Chem.* **2010**, *293*, 1-33.
79. Chakraborty, S.; Colón, Y. J.; Snurr, R. Q.; Nguyen, S. T. *Chem. Sci.* **2015**, *6*, 384-389.
80. Yuan, S.; Dorney, B.; White, D.; Kirklin, S.; Zapol, P.; Yu, L.; Liu, D. J. *Chem. Commum.* **2010**, *46*, 4547-4549.
81. Du, R.; Zhang, N.; Xu, H.; Mao, N.; Duan, W.; Wang, J.; Zhao, Q.; Liu, Z.; Zhang, J. *Adv. Mater.* **2014**, *26*, 8053-8058.
82. Lim, Y.; Cha, M. C.; Chang, J. Y. *Sci. Rep.* **2015**, *5*, 15957.

Chapter II.

Preparation of Thermochromic Polymer Nanocomposite Films from Polymerizable Organogels of Oligothiophene-Based Organogelators

II-1. Introduction

Oligothiophenes have been extensively studied for applications in molecular electronics because of their π-conjugated structures and the ease of synthesis and derivatization. Thiophene rings are connected in various ways, in particular by metal catalyzed cross-coupling reactions. The electronic structures and properties of oligothiophenes can be controlled depending on the number of thiophene rings. In addition, their physicochemical properties are further modified by introducing the second functional groups on the rings.[1-10]

A number of derivatized oligothiophenes showed self-assembly properties, forming supramolecular structures such as liquid crystals and organogels. These materials usually displayed thermochromism. Thermochromism is a phenomenon of color change in materials with change of temperature, which is generally triggered by the morphological change [11-14] or chemical structural change.[11] A thermotropic liquid crystal is a typical example of a thermochromic material, which exhibits a different phase as temperature is changed. A variety of liquid crystalline oligothiophenes were reported; most of them consisting of a rigid oligthiophene core and flexible side groups.[16-19]

The organogel is thermally reversible viscoelastic materials comprised of an organic liquid and low concentrations of low molecular mass molecules.[20-22]

Only a few oligothiophene-based organogelators were reported.[23-28] Shinkai group prepared a series of organogelators by attaching two cholesterol groups to the quater-, quinque-, and sexithiophenes.[23] These oligothiophenes showed thermochromic behavior through the sol-gel phase transition, in which a blue shift occurred due to H-type aggregation by gelation. In another approach, they reported crown-appended quaterthiophene that showed an alkali metal cation responsive gel-to-sol transition with enhanced fluorescence emission in the gel state.[25] Pratihar and coworkers synthesized an amide group-functionalized quaterthiophene. In non-polar solvents, this quaterthiophene π-system formed fibril aggregates with an H-type molecular arrangement due to synergistic effect of hydrogen bonding and π-stacking.[26]

The thermochromic organogel has a potential use in external stimuli sensing, but its poor structural stability is an obstacle to their practical application. The gel-state polymerization is often carried out in an effort to achieve a physically stable material with an assembled structure of gelator molecules. The polymerization of an organogel formed in a monomeric solvent has been studied by Chang et al. The resulting polymer had a composite structure where the supramolecular nanofibers were uniformly distributed in the polymer matrix.[29-31]

Herein the synthesis of thermochromic polymer nanocomposite films from

oligothiophene organogelators and a monomeric solvent was investigated. The different thermal behaviors of the organogel nanofibers depending on their derivatizing group structures when embedded in the polymer were discussed.

II-2. Experimental

Materials. Methyl 3,4,5-trihydroxybenzote, ethylenediamine, (benzotriazol-1-yloxy) tripyrrolidinophosphonium hexafluorophosphate (PyBOP), dicyclohexylcarbodiimide (DCC), 4-(dimethylamino)pyridine (DMAP), 10-bromodecane, 5,5'-bis(trimethylstannyl)-2,2'-bithiophene, tetrakis(triphenylphosphine)palladium(0) were purchased from Aldrich. 10-Bromo-1-decene, 5-bromothiophene-2-carboxylic acid was purchased from TCI. Potassium carbonate, potassium hydroxide, magnesium sulfate, and diethyl ether were purchased from Daejung Chemical & Metals Co. N,N-Dimethylformamide (DMF), n-hexane, ethyl acetate, ethanol, tetrahydrofuran (THF), dichloromethane, and chloroform were purchased from Junsei. Silica gel (Merck 60) was used for column chromatography. THF was distilled with sodium before use. DMF was distilled with magnesium sulfate before use.

Preparation of 1a. Methyl 3,4,5-trihydroxybenzote (1.27 g, 6.9 mmol) and potassium carbonate (5.73 g, 41.4 mmol) were added in DMF (100 mL). After being stirred at 80 °C for 2 h, 10-bromo-1-decene (5 g, 22.8 mmol) was added dropwise. The reaction mixture was stirred at the same temperature for 12 h. After filtration and evaporation, the product was purified by column

chromatography (silica gel, n-hexane/ethyl acetate = 39:1). The transparent liquid was obtained. Yield: 80.5 %. ^{1}H NMR (300 MHz, $CDCl_3$, δ): 7.26 (s, 2H, Ar-H), 5.87-5.74 (m, 3H, C*H*=CH_2), 5.01-4.91 (m, 6H, =CH_2), 4.0 (t, overlap, 6H, OCH_2), 3.89 (s, 3H, OCH_3), 2.05-2.03 (m, 6H, OCH_2CH_2), 1.81-1,60 (m, 6H, =CHC*H_2*), 1.48-1.33 (m, 30H, alkyl chain proton).

Preparation of 2a. This compound was synthesized by the same procedure described for 1a from methyl 3,4,5-trihydroxybenzote (5.54 g, 30 mmol), potassium carbonate (25 g, 180 mmol), and 10-bromodecane (19.5ml, 99 mmol). The white solid was obtained. Yield: 90.5 %. ^{1}H NMR (300 MHz, $CDCl_3$, δ): 7.26 (s, 2H, Ar-H), 4.0 (t, overlap, 6H, OCH_2), 3.89 (s, 3H, OCH_3), 2.05-2.03 (m, 6H, OCH_2C*H_2*), 1.48-1.33 (m, 42H, alkyl chain proton), 0.93 (t, *J* = 6.5 Hz, 9H, CH_3).

Preparation of 1b. To a solution of 1a (2 g, 3.34 mmol) in ethanol (100 mL) was added potassium hydroxide (1.12 g, 20.0 mmol). After being refluxed for 3 h, the mixture was cooled to room temperature and poured to 1 L of distilled water. The pH of the aqueous solution was adjusted to 1 with 10 N hydrochloric acid. The product was isolated by filtration and used for the next reaction without further purification. The white solid was obtained. Yield:

82.5 %. ^{1}H NMR (300 MHz, $CDCl_3$, δ): 7.26 (s, 2H, Ar-H), 5.87-5.74 (m, 3H, C*H*=CH_2) 5.01-4.91 (m, 6H, =CH_2), 4.0 (t, overlap, 6H, OCH_2), 2.05-2.03 (m, 6H, OCH_2CH_2), 1.81-1,60 (m, 6H, =$CHCH_2$), 1.48-1.33 (m, 30H, alkyl chain proton).

Preparation of 2b. This compound was synthesized by the same procedure described for 1b from 2a (3.03 g, 5.00 mmol) and potassium hydroxide (1.68 g, 30.0 mmol). The white solid was obtained. Yield: 85.5 %. ^{1}H NMR (300 MHz, $CDCl_3$, δ): 7.26 (s, 2H, Ar-H), 4.0 (t, overlap, 6H, OCH_2), 2.05-2.03 (m, 6H, OCH_2CH_2), 1.48-1.33 (m, 42H, alkyl chain proton), 0.93 (t, *J* = 6.5 Hz, 9H, CH_3).

Preparation of 1c. To a solution of 1b (2 g, 3.42 mmol) in anhydrous THF (100 mL) was added ethylene diamine (2.28 mL, 34.2 mmol) with PyBOP (2.13 g, 4.10 mmol). After being stirred at 80 °C for 12 h, the mixture was cooled to room temperature. The mixture was extracted with chloroform and the organic layer was washed with brine and dried over anhydrous $MgSO_4$. After filtration and evaporation, the product was further purified by column chromatography (silica gel, dichloromethane/methanol = 19:1). The pale white powder was obtained. Yield: 55.5 %. ^{1}H NMR (300 MHz, $CDCl_3$, δ): 7.26 (s, 2H, Ar-H),

7.0 (br s, 1H, CONH), 5.87-5.74 (m, 3H, C*H*=CH_2), 5.01-4.91 (m, 6H, =CH_2), 4.0 (t, overlap, 6H, OCH_2), 3.52 (t, *J* = 5.6 Hz, 2H, CONHC*H_2*), 2.97 (t, *J* = 5.6 Hz, 2H, NH_2C*H_2*), 2.05-2.03 (m, 6H, OCH_2CH_2), 1.81-1,60 (m, 6H, =$CHCH_2$), 1.48-1.33 (m, 30H, alkyl chain proton).

Preparation of 2c. This compound was synthesized by the same procedure described for 1c from 1b (2 g, 3.38 mmol), ethylenediamine (2.26 mL, 33.8 mmol), and PyBOP (2.11 g, 4.06 mmol). The pale white powder was obtained. Yield: 53.2 %. ^{1}H NMR (300 MHz, $CDCl_3$, δ): 7.26 (s, 2H, Ar-H), 7.0 (br s, 1H, CONH), 4.0 (t, overlap, 6H, OCH_2), 3.52 (t, *J* = 5.6 Hz, 2H, CONHC*H_2*), 2.97 (t, *J* = 5.6 Hz, 2H, NH_2C*H_2*), 2.05-2.03 (m, 6H, OCH_2C*H_2*), 1.48-1.33 (m, 42H, alkyl chain proton), 0.93 (t, *J* = 6.5 Hz, 9H, CH_3).

Preparation of 1d. To a solution of 1c (1 g, 1.6 mmol) in dichloromethane (100 mL) were added 5-bromothiophene-2-carboxylic acid (0.39 g, 1.9 mmol), DMAP (10 mg, 0.08 mmol), and DCC (1.95 g, 9.5 mmol). After being stirred at room temperature for 12 h, the mixture was filtrated. After evaporation, the product was further purified by column chromatography (silica gel, dichloromethane/methanol = 15 : 1) The waxy white solid was obtained. Yield : 53.0 % ^{1}H NMR (300 MHz, $CDCl_3$, δ): 7.29 (d, *J* = 3.9 Hz, 1H, thiophene-H),

7.08 (br s, 1H, Ar-CONH), 7.0 (d, *J* = 3.9 Hz, 1H, thiophene-H), 6.99 (s, 2H, Ar-H), 6.93 (br s, 1H, thiophene-CONH), 5.87-5.74 (m, 3H, C*H*=CH_2), 5.01-4.91 (m, 6H, =CH_2), 4.0 (t, overlap, 6H, OCH_2), 3.63 (t, *J* = 2.1 Hz, 4H, CH_2), 2.05-2.03 (m, 6H, OCH_2C*H_2*), 1.81-1,60 (m, 6H, =CHC*H_2*), 1.48-1.33 (m, 30H, alkyl chain proton).

Preparation of 2d. This compound was synthesized by the same procedure described for 1d from 2c (1 g, 1.6 mmol), 5-bromothiophene-2-carboxlic acid (0.39 g, 1.9 mmol), DMAP (10 mg, 0.08 mmol), and DCC (1.95 g, 9.5 mmol). The waxy white solid was obtained. Yield: 55.0 %. ^{1}H NMR (300 MHz, $CDCl_3$, δ): 7.29 (d, *J* = 3.9 Hz, 1H, thiophene-H), 7.08 (br s, 1H, Ar-CONH), 7.0 (d, *J* = 3.9 Hz, 1H, thiophene-H), 6.99 (s, 2H, Ar-H), 6.93 (br s, 1H, thiophene-CONH), 4.0 (t, overlap, 6H, OCH_2), 3.63 (t, *J* = 2.1 Hz, 4H, CH_2), 2.05-2.03 (m, 6H, OCH_2C*H_2*), 1.48-1.33 (m, 42H, alkyl chain proton), 0.93 (t, *J* = 6.5 Hz, 9H, CH_3).

Preparation of 1. To a solution of 1d (1 g, 1.2 mmol) in DMF (25 mL) were added 5,5'-bis(trimethylstannyl)-2,2'-bithiophene (0.36 mL, 0.6 mmol) and tetrakis(triphenylphosphine)palladium(0) (70 mg, 0.06 mmol). After being stirred at 80 °C for 12 h, the mixture was cooled to room temperature and then

filtered through a silica plug. The product was recrystallized from chloroform/methanol. The dark yellow solid was obtained. Yield: 52.1 % ^{1}H NMR (300 MHz, $CDCl_3$, δ): 7.45 (m, 4H, thiophene-H) 7.24 (br s, 2H, Ar-CONH), 7.05 (s, 4H, Ar-H), 6.95 (m, thiophene-H, 4H), 6.82 (br s, 2H, thiophene-CONH), 5.87-5.74 (m, 6H, CH=CH_2), 5.01-4.91 (m, 12H, =CH_2), 4.0 (t, overlap, 12H, OCH_2), 3.63 (t, overlap, 8H, CH_2), 2.05-2.03 (m, 12H, OCH_2CH_2), 1.81-1,60 (m, 12H, =CHCH_2), 1.48-1.33 (m, 60H, alkyl chain proton); ^{13}C NMR (125 MHz, $CDCl_3$, δ): 169.0, 163.4, 153.3, 142.0, 139.4, 137.1, 137.0, 135.7, 129.2, 129.0, 125.9, 124.9, 124.1, 114.4, 105.7, 77.5, 77.2, 77.0, 73.7, 69.4, 41.4, 34.0, 30.5, 30.0, 29.9, 29.8, 29.7, 29.6, 29.4, 29.3, 29.2, 26.3, 26.2; IR (KBr, cm^{-1}): 3295, 3073, 2926, 2855, 1626, 1581, 1539, 1498, 1464, 1453, 1429, 1388, 1339, 1300, 1231, 1120, 1067, 996, 966, 909, 841, 790, 744, 723, 670; Anal. Calcd. for $C_{96}H_{138}N_4O_{10}S_4$: C 70.46, H 8.50, N 3.42, S 7.84; Found: C 70.3, H 8.40, N 3.42, S 8.06.

Preparation of 2. This compound was synthesized by the same procedure described for 1 from 2d (1 g, 1.2 mmol), 5,5'-bis(trimethylstannyl)-2,2'-bithiophene (0.36 mL, 0.6 mmol), and tetrakis(triphenylphosphine) palladium(0) (70 mg, 0.06 mmol). The dark yellow solid was obtained. Yield: 53.0 % ^{1}H NMR (300 MHz, $CDCl_3$, δ): 7.45 (m, 4H, thiophene-H), 7.24 (br s,

2H, Ar-CONH), 7.07 (s, 4H, Ar-H), 6.92 (m, 4H, thiophene-H), 6.82 (br s, 2H, thiophene-CONH), 4.0 (t, overlap, 12H, OCH_2), 3.63 (t, overlap, 8H, CH_2), 2.05-2.03 (m, 12H, OCH_2CH_2), 1.48-1.33 (m, 84H, alkyl chain proton), 0.93 (t, overlap, 18H, CH_3); ^{13}C NMR (125 MHz, $CDCl_3$, δ): 169.1, 163.4, 153.3, 141.9, 139.4, 137.2, 129.2, 129.0, 125.9, 124.9, 124.1, 105.7, 77.5, 77.2, 77.0, 69.5, 32.2, 30.0, 29.9, 29.7, 29.6, 26.4, 22.3, 14.3; IR (KBr, cm^{-1}): 3286, 3083, 2924, 2854, 1625, 1583, 1538, 1496, 1466, 1452, 1428, 1387, 1339, 1306, 1230, 1118, 1070, 995, 921, 872, 842, 790, 745, 721, 666; Anal. Calcd. for $C_{96}H_{150}N_4O_{10}S_4$: C 69.94, H 9.17, N 3.40, S 7.78; Found: C 69.93, H 9.09, N 3.31, S 7.88.

Preparation of Polymer Nanocomposite Films. The organogel of organogelator 1 or 2 in MMA was placed between two quartz plates and polymerized under UV irradiation (a high-pressure mercury arc lamp 3 mW cm^{-2}) in the presence of photoinitiator (2,2-dimethoxy-2-phenylacetophenone, 1 wt%) and EGDMA (4.5 wt%) for 24 h at room temperature. After washing with THF, the film was dried in vacuo.

Instrumental Characterization. ^1H and ^{13}C NMR spectra were recorded by a Bruker Avance 300 (300 MHz) and Bruker Avance 500 (125 MHz)

spectrometer, respectively. Fourier transform infrared (FT-IR) spectra were obtained with a Perkin–Elmer Spectrum GX I instrument using KBr pellets. DSC measurements were made on a TA modulated DSC Q10 with a scanning rate of 10 ^{o}C min^{-1} under nitrogen. Elemental analysis was performed by a CE Instrument Flash 1112 elemental analyzer. UV-Vis spectra were recorded by a SCINCO S-3150 instrument. Photoluminescence spectra were obtained with a Shimadzu RF-5301 PC spectrofluorometer. FE-SEM images were obtained by using a JEOL JSM-6700F microscope. TEM images were obtained by using a JEOL JEM-2010 microscope at 200 keV. Raman spectra were recorded by Raman plus confocal laser Raman microscope (Nanophoton) with a 785 nm.

II-3. Results and Discussion

II-3-1. Synthesis and Characterization

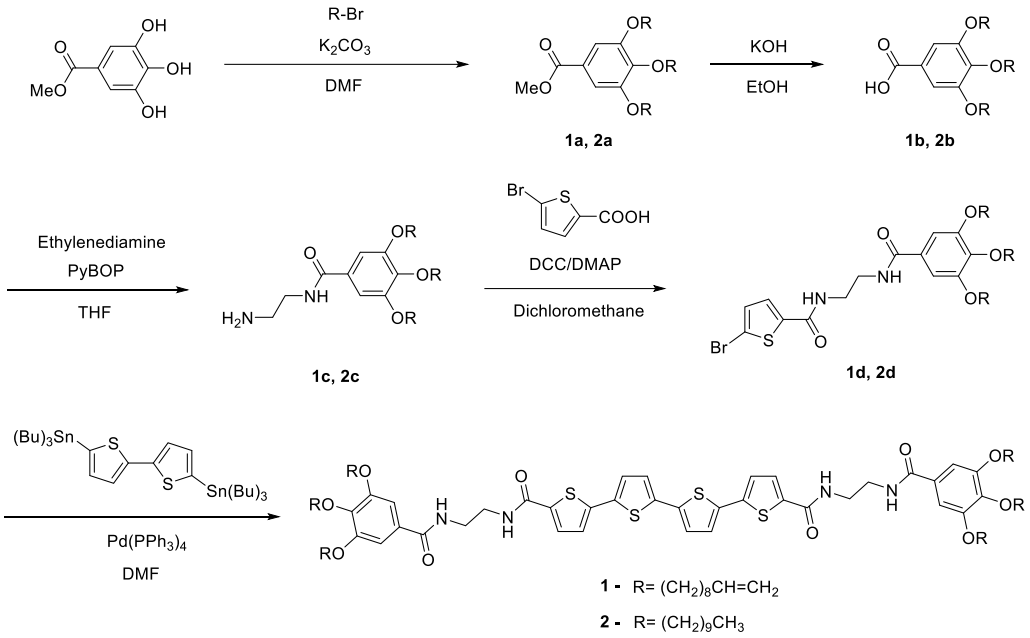

Scheme II-1. Synthesis of organogelators **1** and **2**.

Organogelator **1** having polymerizable vinyl groups was synthesized according to Scheme 1. Three long alkyl chains were introduced to methyl 3,4,5-trihydroxybenzoate by substitution reaction with 10-bromo-1-decene. After saponification, ethylene diamine was reacted with the benzoic acid to form compound **1c**. Compound **1d** having a bromothiophene unit and two

amide bonds were synthesized by reaction of **1c** with 5-bromothiophene-2-carboxylic acid. Organogelator **1** was obtained by the Pd-catalyzed Stille-coupling reaction of **1d** and bis(trimethylstannyl)-2,2'-bithiophene. Organogelator **2** with no polymerizable groups was prepared in the same manner described for the preparation of **1** except that 1-bromodecane was used as a long alkyl chain instead of 10-bromo-1-decene. Both organogelators had four amide bonds and a quaterthiophene unit, which could produce strong intermolecular interactions such as hydrogen bonding and π-π interaction.

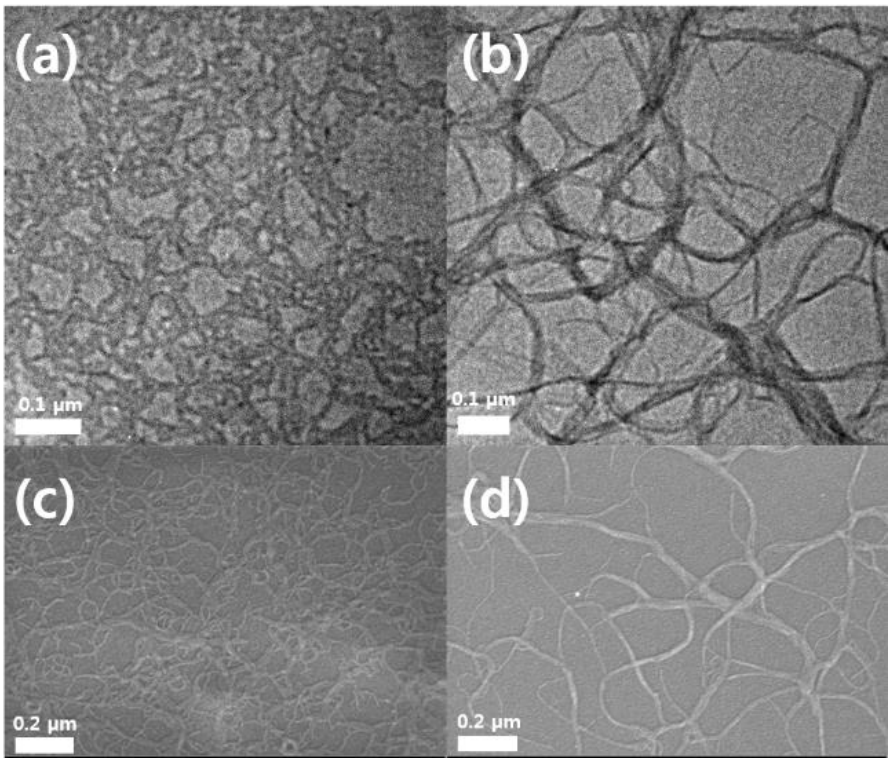

Figure II-1. TEM and SEM images of dried gels obtained from **1** (a, c) and **2** (b, d) in MMA.

Organogelators **1** and **2** showed an ability to gelate aromatic organic solvents such as toluene, xylene, and benzene. They also formed stable organogels in monomeric solvents including methyl methacrylate (MMA), hexyl methacrylate, and ethyleneglycol dimethacrylate (EGDMA) with low critical gelation concentrations. The gelation properties of both compounds are summarized in Table II-1. Organogels formed in MMA would be

photopolymerizable to form a transparent film. The organogels were prepared by cooling the solutions of **1** and **2** (1 wt%) in MMA at 90 ^{o}C down to room temperature. Figure 1 shows TEM and SEM images of the dried gels obtained from the organogels of **1** and **2** formed in MMA. Organogelators **1** and **2** formed fibrous network structures with fiber diameters of about 1-30 and 2-50 nm, respectively.

Table II-1. Gelation Properties of Organogelators **1** and **2**.

Solvent	**1**	**2**
Toluene	G (1.0)	G (0.2)
Xylene	G (1.0)	G (0.3)
Dichloromethane	G (0.5)	G (0.4)
Chloroform	S	S
THF	S	0.4
MMA	G (0.1)	G (0.1)
Hexyl Methacrylate	G (0.1)	G (0.1)
EGDMA	G (0.1)	G (0.1)

G = gel at room temperature, S = Soluble; Critical gelation concentrations are given in parentheses (wt%).

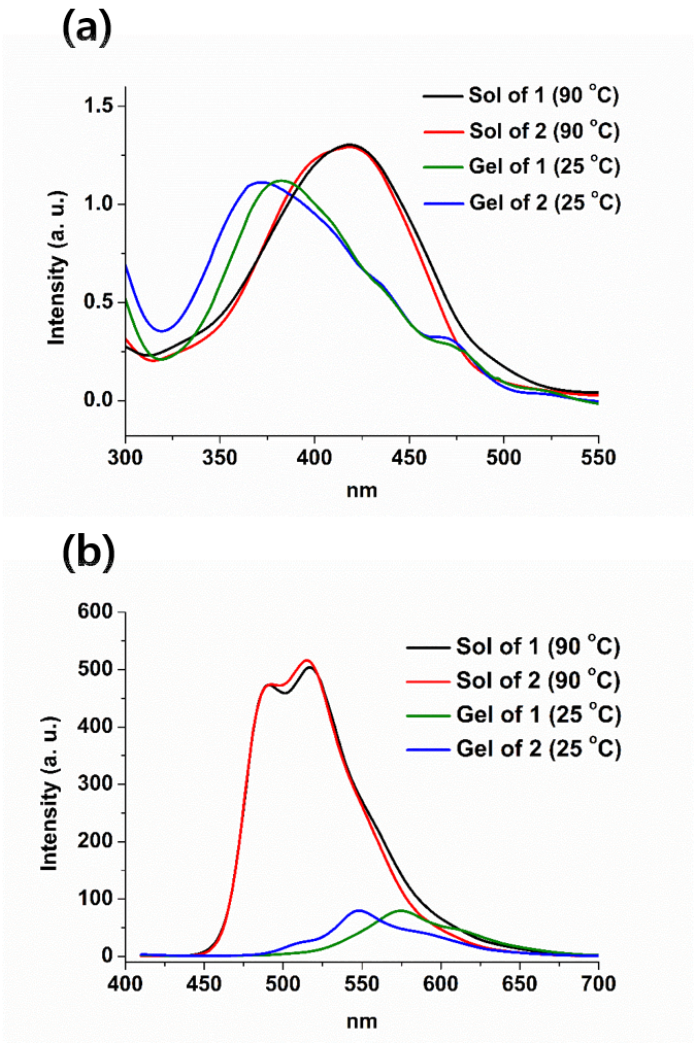

Figure II-2. (a) Absorption and (b) emission spectra of **1** and **2** (0.1 wt%) in MMA in sol and gel states (λ_{ex} = 380 nm).

Absorption and emission spectra of **1** and **2** in MMA are shown in Figure II-2. In the sol state, **1** and **2** showed the maximum absorption peak at 423 nm.

After gelation, they were blue-shifted to 382 and 370 nm, respectively, and they showed absorption shoulders, which were attributed to a self-aggregation of core oligothiophene units in gelators and conformational change (Figure II-2a).[26,27,31] In the case of emission spectra obtained by excitation at 380 nm, the maximum peaks were shown at 518 and 515 nm for **1** and **2**, respectively in the sol state. In the gel state, the maximum peaks of **1** and **2** were bathochromic shifted to 575 and 550 nm, respectively, probably due to the aggregation. The Raman spectra of the dried gels of **1** and **2** showed the strong peak at 1461 cm^{-1} corresponding to the C=C symmetric ring stretch, which was known to be very sensitive to the planarity of the thiophene backbone (Figure II-3).[23,32-34]

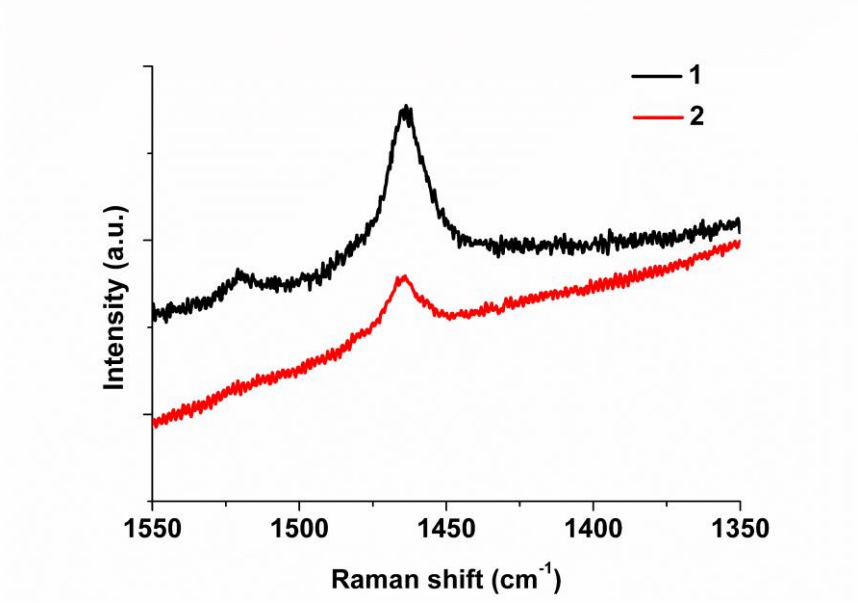

Figure II-3. Raman spectra of **1** and **2** in dried gel state.

Organogelators **1** and **2** had 10-decenyl and *n*-decanyl tails, respectively. The different terminal groups of **1** and **2** influenced their assembled structures. Results of the DSC study also suggested the different assembled structures of **1** and **2** (Figure II-4). The dried gel of **1** showed a melting transition at 110 ^{o}C on heating, and crystallization at 97 ^{o}C on cooling. The dried gel of **2** displayed higher thermal stability than **1** with a melting transition at 124 ^{o}C on heating and recrystallization at 116 ^{o}C on cooling, indicating the better packing ability of **2**.

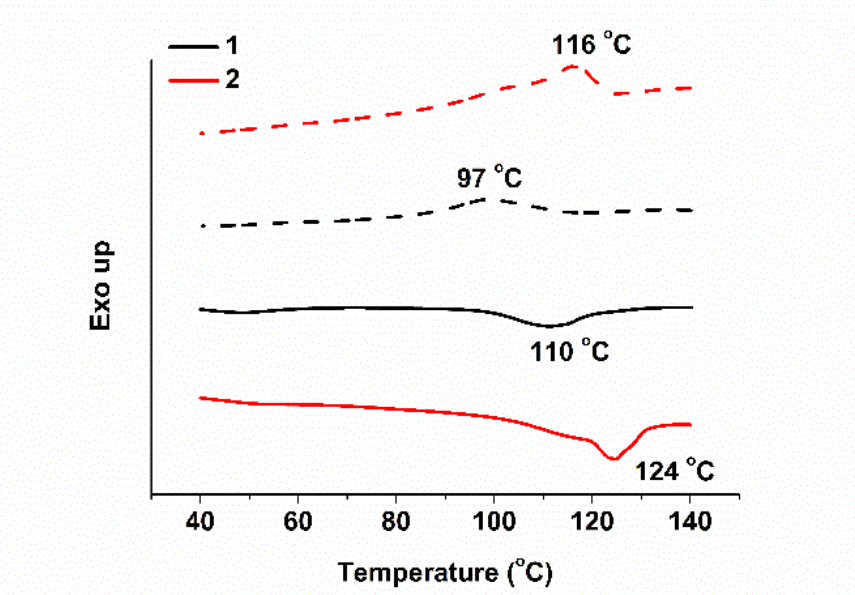

Figure II-4. DSC thermograms of **1** and **2**.

II-3-2. Optical Properties of Organogel

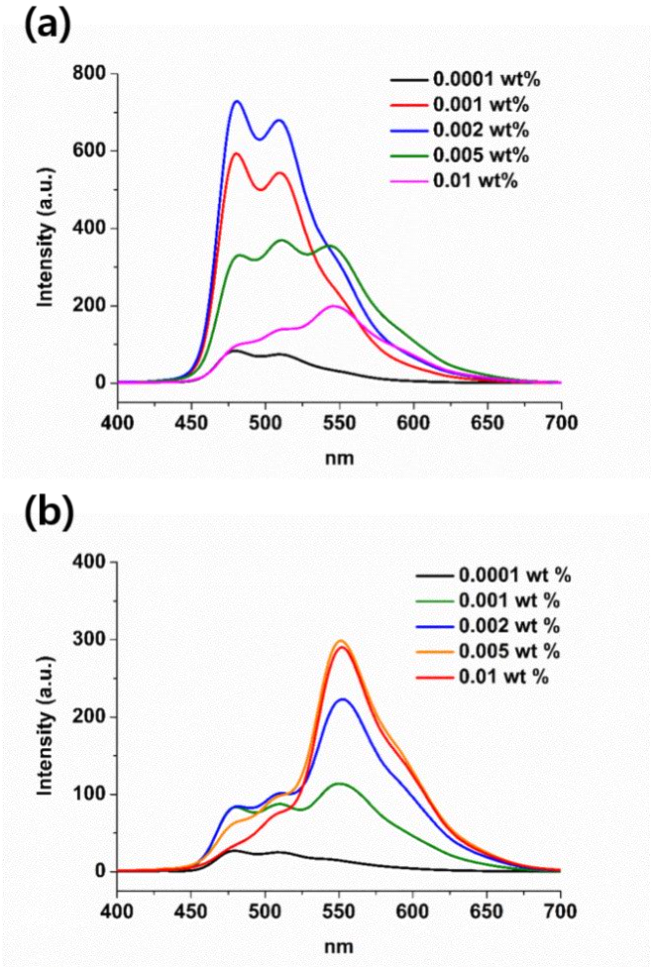

Figure II-5. Emission spectra of (a) **1** and (b) **2** in MMA (λ_{ex} = 380 nm).

Organogelators **1** and **2** showed different emission behaviors with respect to a concentration (Figure II-5). As the concentration of **1** increased from 0.0001

to 0.002 wt%, the overall emission intensity increased. However, at concentrations higher than 0.005 wt%, the intensity of the peaks at 480 and 515 nm, from individual molecules in the sol state, decreased and a new peak developed at 550 nm from its aggregation state. As mentioned above, **2** has a greater tendency to aggregate than **1** so that the monomeric emission of **2** was more quenched than that of **1** at the same concentration. The peak of the aggregate appeared from the concentration of 0.001 wt%. The emission color change was observed by the naked eye.

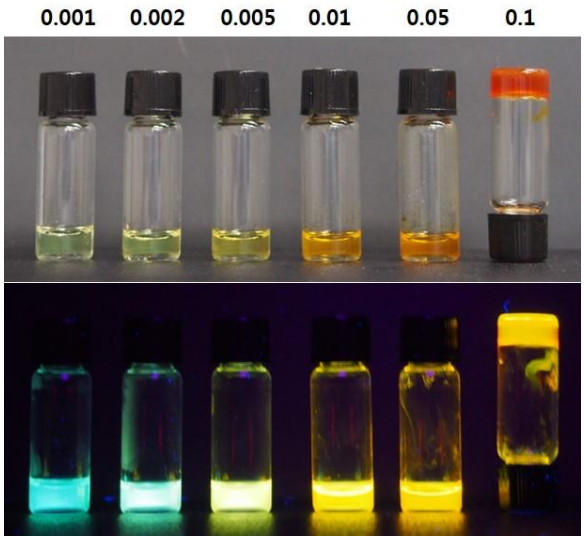

Figure II-6. Photographs of **1** in MMA at various concentrations (wt%) taken in daylight (up) and under 365 nm irradiation (down).

Figure II-6 shows the photographs of **1** in MMA taken in daylight (up) and under 365 nm irradiation (down) at concentrations ranging from 0.001 to 0.1 wt%. As the concentration was increased, the emission color changed from cyan blue to orange. The calculated CIE color coordinates were x = 0.18, y = 0.45 at 0.001 wt% and x = 0.49, y = 0.48 at 0.1 wt% (Figure II-7).

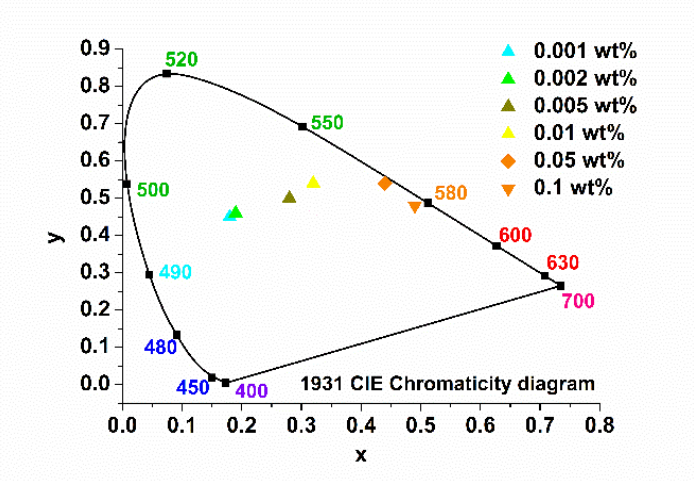

Figure II-7. CIE color coordinates of **1** in MMA at various concentrations.

The fluorescent films containing 0.001 wt% and 0.1 wt% of **1** were prepared from the solution and the organogel of **1** in MMA, respectively, by photopolymerization in the presence of a photoinitiator and a cross-linker (EGDMA, 4.5 wt%) (Figure II-8a). The films showed similar emission patterns to those observed before polymerization (Figure II-8b). Their CIE coordinates

were almost same as those of the corresponding solution and organogel. The CIE coordinates of the films containing 0.001 and 0.1 wt% of **1** were x = 0.2, y = 0.45 and x = 0.48, y = 0.49, respectively. The fluorescent gel fibers embedded in the film could be visualized by confocal laser scanning microscopy (Figure II-9). The film was excited at 380 nm and the emission of 580 nm was collected. The wholly dispersed fibrous structure appeared as shown although individual fibers were not discernible due to the resolution limit of the instrument.

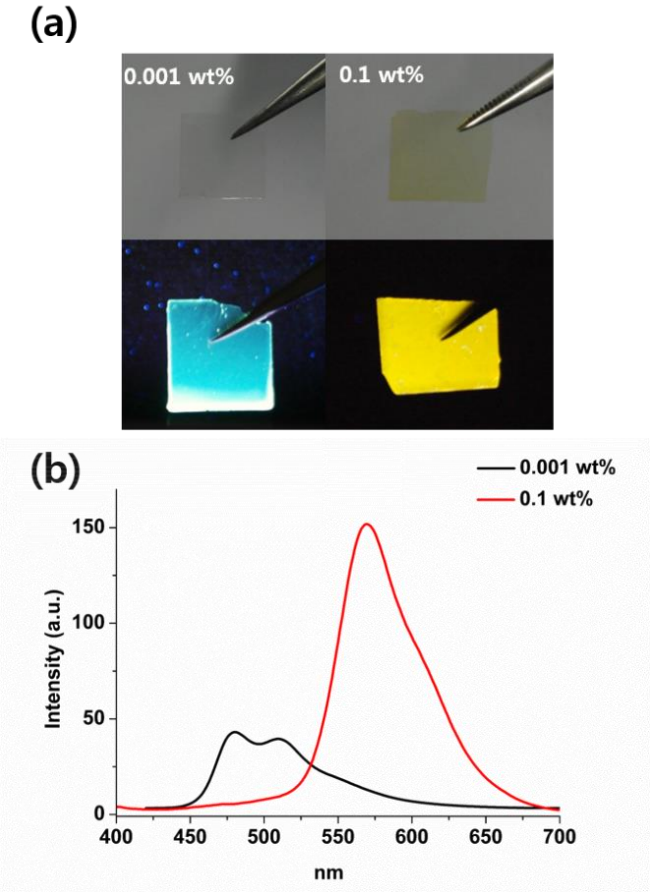

Figure II-8. (a) Photographs of the PMMA – **1** (0.001 wt% and 0.1 wt%) films taken in daylight (up) and under 365 nm irradiation (down). (b) Emission spectra of the films excited at 380 nm.

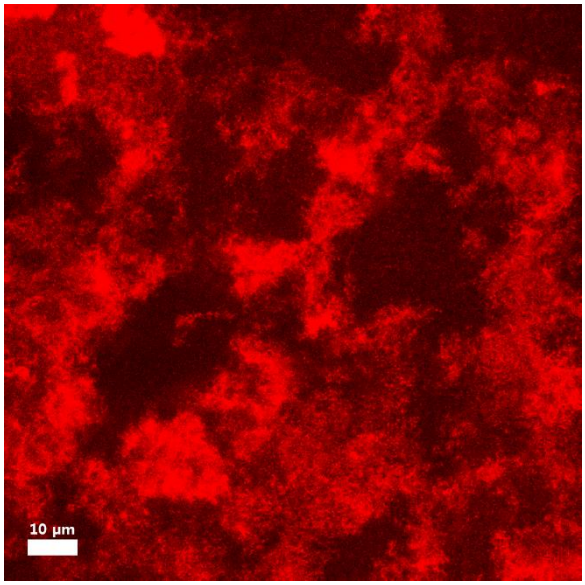

Figure II-9. CLSM image of the PMMA – **1** (0.1 wt%) film excited at 380 nm.

II-3-3. Thermochromic Properties of Polymer Nanocomposites

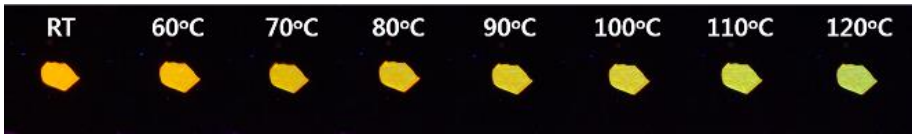

Figure II-10. Photographs of the PMMA - **1** (0.5 wt%) film taken under 365 nm irradiation at the temperature ranging from room temperature to 120 ^{o}C

The reversible thermochromism of the PMMA–**1** (0.5 wt%) polymer composite film was investigated. The temperature dependent emission color change was observed by the naked eyes under 365 nm irradiation (Figure II-10).

When the temperature increased up to 120 ^{o}C from room temperature, the emission was gradually changed to bright green from orange. The emission color of the film returned to its initial orange when it cooled to room temperature. The emission spectrum and the CIE color coordinates also recovered their original states (Figure II-11). The film didn't show a monomeric emission of **1** even at 180 ^{o}C, indicating limited mobility of the gelator molecules in the film. Otherwise, the PMMA film prepared from the organogel of **2** (0.5 wt%) didn't show a reversible thermochromic property. When the film was heated up to 130 ^{o}C over the melting temperature of **2**, the orange emission under 365 nm irradiation was changed to pale green. When the film was cooled to room temperature, the emission color turned yellow green, not the initial orange color (Figure II-12). The thermochromism properties of the PMMA films containg **1** and **2** coressponds to CIE coordinates were shown in Figure II-13.

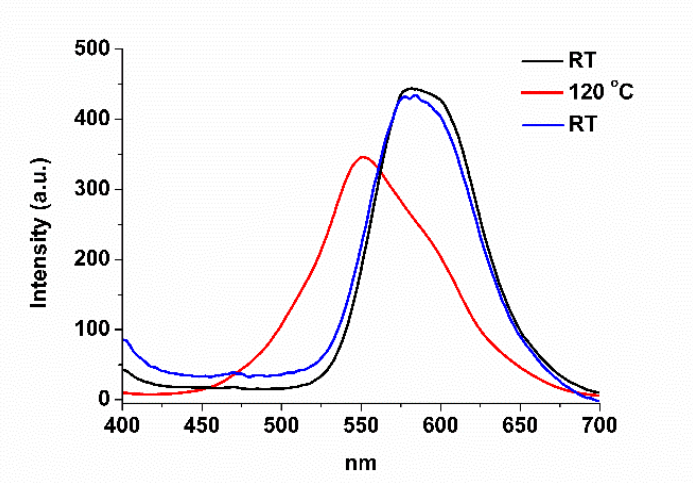

Figure II-11. Emission spectra of the PMMA – **1** (0.5 wt%) film measured at room temperature, after heating to 120 °C, and after cooling to room temperature (λ_{ex} = 380 nm).

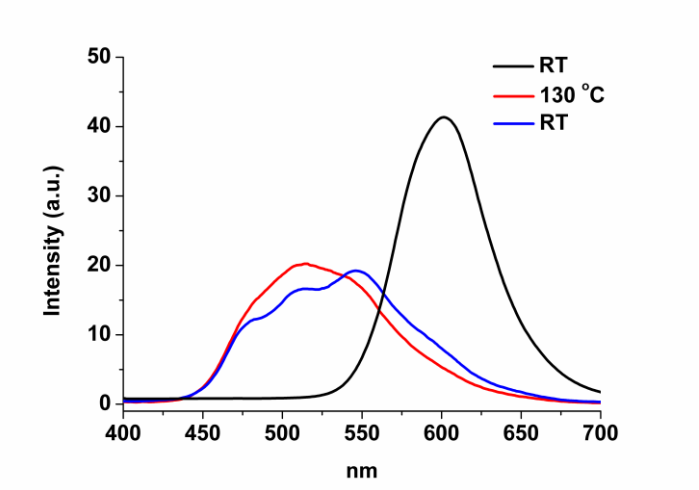

Figure II-12. Emission spectra of the PMMA – **2** (0.5 wt%) film measured at room temperature, after heating to 130 °C, and after cooling to room temperature (λ_{ex} = 380 nm).

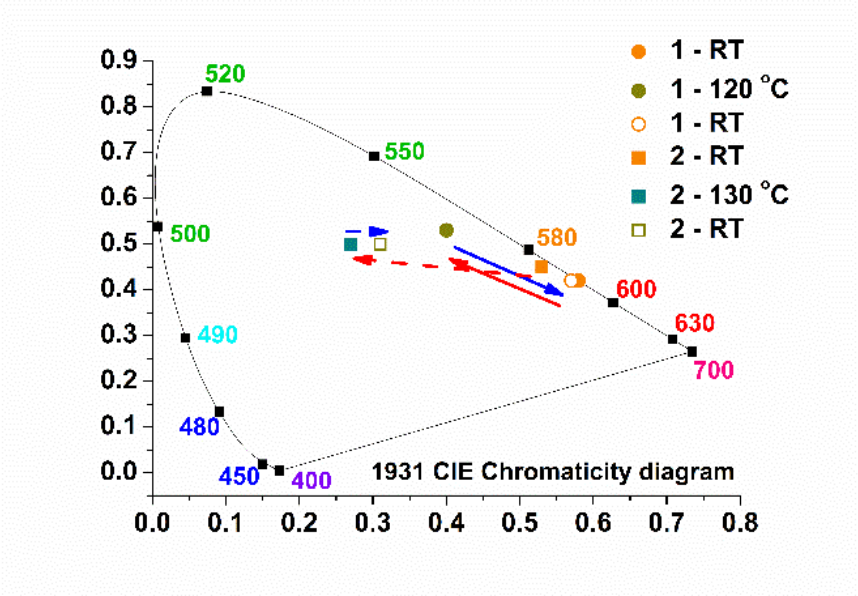

Figure II-13. CIE color coordinates of the PMMA-**1** and PMMA-**2** at different temperatures.

Organogelator **1** had six vinyl groups which participated in the polymerization reaction to form a cross-linked structure. It was assumed that they were loosely connected to each other and to the polymer matrix. The reversible emission color change of the film containing **1** was derived from morphological change of the polymerized gelator molecules.[35-38] A fiber structure formed by self-assembly of organogelator **2** in MMA was maintained in the polymer matrix, but it was readily disrupted by heating and no more reassembled, since **2** had no terminal vinyl groups. The solubility test results also corroborated the proposed polymer nanocomposite structures. When the

emission spectra of the PMMA films were measured after soaking in THF, the film of **1** showed the same emission pattern, while the emission intensity of the film of **2** gradually decreased with increasing soaking time (Figure II-14). Since THF was a good solvent for both gelators, it could dissolve out the gelator molecules.

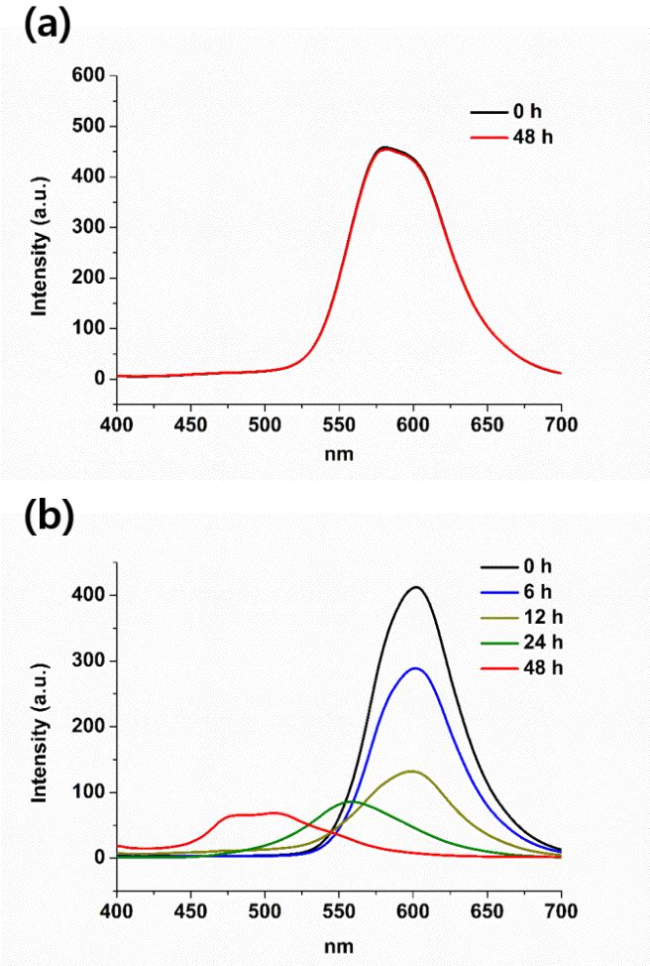

Figure II-14. Emission spectra of (a) the PMMA-**1** and (b) PMMA-**2** immersed in THF for 48 h (λ_{ex} = 380 nm).

II-4. Conclusions

The quaterthiophene-based organogelators showed an ability to gelate several acrylate monomers. The organogels formed in MMA displayed thermochromc behaviors caused by the sol-gel transition. Especially, the emission color of the organogel of **1** containing terminal vinyl groups was tunable from cyan blue to orange by changing the concentration or temperature. The composite film was prepared by the photopolymerization of the organogel of **1** formed in MMA. The terminal vinyl groups of **1** participated in the polymerization to produce polymer fibers covalently embedded in the PMMA matrix. The composite film also showed reversible thermochromism. It was presumed that the thermally reversible conformational change of quarterthiophene units in the polymer fibers was responsible for the thermochromism.

II-5. References

1. Mishira, A.; Ma, C. Q.; Bäuerle, P. *Chem. Rev.* **2009**, *109*, 1141-1276.
2. Amir, E.; Sivanandan, K.; Cochran, J. E.; Cowart, J. J.; Ku, S. –Y.; Seo, J. H.; Chabinyc, M. L.; Hawker, C. J. *J. Polym. Sci., Part A: Polym. Chem.* **2011**, *49*, 1933-1941.
3. Takagi, K.; Kawagita, E.; Kouchi, R. *J. Polym. Sci., Part A: Polym. Chem.* **2014**, *52*, 2166-2174.
4. Nguyen, T. L.; Song, S.; Ko, S. –J.; Choi, H.; Jeong, J. –E.; Kim, T.; Hwang, S.; Kim, J. Y.; Woo, H. Y. *J. Polym. Sci., Part A: Polym. Chem.* **2015**, *53*, 854-862.
5. Liu, Y. –R.; Chan, L. –H.; Tang, H. –Y. *J. Polym. Sci., Part A: Polym. Chem.* **2015**, *53*, 2878-2889.
6. Sun, Y.; Zhang, C.; Dai, B.; Lin, B.; Yang, H.; Zhang, X.; Guo, L.; Liu, Y. *J. Polym. Sci., Part A: Polym. Chem.* **2015**, *53*, 1915-1926.
7. Kim, H. N.; Park, S. M.; Shin, S. C.; Kim, Y. -H. *Macromol. Res.* **2014**, *22*, 1012-1017.
8. Fang, K.; Huang, Y.; Chang, G.; Yang, J.; Shen, Y.; Ye, X. *Macromol. Res.* **2015**, *23*, 545-551.
9. Basavaraja, C.; Kim, J. K.; Huh, D. S. *Macromol. Res.* **2015**, *23*, 649-

657.

10. Basavaraja, C.; Jo, E. J.; Huh, D. S. *Macromole. Res.* **2016**, *24*, 267-275.
11. Crenshaw, B. R.; Weder, C. *Chem. Mater.* **2003**, *15*, 4717-4724.
12. Zhao, Z.; Lamb, J. W. Y.; Tang, B. Z. *Soft Matter* **2013**, *9*, 4564-4579.
13. An, B. –K.; Gierschner, J.; Park, S. Y. *Acc. Chem. Res.* **2012**, *45*, 544-554.
14. Liu, C.; Lu, Y.; He, S.; Wang, Q.; Zhao, L.; Zeng, X. *J. Mater. Chem. C* **2013**, *1*, 4770-4778.
15. Bao, S.; Fei, B.; Li, J.; Yao, X.; Lu, X.; Xin, J. H. *Dyes Pigments* **2013**, *99*, 99-104.
16. Prehm, M.; Götz, G.; Bäuerle, P.; Liu, F.; Zeng, X.; Ungar, G.; Tschierske, C. *Angew. Chem. Int. Ed.* **2007**, *46*, 7856-7859.
17. Li, W. S.; Yamamoto, Y.; Fukushima, T.; Saeki, A.; Seki, S.; Tagawa, S.; Masunaga, H.; Sasaki, S.; Takata, M.; Aida, T. *J. Am. Chem. Soc.* **2008**, *130*, 8886-8887.
18. Yasuda, T.; Ooi, H.; Morita, J.; Akama, Y.; Minoura, K.; Funahashi, M.; Shimomura, T.; Kato, T. *Adv. Funct. Mater.* **2009**, *19*, 411-419.
19. Hu, N.; Shao, R.; Shen, Y.; Chen, D.; Clark, N. A.; Walba, D. M. *Adv. Mater.* **2014**, *26*, 2066-2071.
20. Terech, P.; Weiss, R. G. *Chem. Rev.* **1997**, *97*, 3133-3159.

21. Abdallah, D. J.; Weiss, R. G. *Adv. Mater.* **2000**, *12*, 1237-1247.

22. Sangeetha, N. M.; Maitra, U. *Chem. Soc. Rev.* **2005**, *34*, 821-836.

23. Kawano, S. –I.; Fujita, N.; Shinkai, S. *Chem. Eur. J.* **2005**, *11*, 4735–4742.

24. Melucci, M.; Barbarella, G.; Gazzano, M.; Cavallini, M.; Biscarini, F.; Bongini, A.; Piccinelli, F.; Monari, M.; Bandini, M.; Umani-Ronchi, A.; Biscarini, P. *Chem. Eur. J.* **2006**, *12*, 7304-7312.

25. Sobczuk, A. A.; Tamaru, S. –I.; Shinkai, S. *Chem. Commun.* **2011**, *47*, 3093-3095.

26. Pratihar, P.; Ghosh, S.; Stepanenko, V.; Patwardhan, S.; Grozema, F. C.; Siebbeles, L. D. A.; Würthner, F. *Beilstein J. Org. chem.* **2010**, *6*, 1070-1078.

27. Stone, D. A.; Tayi, A. S.; Goldberger, J. E.; Palmer, L. C.; Stupp, S. I. *Chem. Commun.* **2011**, *47*, 5702-5704.

28. Sobczuk, A. A.; Tsuchiya, Y.; Shiraki, T.; Tamaru, S. –I.; Shinkai, S. *Chem. Eur. J.* **2012**, *18*, 2832-2838.

29. Kang, S. H.; Jung, B. M.; Chang, J. Y. *Adv. Mater.* **2007**, *19*, 2780-2784.

30. Kim, W. J.; Jung, B. M.; Kang, S. H.; Chang, J. Y. *Soft Matter* **2011**, *7*, 4160-4162.

31. Kim, H.; Chang, J. Y. *Langmuir* **2014**, *30*, 13673-13679.

32. Benincori, T.; Bongiovanni, G.; Botta, C.; Cerullo, G.; Lanzani, G.; Mura, A.; Rossi, L.; Sannicolò, F.; Tubino, R. *Phys. Rev. B* **1998**, *58*, 9082-9086.

33. Tsoi, W. C.; James, D. T.; Kim. J. S.; Nicholson, P. G.; Murphy, C. E.; Bradley, D. D. C.; Nelson, J.; Kim, J. –S. *J. Am. Chem. Soc.* **2011**, *133*, 9834-9843.

34. Kim, J. S.; Wood, S.; Shoaee, S.; Spencer, S. J.; Casatro, F. A.; Tsoi, W. C.; Murphy, C. E.; Sim, M.; Cho, K.; Durrant, J. R.; Kim, J. –S. *J. Mater. Chem. C* **2015**, *3*, 9224-9232.

35. Thienpont, H.; Rikken, G. L. J. A.; Meijer, E. W.; ten Hoeve, W.; Wynberg, H. *Phys. Rev. Lett.* **1990**, *65*, 2141-2144.

36. DiCésare, N.; Belletête, M.; Marrano, C.; Leclerc, M.; Durocher, G.; *J. Phys. Chem. A* **1988**, *102*, 5142-5149.

37. Lukeš, V.; Breza, M.; Pálszegi, T.; Laurinc, V.; Vrábel, I. *Macromol. Theory Simul.* **2001**, *10*, 592-599.

38. Elmacı, N.; Yurtsever, E. *J. Phys. Chem. A* **2002**, *106*, 11981-11986.

Chapter III.

Monolithic Catalysts Based on Acid- and Base-Functionalized Hierarchically Porous Polymers for Continuous Sequential Reactions

III-1. Introduction

The synthetic methods to perform sequential reactions continuously using different catalytic systems provide environmental and economical advantages by reducing work-up and purification process.[1] For continuous sequential catalytic reactions, the catalytic active sites for one reaction should be isolated from those of the other to avoid cross-poisoning between the catalysts. Several supporting materials have been used for the catalytic site-isolation, including highly sterically demanding polymers,[2] silica,[3-6] metal-organic frameworks (MOFs).[7] Recently porous organic polymers (POPs)[8-11] have also received much attention as supporting materials for the catalytic site-isolation, because of their large surface area and physicochemical stability. In addition, it is easy to control the functionality of POPs by taking advantages of diversity of building blocks. Corma and Sánchez et al nicely demonstrated acid and base functionalized porous organic polymers, specifically porous aromatic frameworks(PAFs) series.[8,9] Briefly, they prepared PAFs by Suzuki-Miyaura coupling reaction with tetraiodo monomers such as 2,2',7,7'-tetraiodo-9,9'-spiro-bisfluorene or tetrakis-(4-iodophenyl)methane and 1,4-benzenedibornic acid. Acid functionalities (-SO_3H) were introduced by treatment with chlorosulfonic acid and base functionalities (-NH_2) were introduced by nitration

and reduction. They used it for sequential reactions of deacetalization and Knoevenagel condensation. Ma group also reported acid and base functionalized PAFs. After preparing amine functionalized PAF-1 by nitration and reduction of PAF-1, protected primary amine was grafted.[10] While sulfonation with chlorosulfonic acid, deprotection of primary amine gave rise to acid and base functionalized PAF-1.They used it for sequential reactions of deacetalization and Henry reaction.

Herein, acid and base functionalized monolithic porous polymers with compressibility were prepared and used as a heterogeneous catalyst. Most of POPs mentioned above were geneally obtained as apowders, which restricted their practical applications.[14,15] The monolithic porous polymer based catalysts studied in this work were easily cut by a knife and successfully used for a semi-continuous flow reactor. To demonstrate the easy processability and catalytic active site isolation property of the catalyst, two sequential reactions, an acid-catalyzed decaetalization and a base-catalyzed Knoevenagel condensation reaction were carried out.

III-2. Experimental

Materials. 1,3,5-Triethynylbenzne, 2,5-dibromoaniline, 1,4-diiodobenzene, benzaldehyde dimethyl acetal and bis(triphenylphospine)Palladium(II) dichloride were purchased from TCI. Chlorosulfonic acid, malononitrile and copper iodide were purchased from Sigma-Aldrich. Toluene and triethylamine (TEA) were purchased from Junsei. All chemicals were used without any further purification. All other solvents and reagents were in chemically pure grade and used as purchased.

Preparation of HM. 1,3,5-triethynylbenzene (150 mg, 1 mmol), 1,4-diiodobenzne (330 mg, 1 mmol) and $PdCl_2(PPh_3)_2$ (35 mg, 0.05 mmol) were dissolved in toluene and TEA (9 mL, 2:1, v/v) and the solution was transferred to a 20 mL vial. A solution of CuI (9 mg, 0.05 mmol) in toluene and TEA (1 mL, 2:1, v/v) was added to the mixture quickly. The reaction was carried out at room temperature for 12 h without stirring. The polymer composite was taken out of the vial and washed with methanol, tetrahydrofuran and acetone. After Soxhlet extraction with methanol, the resulting polymer was dried in vacuo at 90 ^oC for 48 h. HM was obtained as yellowish sponge (230 mg). FT-IR (KBr, cm^{-1}): 3297, 3050, 2963, 2208, 1777, 1671, 1584, 1502, 1431, 1409, 1351, 1272, 1184, 1094,

1017, 960, 876, 832, 680, 597, 540. Elemental analysis: C; 89.3, H; 3.62, N; 0.04.

Preparation of HM-B. 1,3,5-triethynylbenzene (150 mg, 1 mmol), 1,4-diiodobenzne (330 mg, 1 mmol) and $PdCl_2(PPh_3)_2$ (35 mg, 0.05 mmol) were dissolved in toluene and TEA (9 mL, 2:1, v/v) and the solution was transferred to a 20 mL vial. A solution of CuI (9 mg, 0.05 mmol) dissolved in toluene and TEA (1 mL, 2:1, v/v) was added to the mixture quickly. The reaction was carried out at room temperature for 12 h without stirring. The monolith organogel was transferred to the solution of 2,5-dibromoanilne (150 mg, 0.3 mmol), 1,3,5-triethynylamine (45 mg, 0.3 mmol), $PdCl_2(PPh_3)_2$ (10.5 mg, 0.015 mmol) and CuI (2.7mg, 0.015 mmol) in toluene and TEA (5 mL, 2:1, v/v). The further reaction was carried out at 80 ^oC for 24 h. The polymer composite was taken out of the vial and washed with methanol, tetrahydrofuran and acetone. After Soxhlet extraction with methanol, the resulting polymer was dried in vacuo at 90 ^oC for 48 h. HM-B was obtained as brownish monolithic sponge. (290 mg). FT-IR (KBr, cm^{-1}): 3457, 3297, 3063, 3050, 2969, 2202, 1783, 1686, 1581, 1505, 1425, 1406, 1363, 1277, 1181, 1099, 1015, 960, 876, 832, 678, 594, 540. Elemental analysis: C; 80.2, H; 3.93, N; 1.15.

Preparation of HM-A. After preparing HM, it was transferred to a dichloromethane (20 mL) at 0 ^{o}C and chlorosulfonic acid (2 mL) was added dropwise slowly. After 1 h, the resulting polymer was filtered, washed with dichloromethane, ethanol and water. After Soxhlet extracted with methanol, the polymer was dried in vacuo for 48 h. HM-A was obtained as yellowish sponge (285 mg). FT-IR (KBr, cm^{-1}): 3407, 3304, 3060, 2991, 2946, 2202, 1681, 1588, 1504, 1426, 1405, 1364, 1243, 1213, 1178, 1040, 1003, 884, 837, 770, 687, 592, 540. Elemental analysis: C; 39.63, H; 4.88, S;9.22.

Deacetalization and Knoevenagel condensation in semi-continuous flow reactor. Benzaldehyde dimethyl acetal (15 μL, 0.1 mmol) and malononitrile (24 μL, 0.4 mmol) were dissolved in THF/H_2O (1 ml, 1:1, v/v). HM-A, HM-B and HM (20 mg) cut by knife were packed into a syringe according to reaction condition and they were used as a semi-continuous flow reactor. A flow rate was controlled by a syringe pump with a rate of 0.2 mL/min. For the conventional batch type reaction, HM-A (20 mg) and HM-B (20 mg) were ground for making powder and added to 10 mL of the reaction mixture solution (10 times diluted) and stirred at 300 rpm. The reaction was monitored by TLC and measured by ^{1}H NMR spectroscopy without further purification.

Instrumental Characterization. ^{1}H NMR spectra were recorded on a Bruker Avance 300 spectrometer (300 MHz). Solid-state ^{13}C NMR spectra were recorded on a Bruker Avance 400WB spectrometer (100 MHz) equipped with a CP-MAS probe. TGA measurements were performed on a TA modulated TGA2050 with a heating rate of 10 ^{o}C min^{-1} under nitrogen. FT-IR measurements were made on a PERKIN ELMER Spectrum GX I using KBr pellets. N_2 uptake amounts were measured by using a Belsorp-Max (BEL Japan, Inc.) apparatus. SEM images were obtained by using a JEOL JSM-6330F microscope. Energy-dispersive X-ray spectroscopy (EDS) elemental maps were obtained using Oxford instrument X-Max^{N} detector and analyzed with AZtecEnergy EDS analysis. The compression test was performed on KES-FB3 autometic compression tester.

III-3. Results and Discussion

III-3-1. Synthesis and Characterization

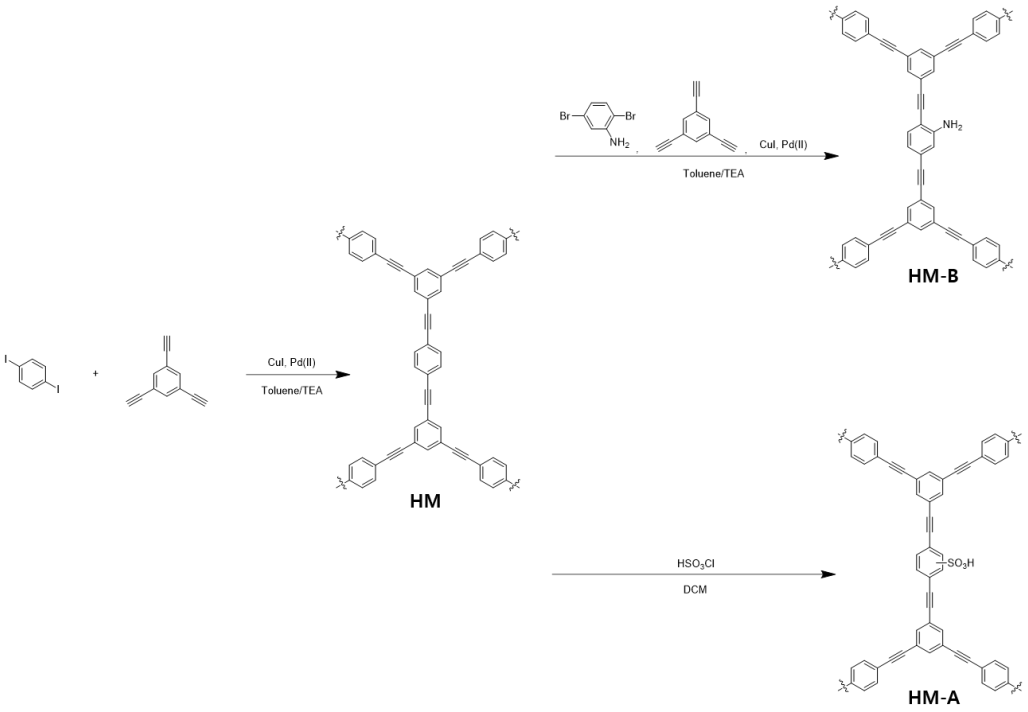

Scheme III-1. Synthesis of HM, HM-A, and HM-B.

Scheme III-1 shows synthesis of acid- and base-functionalized hierarchical porous polymer monoliths. A hierarchically porous polymer monolith (HM) having no acid or base functionality was prepared *via* Sonogashira-Hagihara coupling reaction with 1,3,5-triethynyl benzene and 1,4-diiodobenzene in a vial.

Because of the possible homocoupling of ethynyl groups, the molar ratio between ethynyl group and halogen group was 1.5:1.[16] The reaction mixture turned into an organogel in 5 min (Figure III-1). After the reaction at room temperature for 12 h, the polymer was washed with organic solvents and dried in vacuo at 90 ^{o}C to give a compressible monolith.

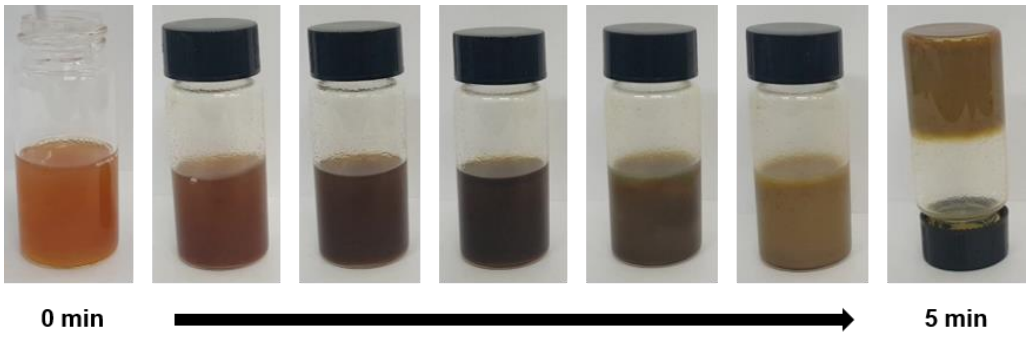

Figure III-1. Photographs of the reaction mixture according to the reaction time.

For the synthesis of a base functionalized porous polymer monolith (HM-B), The Sonogashira-Hagihara coupling reaction of 1,3,5-triethynylbenzene and 1,4-diiodobenzene was perfomed for 12 h in the same manner as for the preparation of HM. The resulting monolithic gel was transferred into a solution of 1,3,5-triethynylbenzene, 2,5-dibromoaniline, and the catalysts in toluene/TEA (2:1. v/v) and the second Sonogashira-Hagihara reaction was

carried out in the HM.[17-19] Even after work-up process, the polymer (HM-B) maintained its original monolithic shape and compressibility. In contrast, the base functionalized polymer (B) prepared from 2,5-dibromoaniline and 1,3,5-triethynylbenzene didn't show compressible and monolithic characteristics and was readily broken into powders. An acid functionalized porous polymer monolith (HM-A) was obtained by the sulfonation reaction of HM with chlorosulfonic acid.[20] HM-A also preserved compressible and monolithic properties. HM, HM-A and HM-B had cylindrical shapes, which were complementary to the inside of the vial reactor. (Figure III-2 and Figure III-3). All the polymers could be cut into various shapes by a knife as shown in Figure III-4.

Figure III-2. Photographs of HM, HM-A and HM-B.

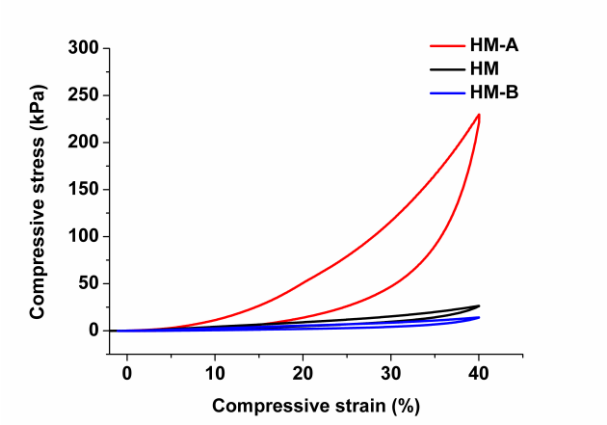

Figure III-3. Compressive stress-strain curves of HM, HM-A, and HM-B.

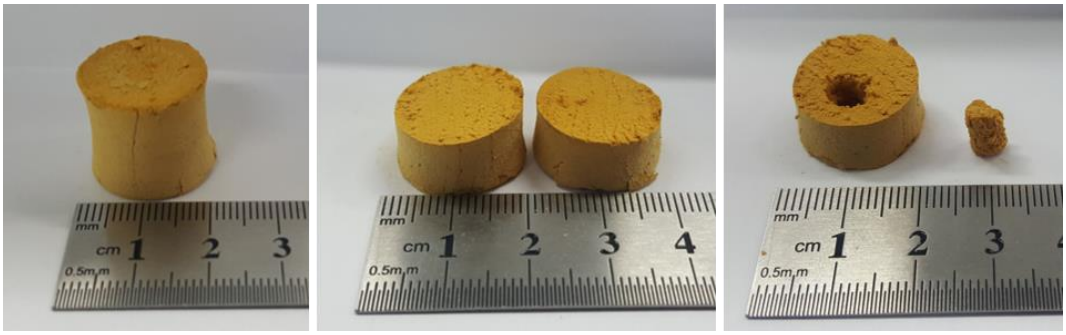

Figure III-4. Photographs of HM-B in various shapes obtained by cutting with a knife.

Special care such as freeze drying was not needed to make sure that the polymer kept the compressible and monolithic properties. It might due to the highly entangled fibrous networks as shown in Figure III-5.[21,22] The SEM images of the polymer showed highly interconnected fibrous structures with

several hundred micrometers in length and spherical particles with several micrometers in diameter. The hollow structures of the fibers were observed in the SEM images as marked by white arrows. The TEM images of the polymers also showed that the fibers had hollow structures (Figure III-6).

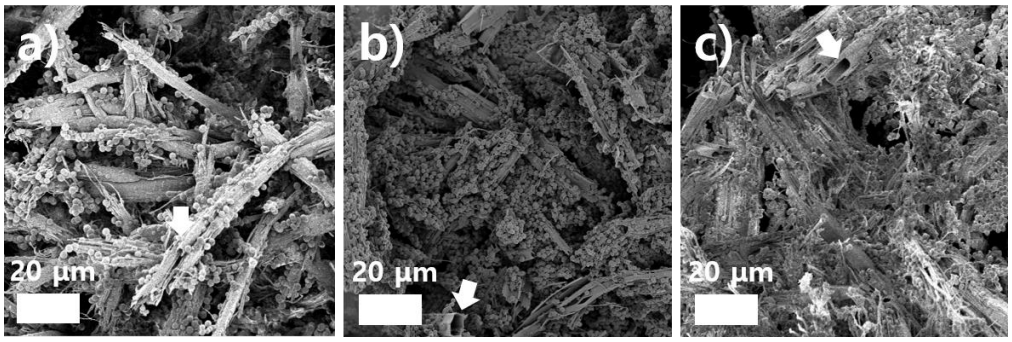

Figure III-5. SEM images of (a) HM, (b) HM-A, and (c) HM-B.

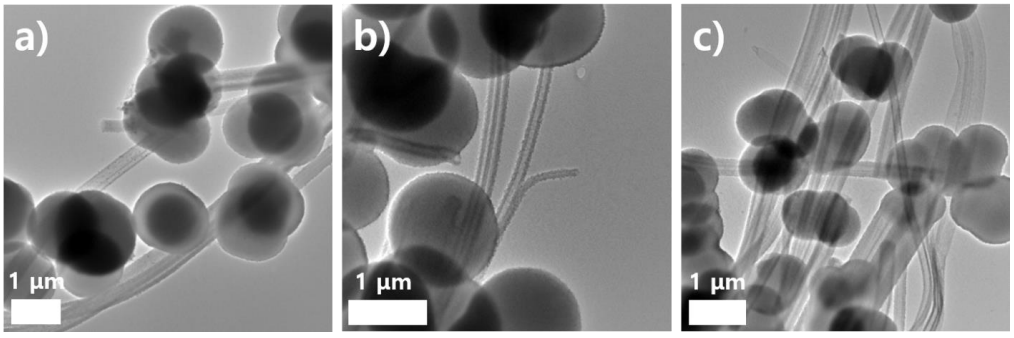

Figure III-6. TEM images of (a) HM, (b) HM-A, and (c) HM-B.

The chemical structures of the polymers were confirmed by ^{13}C cross-polarization/magic angle spinning nuclear magnetic resonance (CP/MAS NMR) spectroscopy (Figure III-7a). Because all the polymers had a HM skeleton, the overall shapes of the spectra were similar. The peaks appeared at 121 ppm and 128 ppm, corresponding to aromatic carbons bonded to acetylene carbons and hydrogen, respectively. HM-B and HM-A showed additional broad peaks at 138 and 134 ppm, respectively[23-25] The FT-IR spectrum of HM showed a band at 3300 cm^{-1} from C-H stretching vibration of terminal alkyne. The acetylene -C≡C- stretching vibration and aromatic C=C stretching vibration occurred at 2201 cm^{-1} and 1584 cm^{-1}, respectively (Figure III-7b). HM-B,showed an additional peak around 3400 cm^{-1} indicating the presence of the amine functional groups. In the spectra of HM-A, the broad peak around 3400 cm^{-1} appeared due to –OH functional group in the SO_3H group. The asymmetric and symmetric stretching vibration of SO_2 were observed at around 1200 cm^{-1} and 1000 cm^{-1}, respectively.[10,25-28]

An elemental analysis showed that HM-A contained 2.88 $mmolg^{-1}$ of acid while HM-B has 0.82 $mmolg^{-1}$ of base functionality. The thermogravimetric analysis showed that HM and HM-B were thermally stable up to 300 ^oC, whereas HM-A with sulfonic groups began to thermally degrade above 200 ^oC (Figure III-7c).[28] There were no noticeable peaks in X-ray diffraction patterns

of HM, HM-A, and HM-B, representing that the polymers have amorphous structures (Figure III-7d).

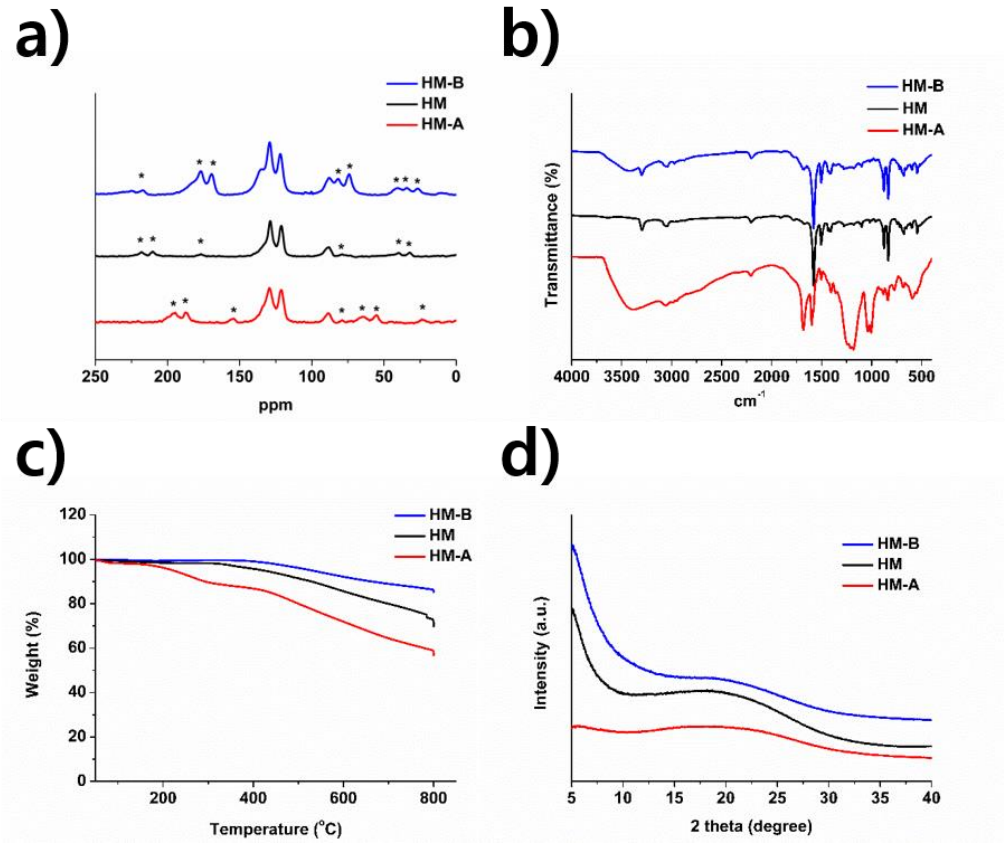

Figure III-7. (a) ^{13}C Solid CP/MAS NMR spectra, (b) FT-IR spectra, (c) TGA thermograms, and (d) XRD patterns of HM, HM-A, and HM-B.

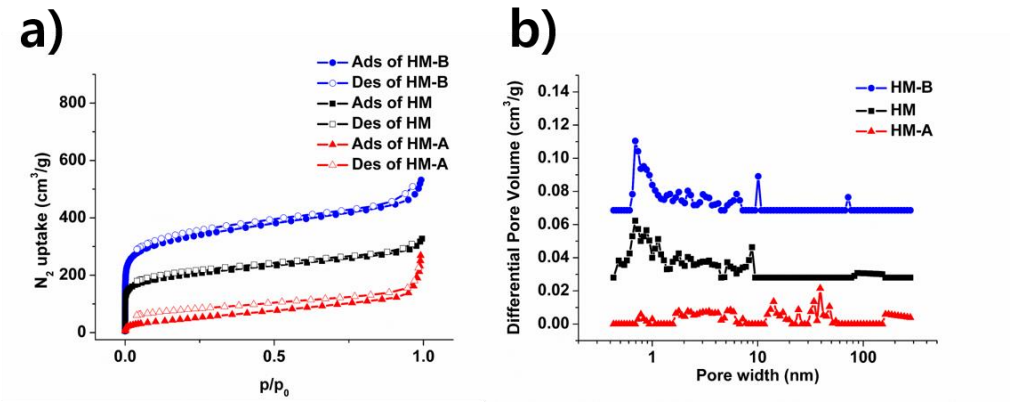

Figure III-8. (a) N_2 adsorption-desorption isotherms measured at 77 K and (b) NL-DFT pore size distribution of HM, HM-A and HM-B.

The polymers had hierarchically porous structures consisting of micro- and meso pores produced by the highly cross-linked structures and macropores generated by the solvent extraction from the gels. Hierarchical pore structures were desirable for catalysis applications because micro- and meso pores provide large surface area while macropores facilitate mass transfer.[29,30] The N_2 adsorption-desorption isotherms were shown in Figure V-8a. The Brunauer-Emmett-Teller (BET) surface area of HM, HM-A, and HM-B were 735, 193, and 1224 m^2g^{-1}, respectively. HM-A had a smaller surface area than HM because of the introduction of sulfonic groups.[25] HM-B showed a significantly larger surface area than HM. The polymer (B) prepared from 2,5-dibromobenzene and 1,3,5-triethynylbenzene showed a large BET surface area

of 1340 m^2g^{-1} (Figure III-9). Even considering the surface area and composition of B (20.7 % when estimated by weighing), however, the surface area of HM-B was larger than expected. This result could be attributed to the fact that more micropores were produced during the second reaction in the synthesis of HM-B. (Figure III-8b). When compared the NL-DFT pore sized distribution of HM-B with that of HM, the micropore volume increased, while the volume of macropores around 100 nm decreased.

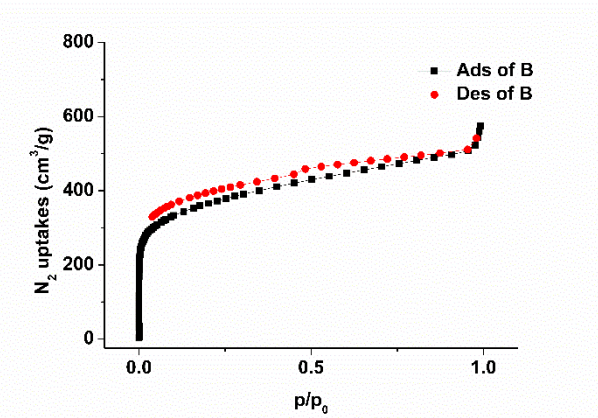

Figure III-9. N_2 adsorption-desorption isotherm of **B**.

III-3-2. Acid and Base Catalyzed Continuous Sequential Reaction in S emi-Continuous Flow Reactors

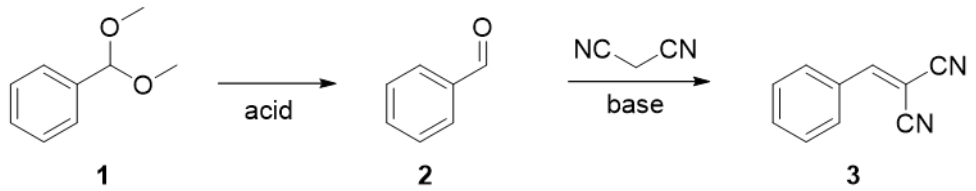

1 2 3

Scheme III-2. A tandem reaction: deacetalization and Knoevenagel condensation reaction.

HM-A and HM-B could be simultaneously used as an acid and base catalyst, repectively. To elucidate this possibility, successive deacetalization and Knoevenagel condensation reactions were carried out using the polymer as catalysts (Scheme III-2). The polymers (20mg of each polymer) were cut and fitted into a syringe in a sequence of HM-B and HM-A and used for a semi-continuous flow reaction. Benzaldehyde dimethyl acetal (0.1 mmol) and malononitrile (0.4 mmol) were dissolved in THF/H_2O (1 mL, 1:1, v/v) and put into the polymers packed syringe. The reaction mixture passed through the porous polymers with the help of syringe pump (0.2 mL/min) (Figure III-10). The product came out fo the syringe was analyzed by 1H NMR spectroscopy without further purification (Figure III-11).

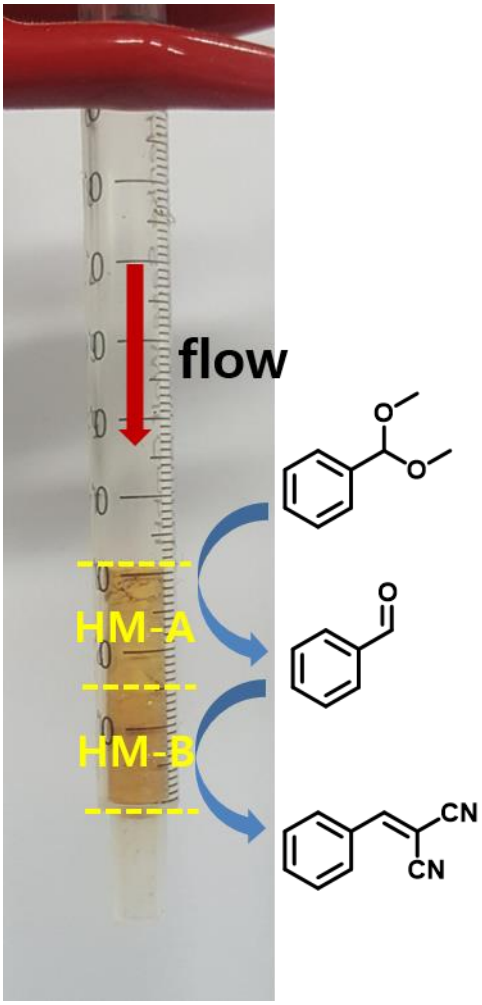

Figure III-10. Semi-continuous flow reactor with HM-A and HM-B.

The deacetalization reaction catalyzed by HM-A occurred first and Knoevenagel condensation reaction catalyzed by HM-B was followed during the reaction mixture flow (Table III-1, entry 1). At a flow rate of 0.2 mL/min, the reaction was completed within 5 min. Deacetalization was observed when

only HM-A was used as a catalyst (Table III-1, entry 2). No product formed with HM-B alone (Table III-1, entry 3). HM having no acid or base functionality didn't show catalytic activity as expected (Table III-1, entry 4). When polymers were packed in a reverse sequence, and so the reaction mixture met HM-B first, only the deacetalization reaction took place (Table III-1, entry 5). When the polymers were ground and dispersed in the reaction mixture as seen in a conventional batch type reactor, the desired reaction still occurred. However, 10 times more amount of the solvent was required for the dispersion and the reaction was completed after 2 h (Table III-1, entry 6). This semi-continuous flow reactor could be used successively after simple washing with water and THF without a significant decrease in reaction efficiency (Figure III-12).

Table III-1. Tandem deacetalization – knoevenagel condensation reaction[a]

Entry	Catalyst	Conversion (%)[c] 1	Yield (%)[c] 2	Yield (%) 3
1	HM-A+HM-B	99	0	100
2	HM-A	99	99	0
3	HM-B	trace	trace	0
4	HM	0	0	0
5	HM-B+HM-A	99	100	0
6	HM-A+HM-B[b]	99	2	98

[a]Reaction conditions: benzaldehyde dimethyl acetal (0.1 mmol), malononitrile (0.4 mmol), THF (0.5 mL) + H_2O (0.5 mL), room temperature for 5 min.

[b]HM-A (20 mg) + HM-B (20 mg) powders were added in 10 mL of mixture solution (10 times diluted) and stirred at 500 rpm, room temperature for 2 h.

[c]Conversion and yield (%): calculated from ^{1}H NMR spectroscopy.

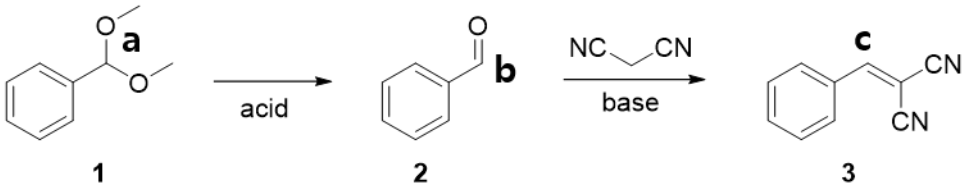

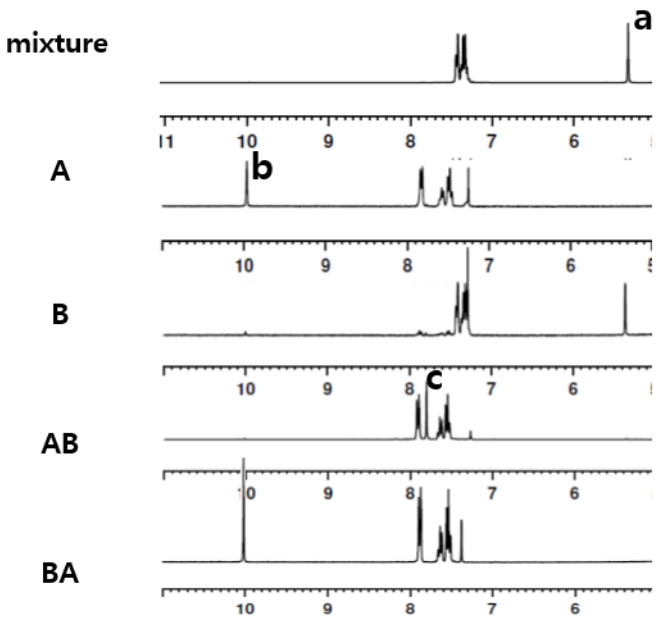

Figure III-11. ^{1}H NMR spectra of the reaction mixtures after passing through the polymers ($CDCl_3$).

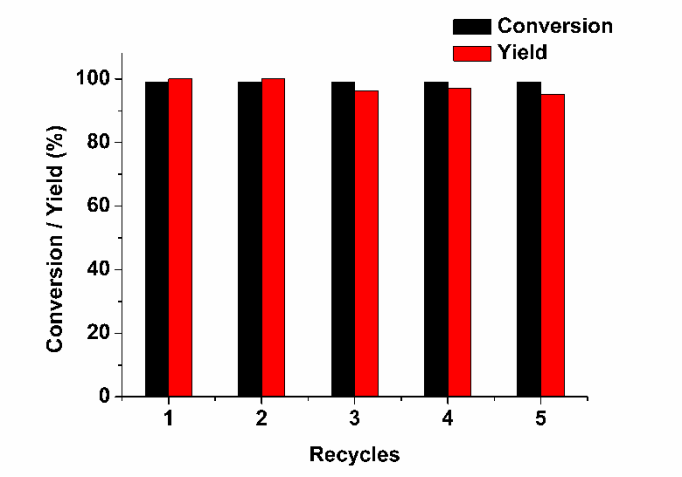

Figure III-12. Recycles of HM-A and HM-B packed semi-continuous flow reactor.

III-4. Conclusion

A compressible and monolithic hierarchical porous polymer, HM was prepared by one-pot synthesis. Sulfonation of HM was carried out to introduce acid functionality. The polymer with base was prepared by an additional Sonogashira-Hagihara reaction with 2,5-dibromoaniline and 1,3,5-triethynylbenzene in the presence of HM. HM-A and HM-B were fit into a syringe sequentially and the syringe was used as a semi-continuous flow reactor for a tandem reaction; deacetalization and Knoevenagel condensation. Because acid and base functionalities were immobilized in the porous organic polymers, they could be used at the same time. The semi-continuous flow reactor required less solvent and reaction time than a conventional batch type reactor. The reactor was recycled with no significant loss in catalytic activity. The monolithic hierarchically porous polymers with compressibility can be promising catalyst supports for various tandem reactions, particularly in a continuous flow-type reactor.

III-5. References

1. Xiong, L.; Zhang, H.; Zhong, A.; He, Z.; Huang, K. *Chem. Commun.* **2014**, *50*, 14778-14781.
2. Helms, B.; Guillaudeu, S. J.; Xie, Y.; McMurdo, M.; Hawker, C. J.; Fréchet, J. M. J. *Angew. Chem. Int. Ed.* **2005**, *44*, 6384-6387.
3. Gelman, F.; Blum, J.; Avnir, D. *Angew. Chem. Int. Ed.* **2001**, *40*, 3647-3649.
4. Shiju, N. R.; Alberts, A. H.; Khalid, S.; Brwon, D. R.; Rothenberg, G. *Angew. Chem. Int. Ed.* **2011**, *50*, 9615-9619.
5. Gianotti, E.; Diaz, U.; Velty, A.; Corma, A. *Catal. Sci. Technol.* **2013**, *3*, 3677-2688.
6. Zhong, L.; Anand, C.; Lakhi, K. S.; Lawrence, G.; Vinu, A. *Sci. Rep.* **2015**, *5*, 12901.
7. Toyao, T.; Fujiwaki, M.; Horiuchi, Y.; Matsuoka, M. *RSC Adv.* **2013**, *3*, 21582-21587.
8. Merino, E.; Verde-Sesto, E.; Maya, E. M.; Iglesias, M.; Sánchez, F.; Corma, A. *Chem. Mater.* **2013**, *25*, 981-988.
9. Merino, E.; Verde-Sesto, E.; Maya, E. M.; Corma, A.; Iglesias, M.; Sánchez, F. *Appl. Catal. A* **2014**, *469*, 206-212.

10. Zhang, Y.; Li, B.; Ma, S. *Chem. Commun.* **2014**, *50*, 8507-8510.
11. Shinde, D. B.; Kandambeth, S.; Pachfule, P.; Kumar, R. R.; Banerjee, R. *Chem. Commun.* **2015**, *51*, 310-313.
12. Xu, Y.; Jin. S.; Xu, H.; Nagai, A.; Jiang, D. *Chem. Soc. Rev.* **2013**, *42*, 8012-8031.
13. Sun, Q.; Dai, Z.; Meng, X.; Wang, L.; Xiao, F. –S. *ACS Catal.* **2015**, *5*, 4556-4567.
14. Cheng, G.; Hasell, T.; Trewin, A.; Adams, D. J.; Cooper, A. I. *Angew. Chem. Int. Ed.* **2012**, *51*, 12727-12731.
15. Gu, C.; Huang, N.; Chen, Y.; Qin, L.; Xu, H.; Zhang, S.; Li, F.; Ma, Y.; Jiang, D. *Angew. Chem. Int. Ed.* **2015**, *54*, 13594-13598.
16. Jiang, J. –X.; Su, F.; Trewin, A.; Wood, C. D.; Niu, H.; Jones, J. T. A.; Khimyak, Y. Z.; Cooper, A. I. *J. Am. Chem. Soc.* **2008**, *130*, 7710-7720.
17. Chinchilla, R.; Nájera, C. *Chem. Rev.* **2007**, *107*, 874-922.
18. Chinchilla, R.; Nájera, C. *Chem. Soc. Rev.* **2011**, *40*, 5084-5121.
19. Shcilz, M.; Plenio, H. *J. Org. Chem.* **2012**, *77*, 2798-2807.
20. Idibie, C. A.; Abdulkareem, S. A.; vZ Pienaar, C. H.; Iyuke, S. E.; vanDyk, L. *Ind. Eng. Chem. Res.* **2010**, *49*, 1600-1604.
21. Du, R.; Zhang, N.; Xu, H.; Mao, N.; Duan, W.; Wang, J.; Zhao, Q.; Liu, Z.; Zhang, J. *Adv. Mater.* **2014**, *26*, 8053-8058.

22. Lim. Y.; Cha, M. C.; Chang, J. Y. *Sci. Rep.* **2015**, *5*, 15957.

23. Dawson, R.; Laybourn, A.; Clowes, R.; Khimyak, Y. Z.; Adams, D. J.; Cooper, A. I. *Macromolecules* **2009**, *42*, 8809-8816.

24. Ratvijitvech, T.; Dawson, R.; Laybourn, A.; Khimyak, Y. Z.; Adams, D. J.; Cooper, A. I. *Polymer* **2014**, *55*, 321-325.

25. Lu, W.; yuan, D.; Sculley, J.; Zhao, D.; Krishna, R.; Zhou, H. –C. *J. Am. Chem. Soc.* **2011**, *133*, 18126-18129.

26. Chackalackal, S. M.; Stafford, F. E. *J. Am. Chem. Soc.* **1966**, *88*, 4815-4819.

27. Kavc, T.; Kern, W. *Chem. Mater.* **2000**, *12*, 1053-1059.

28. Goesten, M. G.; Szécsényi, À.; de Lange, M. F.; Bavykina, A. V.; Gupta, K. B. S. S.; Kapteijn, F.; Gascon, J. *ChemCatChem* **2016**, *8*, 961-967.

29. Liang, Y.; Wu, B.; Wu, D.; Xu, F.; li, Z.; Luo, J.; Zhong, H.; Fu, R.; Matyjaszewski, K. *J. Mater. Chem.* **2011**, *21*, 14424-14427.

30. Seo, M.; Kim, S.; Oh, J.; Kim, S. –J.; Hillmyer, M. A. *J. Am. Chem. Soc.* **2015**, *137*, 600-603.

Chapter IV.

Water Wettable, Compressible, and Hierarchically Porous Polymer Composite

IV-1. Introduction

Hierarchically porous polymers with interconnected micro-, meso- and macropore structures are of great interest because they have large surface areas and excellent pore accessibility at the same time.[1] A large surface area generated by micro and meso- pores is an important parameter in various applications such as gas storage, separation, catalysis and biomedical applications. Macropores provide pathways to meso- and micropores and enhance pore accessibility.[2] To develop hierarchically porous structures, many researchers used sacrificial template approaches to produce meso- or macro-pores and activation or post-reaction strategies to generate micropores. A variety of sacrificial templates that are removed after completion of the reaction have been used such as solvent [3,4], surfactant [5,6], polymer [2,7,8], silica and metal oxides.[9] The activation processes to generate microporosity include carbonization,[10] gas-developing activation.[1,11,12] Hyper-crosslinking reactions are often used as post reactions to form micropores, which is applicable to macroporous polymers with reactive groups.[2,13]

Microporous organic polymers (MOPs) with highly cross-linked structures have been widely investigated as promising functional porous materials with high surface areas and physicochemical stability.[14,15] Most MOPs are prepared

by polymerization of tri- or multi-functional building blocks. Because of their highly cross-linked rigid structures, MOPs are generally obtained as powders, which restricts their practical applications. Recently, Chang et al. reported compressible and monolithic microporous polymers.[16] The polymer monoliths consisted mainly of polymer tubes and their bundles, together with spherical particles. They were easily cut into any form using a knife. The compressibility and monolithic character of the polymers allowed for the facile release of adsorbed chemicals by applying pressure and thereby imparting a good recyclability. The polymer morphology was greatly influenced by the monomer structures and the experimental conditions and only a limited number of monomers produced satisfactory results. The use of synthetic sponges as a template is an alternative way for microporous polymers to be given a monolithic character. A number of studies have nicely demonstrated the efficacy of this approach, where microporous polymers were loaded[17,18] or were synthesized in a synthetic sponge.[19]

In this study, compressible and hierarchically porous polymer composites were prepared by carrying out the Sonogashira-Hagihara coupling reaction between aryl halides and an alkyne in a polyurethane sponge. Most microporous polymers obtained by carbon-carbon coupling reactions usually have hydrophobic networks which are not suitable for use in aqueous

environments. To address this problem, 2,5-diiodobenzoic acid was used as an aryl halide co-monomer. Here, pore structures, adsorption behaviors and mechanical properties of the hierarchically porous polymeric materials were discussed.

IV-2. Experimental

Materials. 1,3,5-Triethynylbenzne and 1,4-diiodobenzene were purchased from TCI. 2,5-Diiodobenzoic acid, bis(triphenylphosphine)palladium(II) dichloride and copper iodide were purchased from Sigma-Aldrich. Toluene and triethylamine (TEA) were purchased from Junsei. A urethane sponge was purchased from 3M.

Synthesis of PUS-MOP-A and MOP-A. 1,3,5-Triethynyl benzene (150 mg, 1 mmol), 1,4-diiodobenzne (264 mg, 0.8 mmol) and 2,5-diiodobenzoic acid (75 mg, 0.2 mmol) were dissolved in toluene and TEA (9 mL, 2:1, v/v) and the solution was transferred to a 20 mL vial. After adding $PdCl_2(PPh_3)_2$ (70 mg, 0.1 mmol) to the solution, a polyurethane sponge (1.5 x 1.5 x 1.5 cm^3, 90 mg) was placed in the vial. A solution of CuI (19 mg, 0.1 mmol) in toluene and TEA (1 mL, 2:1, v/v) was added to the mixture quickly. The reaction was carried out at room temperature for 12 h without stirring. The polymer composite was taken out of the vial and washed with methanol, tetrahydrofuran and acetone. After Soxhlet extraction with methanol, PUS-MOP-A was dried in vacuo at 90 ^oC (yield: 220 mg). FT-IR (KBr, cm^{-1}): 3369, 3289, 3050, 2982, 2208, 1796, 1718, 1580, 1508, 1438, 1406, 1359, 1094, 1012, 958, 875, 836, 680, 540.

MOP-A was prepared in the same manner as described above except that a polyurethane sponge was not added (yield: 251 mg). FT-IR (KBr, cm^{-1}): 3417, 3295, 3050, 2976, 2202, 1792, 1714, 1580, 1508, 1438, 1406, 1359, 1094, 1012, 958, 875, 836, 680, 540.

Preparation of PUS-MOP-Aa. PUS-MOP-A (25 mg) was added in a 0.01 M KOH solution in ethanol/water (10 mL, 1:1, v/v). PUS-MOP-A was compressed and released 100 times and was stirred for 12h. After washing with water and ethanol, the product was dried in vacuo at 90 ºC. The content of carboxylic acids in PUS-MOP-A was measured by titration with an aqueous KOH solution. The amount of KOH required for the titration was determined by ICP analysis.

Absorption test. For the static absorption, PUS or PUS-MOP-Aa (20 mg) was immersed in a dye solution (10 mL, 5.0×10^{-5} M) and UV-Vis spectra of the solution were measured at different time intervals. For the dynamic absorption, PUS-MOP-Aa (20 mg) was manually compressed and released in a dye solution (10 mL, 5.0×10^{-5} M) at a rate of about 5 s per cycle. For the absorption capacity measurement, PUS-MOP-Aa (20 mg) was saturated with

the dye in a 1.5 M dye solution (10 mL) and the remaining dye concentration in the solution was determined by UV-Vis spectroscopy (ε = 54447 $M^{-1}cm^{-1}$).

Desorption. A dye-absorbed PUS-MOP-Aa was immersed in a 0.01 M HCl solution in ethanol/water (1:1, v/v) for 1 h, washed by Soxhlet extraction with ethanol and dried in vacuo.

Instrumental Characterization. Solid-state ^{13}C NMR spectra were recorded on a Bruker Avance 400WB spectrometer (100 MHz) equipped with a CP-MAS probe. TGA measurements were performed on a TA modulated TGA2050 with a heating rate of 10 ^{o}C min^{-1} under nitrogen. The FT-IR spectra were measured by a Thermo Scientific Nicolet 6700 FT-IR spectrometer using KBr pellets. N_2 uptake amounts were measured using a Belsorp-Max (BEL Japan, Inc.) apparatus. UV-Vis spectra were obtained using a Sinco S-3150 spectrometer. SEM images were obtained using a JEOL JSM-6330F microscope. Energy-dispersive X-ray spectroscopy (EDS) elemental maps were obtained using an Oxford instrument X-MaxN detector and analyzed with an AZtecEnergy EDS analysis. Transmission electron microscopy images were obtained using a JEOL JEM-2010 microscope at 200 keV. The compression test was performed on a KES-FB3 autometic compression tester. The concentration

of potassium ion was measured by an ICP (Inductively Coupled Plasma) emission spectrometer VARIAN 730ES.

IV-3. Results and Discussion

IV-3-1. Synthesis and Characterization

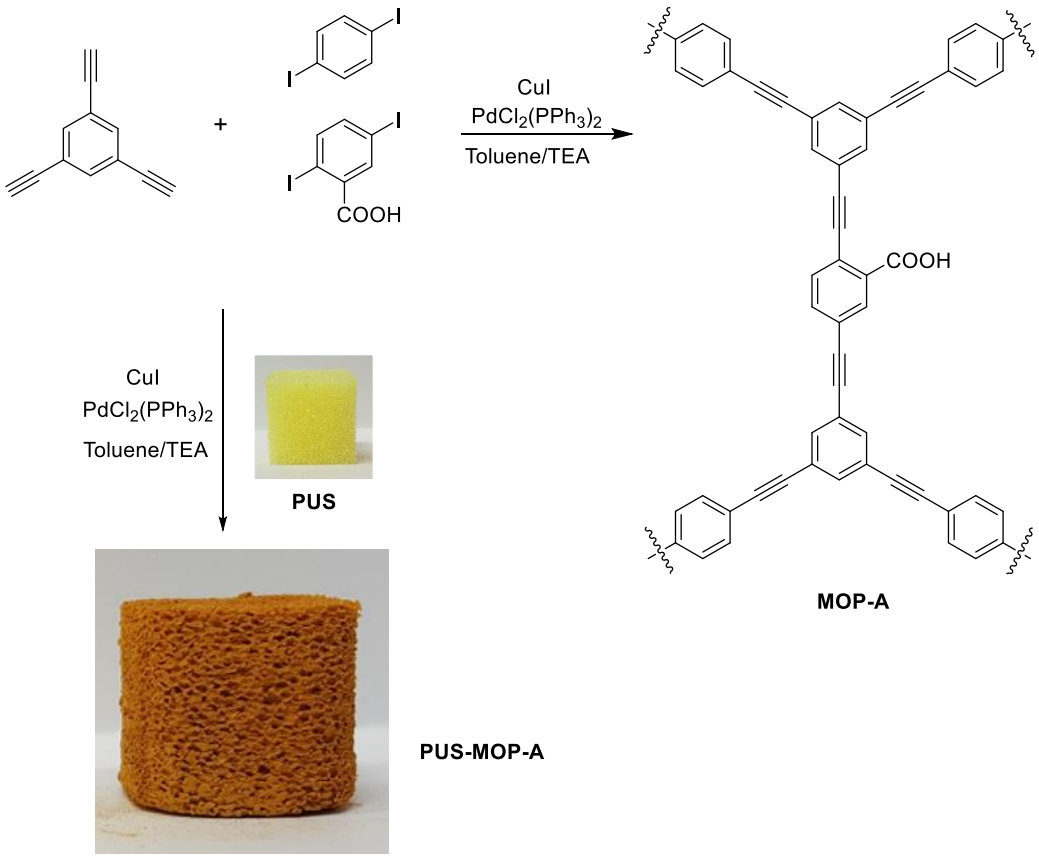

Scheme IV-1. Synthesis of PUS-MOP-A.

Scheme IV-1 shows the synthetic routes for a microporous organic polymer (MOP-A) and a hierarchically porous polymer composite (PUS-MOP-A). MOP-A was synthesized by the Sonogashira-Hagihara coupling reaction of

1,3,5-triethynyl benzene, 1.4-diiodobenzene and 2,5-diiodobenzoic acid in toluene/TEA (2:1, v/v) at room temperature. The molar ratio between ethynyl and iodo groups was fixed to 1.5:1, considering the possible homocoupling reaction between the ethynyl groups.[20] 2,5-Diiodobenzoic acid was used as a co-monomer to provide carboxyl functionality to the pore surface. The polymer showed fibrous morphology when 1,4-diiodobenzene was used as a major aryl halide. An increase in the amount of 2,5-diiodobenzoic acid adversely affected the formation of the fibrous structure and spherical particles formed dominantly when the ratio of 2,5-diiodobenzoic acid to 1,4-diiodobenzene was higher than 2:1 (Figure IV-1). For the synthesis of a hierarchically porous polymer composite (PUS-MOP-A), a polyurethane sponge (PUS) was soaked in a solution of 1,3,5-triethynyl benzene, 1.4-diiodobenzene, and 2,5-diiodobenzoic acid in toluene/TEA (2:1, v/v) and the Sonogashira-Hagihara coupling reaction was carried out at room temperature without stirring. The molar ratio between 1,4-diiodobenzene, and 2,5-diiodobenzoic acid was chosen as 4:1.

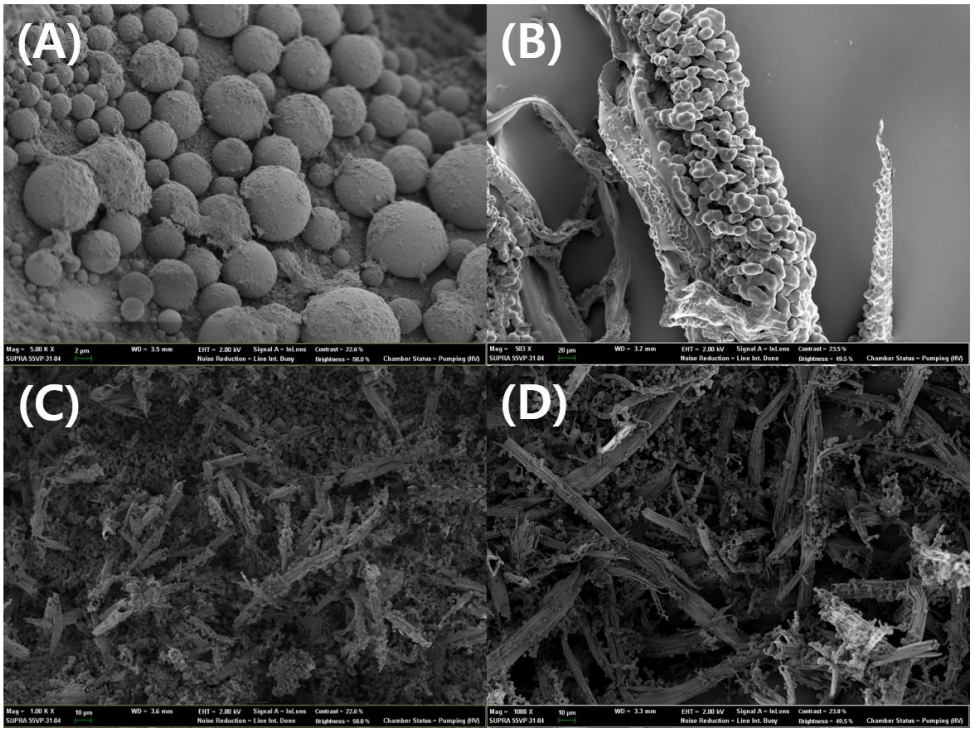

Figure IV-1. SEM images of microporous polymers obtained when the ratios between 1,4-diiodobenzene and 2,5-diiodobenzoic acid were (a) 0:1, (b) 1:1, (c) 4:1, (d) 1:0.

The polymer structures were characterized by solid state ^{13}C cross-polarization/magic-angle spinning NMR (CP/MAS NMR) spectroscopy (Figure IV-2). PUS-MOP-A showed peaks at 131 and 123 ppm which corresponded to aromatic carbons bonded to hydrogen and acetylene carbon, respectively. The peak at 90 ppm was assigned to acetylene carbons. The carbon peaks of a polyurethane sponge appeared at 157 ppm, 75 ppm and 17 ppm.[21]

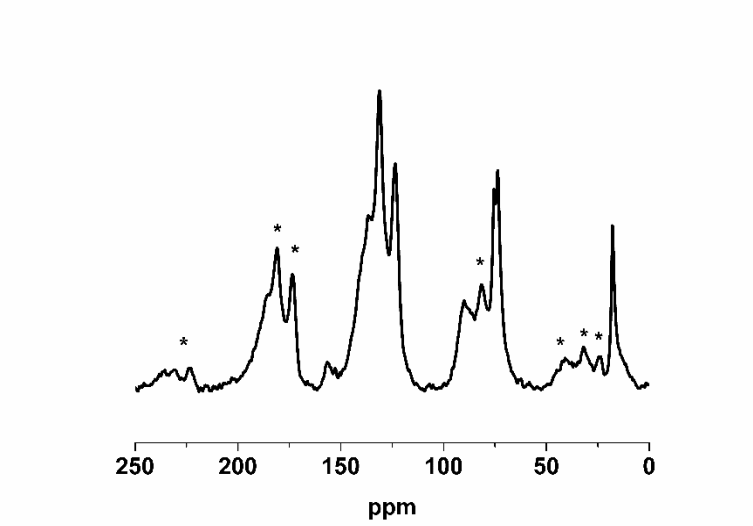

Figure IV-2. ^{13}C CP/MAS solid NMR spectrum of PUS-MOP-A.

The X-ray diffraction study showed that PUS-MOP-A had an amorphous structure (Figure IV-3). The FT-IR spectrum of PUS-MOP-A (Figure IV-4) showed all the bands observed from PUS and MOP-A, including the peaks at 3300 cm^{-1} from C-H stretching vibration of the terminal alkynes, at 2201 cm^{-1} for -C≡C- stretching vibration and at 1718 cm^{-1} for C=O stretching from the carboxyl groups. The content of the microporous polymer in PUS-MOP-A was about 60 wt% when estimated by weighing PUS and PUS-MOP-A and TGA analysis (Figure IV-5).

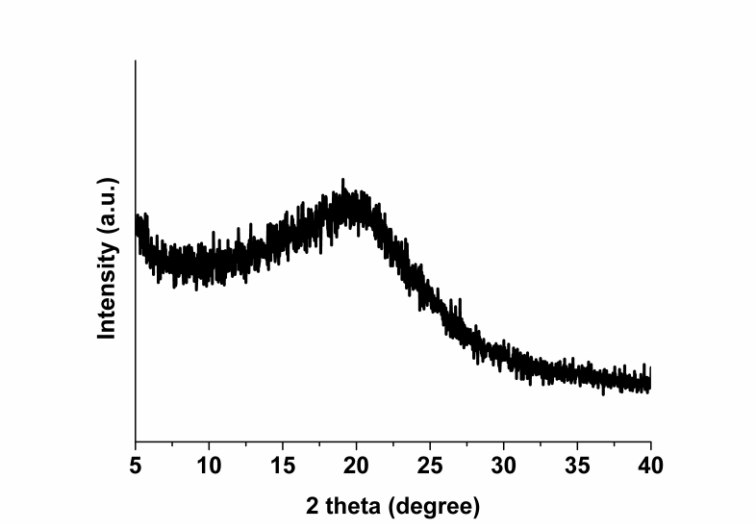

Figure IV-3. XRD pattern of PUS-MOP-A.

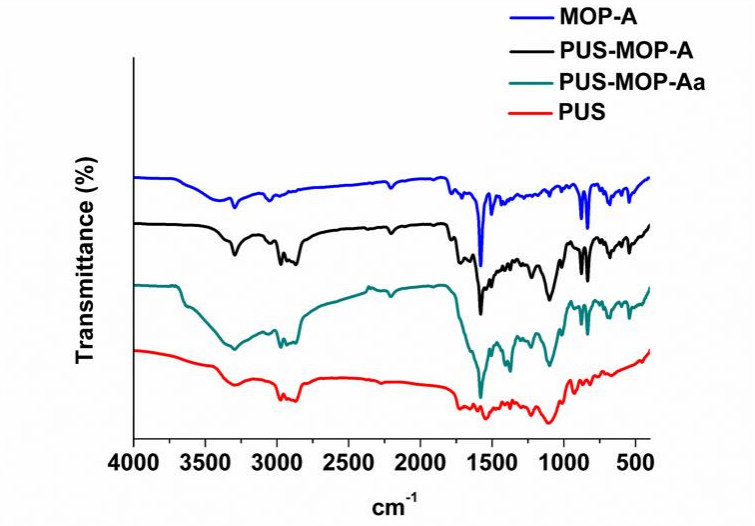

Figure IV-4. FT-IR spectra of MOP-A, PUS-MOP-A, PUS-MOP-Aa and PUS.

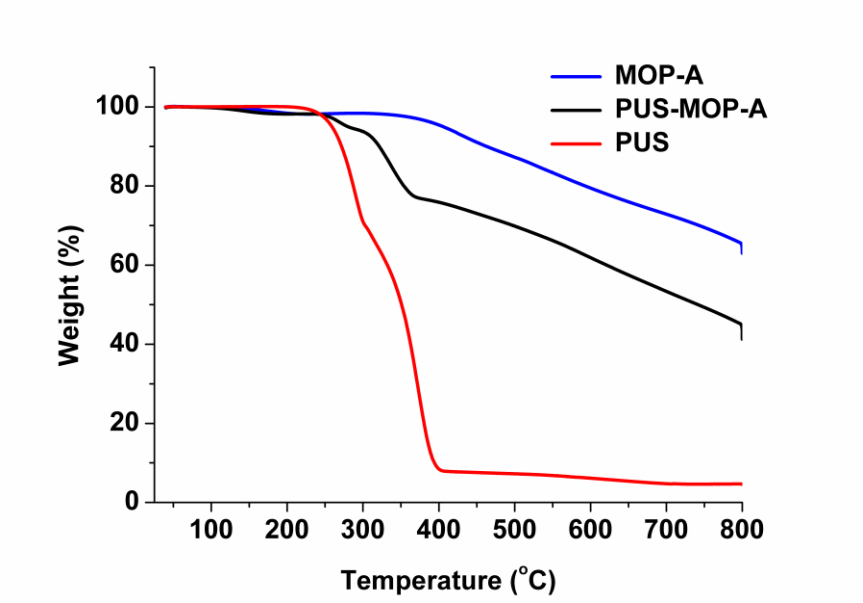

Figure IV-5. TGA thermograms of MOP-A, PUS-MOP-A and PUS.

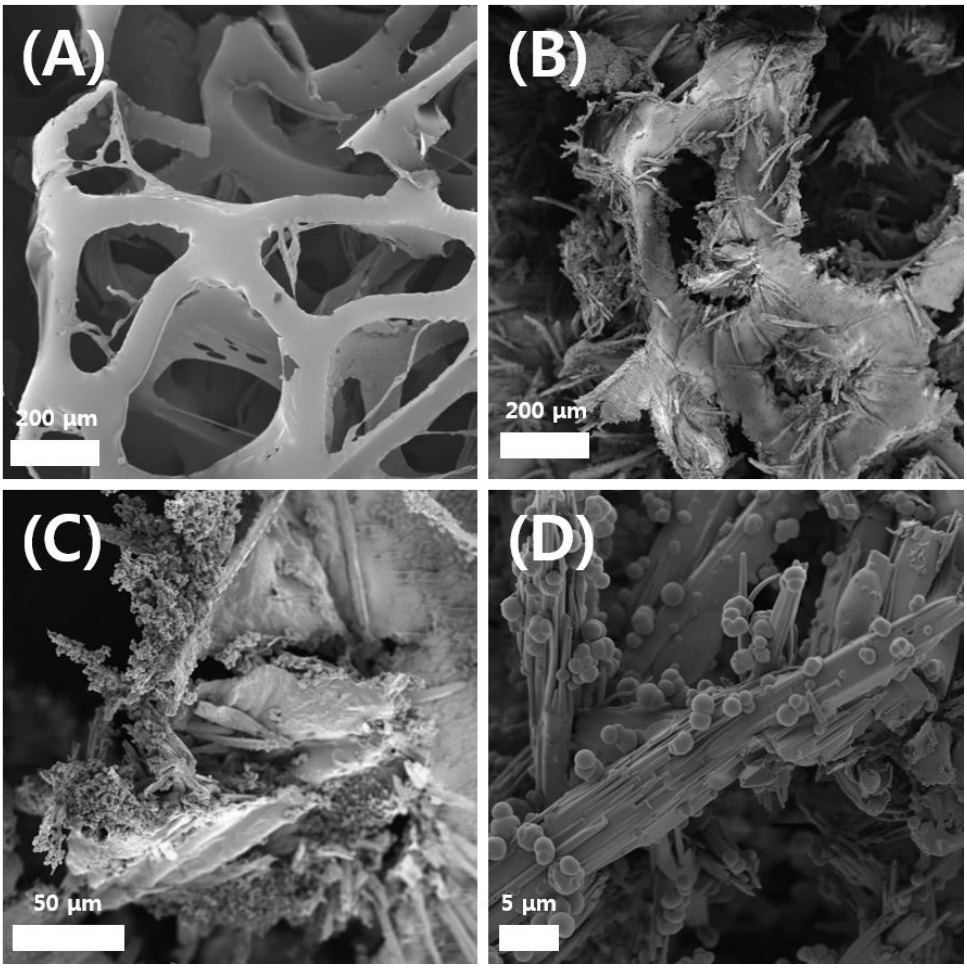

Figure IV-6. SEM images of (a) PUS, (b), (c), and (d) PUS-MOP-A.

The SEM images of PUS and PUS-MOP-A are shown in Figure IV-6. Several hundreds of micrometer scale pores were observed in PUS (Figure IV-6a). After the polymerization, these pores were partially filled by the microporous polymer as seen in Figure IV-6b, c. The microstructure of the

microporous polymer incorporated in PUS-MOP-A was essentially same as that of MOP-A (Figure IV-6d, Figure IV-1c), showing fibers with several tens of micrometer in length and spherical particles with a size of several micrometer. To examine the participation of 2,5-diiodobenzoic acid in the polymerization, the EDS element mapping of oxygen in the microporous polymer was performed. As shown in Figure IV-7, oxygen was wholly distributed over the fibers and spherical particles, suggesting the homogeneous incorporation of the acid moiety into the microporous polymer structure.

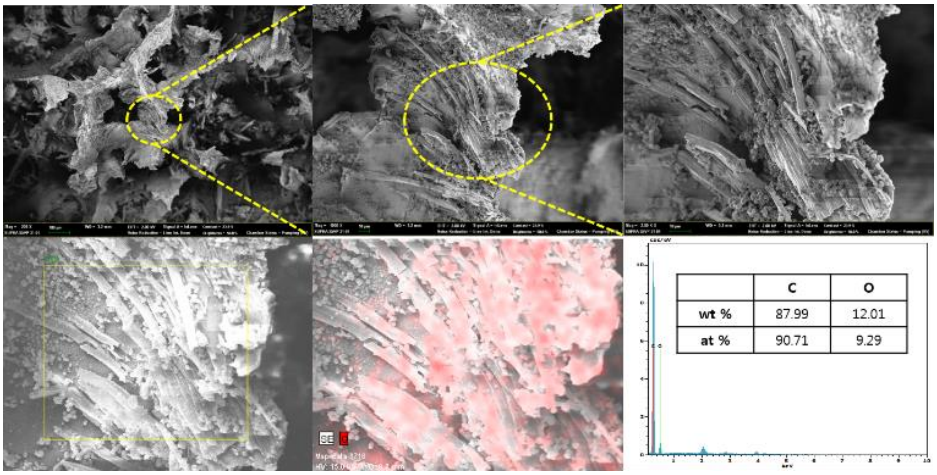

Figure IV-7. EDS element mapping for oxygen

The TEM images of PUS-MOP-A showed that the fibers had a tubular structure with open ends (Figure IV-8).

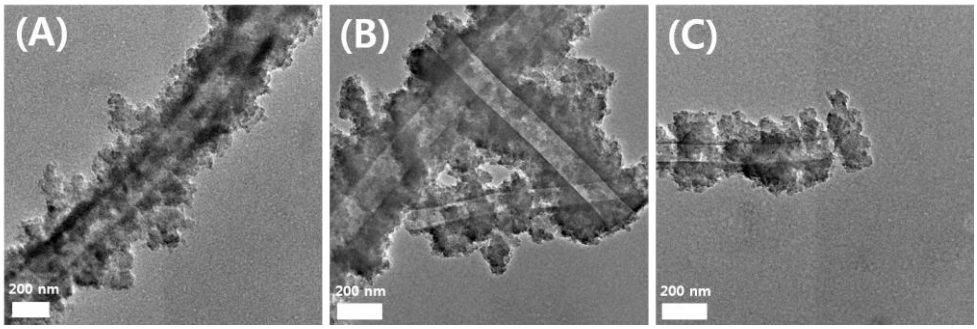

Figure IV-8. TEM images of MOP-A in PUS-MOP-A.

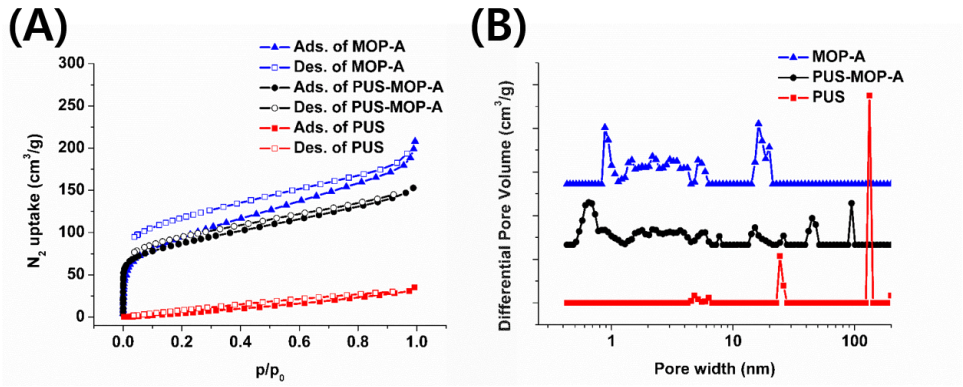

Figure IV-9. (a) N_2 adsorption-desorption isotherms measured at 77 K and (b) NL-DFT pore size distribution of PUS, PUS-MOP-A and MOP-A.

The N_2 adsorption/desorption isotherms and pore size distributions of PUS, PUS-MOP-A and MOP-A are shown in Figure IV-9. The Brunauer-Emmett-Teller (BET) surface area of PUS-MOP-A calculated from the N_2 adsorption isotherm at 77 K was 306 m^2g^{-1}. BET surface area of MOP-A and PUS were

340 m^2g^{-1} and 55 m^2g^{-1}, respectively. Nonlocal density functional theory (NL-DFT) pore size distribution of PUS-MOP-A showed that the polymer had micro-, meso- and macropores.

IV-3-2. Compressibility and Water Contact Angle

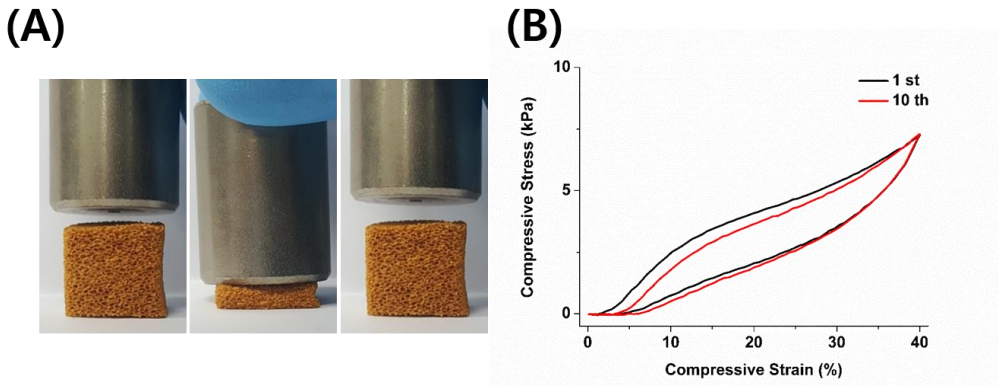

Figure IV-10. (a) Sequential images of PUS-MOP-A in as-prepared, compressed, and released states and (b) compressive stress-strain curves of PUS-MOP-A for the 1st and 10th test cycles.

The compression test results of PUS-MOP-A are shown in Figure IV-10. PUS-MOP-A recovered its initial shape immediately after the removal of external force (Figure IV-10a). Figure IV-10b shows the compressive stress–strain curves measured over 10 cycles of repeated stress loading and unloading.

Only a small change was observed, indicating a high mechanical stability of the polymer against compressive force.

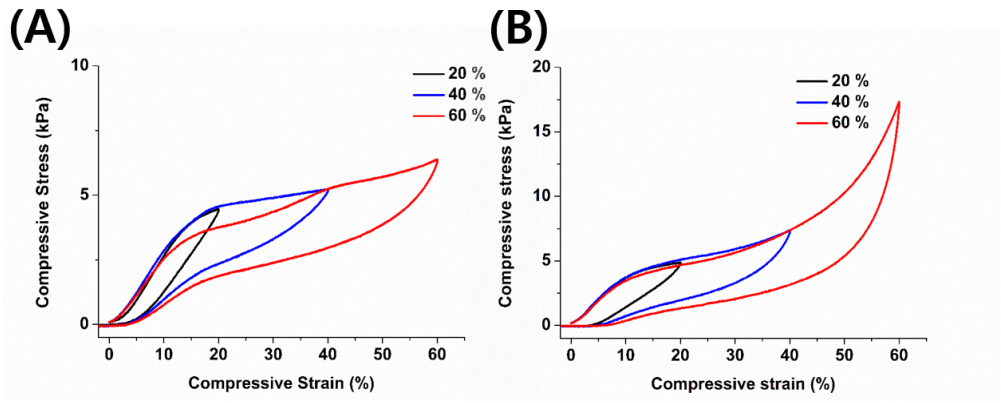

Figure IV-11. Compressive stress-strain curves of (a) PUS and (b) PUS-MOP-A.

PUS-MOP-A and PUS showed a similar shape of the compressive stress-strain curves under 40 % strain, but their compressive behaviors were considerably different under strain of larger than 40% (Figure IV-11). PUS-MOP-A exhibited a steeply sloped curve, indicating that densification occurred and showed much higher compressive stress ($\sigma \sim 17$ kPa) than PUS ($\sigma \sim 6$ kPa) at $\varepsilon = 60$ %. In the compressive stress-strain curve of PUS, only a slow plateau stress increase was observed with increasing stress. These results suggested that

the PUS network structure was significantly reinforced by the incorporation of the microporous polymers.[22]

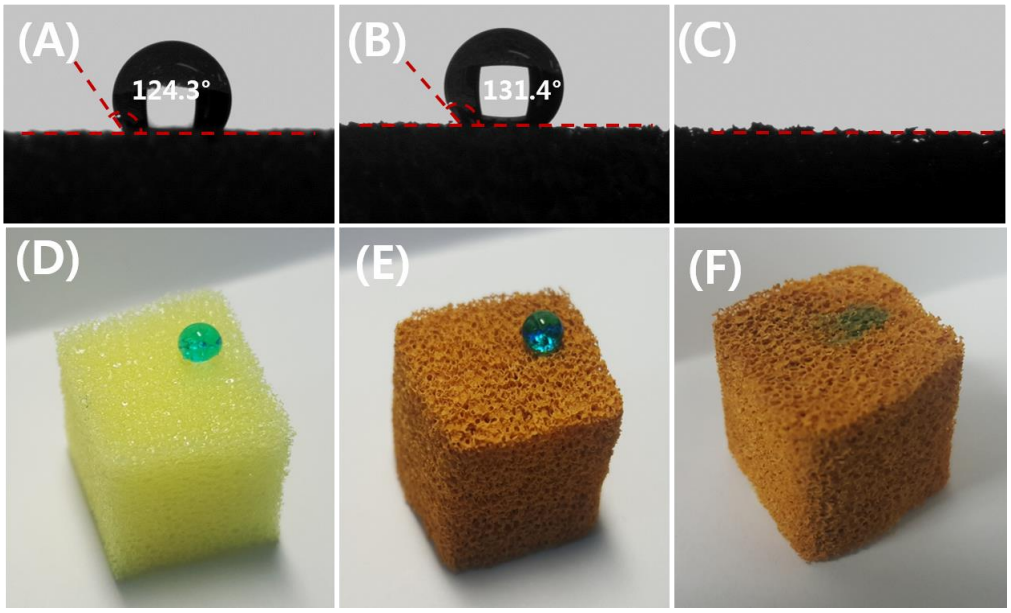

Figure IV-12. Water contact angles of (a) PUS, (b) PUS-MOP-A and (c) PUS-MOP-A treated with KOH (PUS-MOP-Aa) and photo images of a water droplet on (d) PUS, (e) PUS-MOP-A and (f) PUS-MOP-Aa.

The surface properties were investigated by measuring a water contact angle (Figure IV-12). PUS was hydrophobic with a water contact angle of 124.3°. PUS-MOP-A showed a higher water contact angle (131.4°) than PUS. The water contact angle of PUS-MOP prepared by the reaction of 1,4-diiodobenzene

and 1,3,5-triethynyl benzene in PUS was 144.8° (Figure IV-13), suggesting that the carboxyl group of PUS-MOP-A reduced the hydrophobicity.[23]

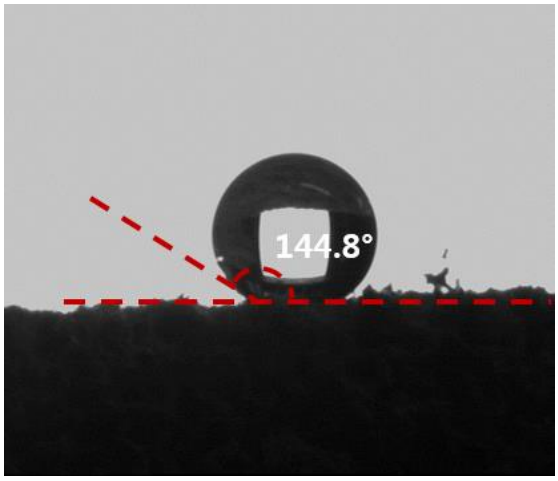

Figure IV-13. Image of a water droplet on the surface of PUS-MOP.

The amount of carboxylic acids in PUS-MOP-Aa estimated by titration was about 0.304 mmol/g (Table IV-1). The carboxyl groups on the MOP-A backbone could be transformed to the carboxylate anions easily by the reaction with a base. After being treated with a KOH solution in EtOH/H_2O (1:1) and dried, PUS-MOP-A absorbed water quickly, showing a water contact angle of 0^o (Figure IV-12c, f). The ionization of the carboxyl groups was confirmed by FT-IR spectroscopy. The C=O stretching peak at 1718 cm^{-1} of PUS-MOP-A disappeared after the KOH treatment and the CO_2^- asymmetric and symmetric

stretching vibration peaks appeared at 1510-1650 cm^{-1} and at ~1400 cm^{-1}, respectively (Figure IV-4). [24]

Table IV-1. Potassium ion concentrations in a KOH solution (10 mL) before and after titration of carboxylic acids in PUS-MOP-A (25 mg).

Sample	Amount of K	
	(mg/L)	(mM)
before	371.8	9.51
after	342.1	8.75

IV-3-3. Molecular Absorption Test

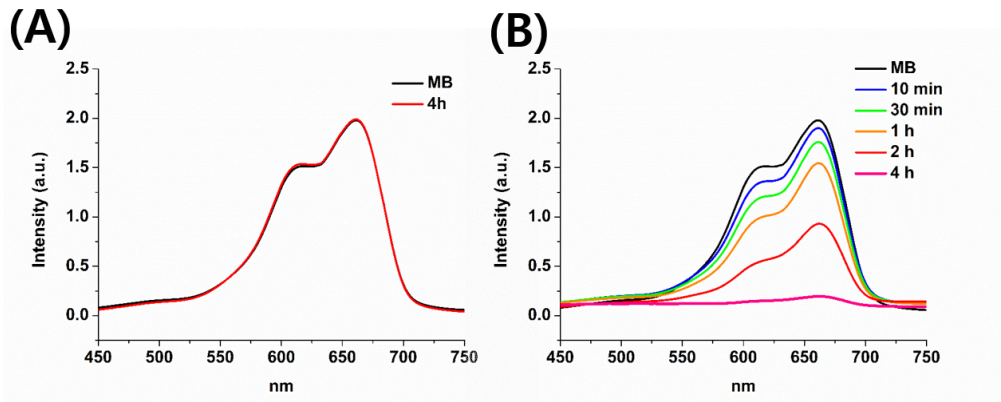

Figure IV-14. UV-Vis spectra of an MB aqueous solution (5.0×10^{-5} M) after static absorption by (a) PUS and (b) PUS-MOP-Aa.

PUS-MOP-A treated with an aqueous KOH solution (PUS-MOP-Aa) could be immersed in an aqueous solution to remove chemicals dissolved in water. Absorption ability of PUS and PUS-MOP-Aa to remove chemical pollutants in an aqueous solution was studied using a cationic dye, Methylene Blue (MB) as a model chemical. A same mass of PUS and PUS-MOP-Aa were immersed in a MB solution and UV-Vis spectra of the solution were measured at different time interval (Figure IV-14). PUS-MOP-Aa removed MB almost completely after 4 h owing to its large surface area and micropores.[16] The carboxylate ions on the surface PUS-MOP-Aa could also capture MB by an ionic interaction.[25] Meanwhile, PUS with only macropores didn't absorb the dye at all.

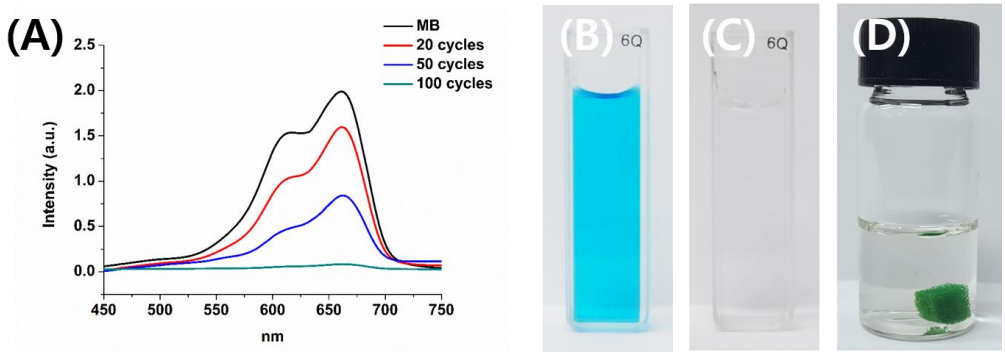

Figure IV-15. (a) UV-Vis spectra of an MB aqueous solution (5.0×10^{-5} M) measured after removing a dye by PUS-MOP-Aa (0, 20, 50, and 100 cycles of compression and release) and (b) photographs of the MB aqueous solution (5.0×10^{-5} M) and (c, d) after absorption.

The fast removal of the dye by PUS-MOP-Aa could be realized by taking an advantage of its compressibility. PUS-MOP-Aa was manually compressed and released in situ at a rate of about 5 s per cycle, which significantly enhanced mass transport to the internal pores.[13,19] The absorption intensity of MB in the solution gradually decreased as the number of the cycles increased (Figure IV-15a). The blue colour of the solution became almost disappeared after 100 cycles, indicating that MB had been absorbed by PUS-MOP-Aa. The MB absorption capacity of PUS-MOP-Aa was 0.75 mmol/g, which was determined after PUS-MOP was saturated with MB by the compression and release method (Figure IV-16).

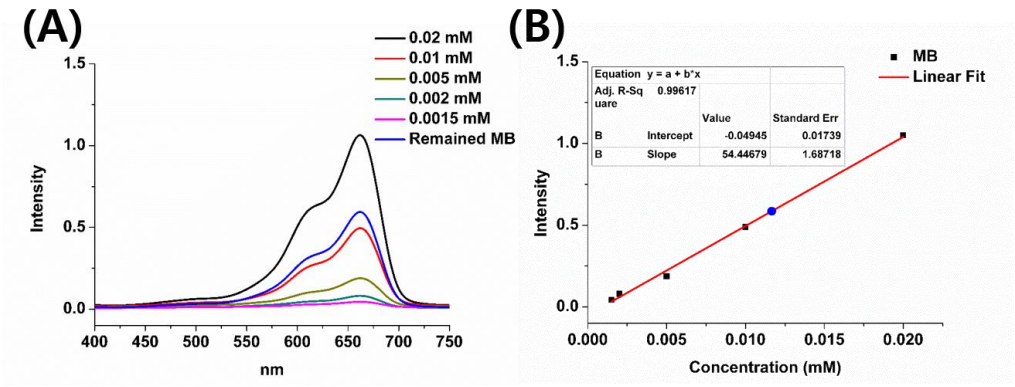

Figure IV-16. (a) UV-Vis absorption spectra of MB aqueous solutions of different concentrations and (b) the plot of the maximum peak intensity as a function of concentration. The blue line in (a) and the blue dot in (b) correspond to the remaining MB concentration (11.6 μM).

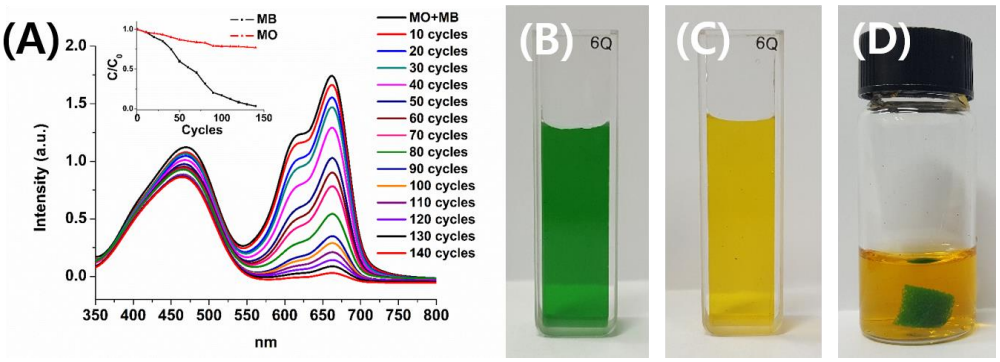

Figure IV-17. (a) UV-Vis spectra of an aqueous solution containing MO and MB (5.0×10^{-5} M, each) measured after removing dyes by PUS-MOP-Aa using the compression and release method and (b) photographs of the aqueous solution and (c,d) after absorption. Inset shows an absorption profiles against MO and MB.

When an aqueous solution contained both an anionic and a cationic dye, PUS-MOP-Aa preferentially removed the cationic dye. An anionic dye, Methylene Orange (MO) was dissolved in water together with an equimolar of MB (Figure IV-17b). PUS-MOP-Aa was immersed in the dye solution and compressed and released at a rate of about 5 s per cycle. The UV-Vis spectra of the solution showed two different absorption maxima at 465 nm from MO and at 665 nm from MB. The absorption intensity of MB decreased much faster than that of MO as the number of cycles increased (Figure IV-17a). The color

of the solution changed from green to orange after 140 cycles, indicating that most MB molecules were removed (Figure IV-17c, d). This result could be attributed to the fact that the carboxylate anions on the surface of PUS-MOP-Aa could impede the access of anions.

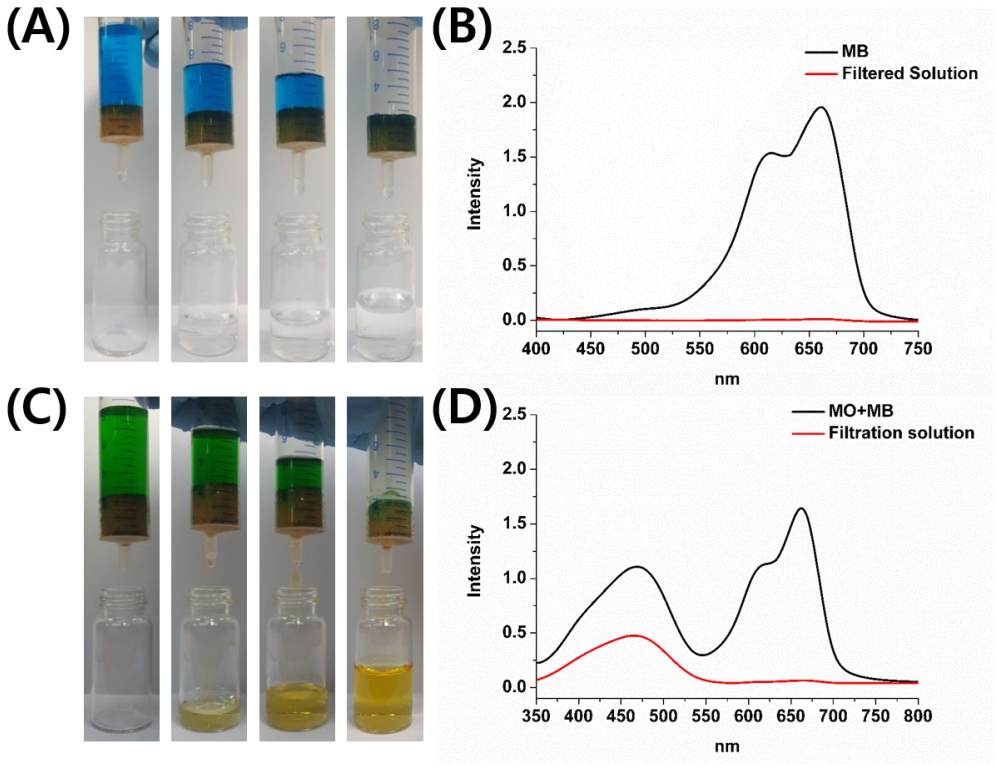

Figure IV-18. (a) Sequential photographs showing removal of MB using a PUS-MOP-Aa syringe filter and (b) UV-Vis spectra of a MB aqueous solution (5×10^{-5} M) and a filtered solution. (c) sequential photographs showing removal of MB over MO using a PUS-MOP-Aa syringe filter and (d) UV-Vis spectra of a MB + MO aqueous solution (5×10^{-5} M) and a filtered solution.

PUS-MOP-Aa could be prepared to have various shapes and sizes, depending on the type of a reaction vessel or by cutting with a knife. A cylindrical PUS-MOP-Aa was prepared that fitted into a syringe and used for

filtration. The blue MB solution turned colorless as it passed through PUS-MOP-Aa, showing that all MB molecules were removed by the syringe filter (Figure IV-18a). The UV-Vis spectrum of the filtrate also supported the results (Figure IV-18b). When the solution of MB and MO was passed, the green solution turned yellow. The UV-Vis spectroscopy showed that MB was completely removed by the filtration. A substantial amount of MO molecules were also removed in the process (Figure IV-18c, d). PUS-MOP-Aa could be reused after removing the absorbed dyes by treating with an acid followed by washing with ethanol as shown in Figure IV-19.

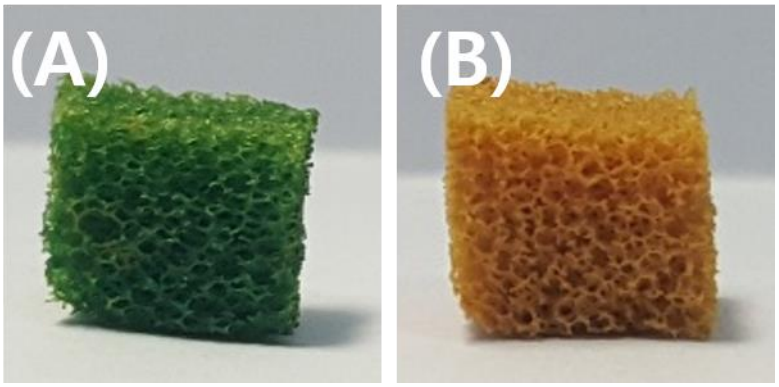

Figure IV-19. Photographs of MB-absorbed PUS-MOP-Aa taken (a) before and (b) after the desorption process.

IV-4. Conclusions

The facile synthesis of a compressible and hierarchically porous polymer composite was demonstrated by using a polymer sponge (PUS) as a template and the Sonogashira-Hagihara coupling reaction between aryl halides and alkynes. pH sensitive carboxyl groups were introduced to the microporous polymer using 2,5-diiodobenzoic acid as an aryl halide co-monomer. The polymer composite had a structure in which the macropores of PUS were filled with tubular and spherical microporous polymers. The polymer composite was treated with KOH, which converted the carboxyl groups to the carboxylate anions. The KOH treated polymer composite (PUS-MOP-Aa) was hydrophilic enough to be used as an absorbent in an aqueous solution. A manual compression and release of PUS-MOP-Aa in a polluted aqueous solution accelerated the absorption of pollutant molecules by pumping the solution into its meso- and micropores. PUS-MOP-Aa was able to preferentially absorb a cationic dye over an anionic dye. Thanks to the monolithic and compressible properties, PUS-MOP-Aa could be used in syringe filtration, which made it possible to remove the dye fast. A compressible and hierarchically porous material with water wettability is an excellent candidate for water purification. Related applications to other environmental concerns are also highly anticipated.

IV-5. References

1. Liang, Y.; Wu, B.; Wu, D.; Xu, F.; Li, Z.; Luo, J.; Zhong, H.; Fu, R.; Matyjaszewski, K. *J. Mater. Chem.* **2011**, *21*, 14424-14427.
2. Seo, M.; Kim, S.; Oh, J.; Kim, S. J.; Hillmyer, M. A. *J. Am. Chem. Soc.* **2015**, *137*, 600–603.
3. Du, R.; Zhang, N.; Xu, H.; Mao, N.; Duan, W.; Wang, J.; Zhao, Q.; Liu, Z.; Zhang, J. *Adv. Mater.* **2014**, *26*, 8053–8056.
4. Muñoz-Bonilla, A.; Fernández-García, M.; Rodríguez-Hernández, J. *Prog. Polym. Sci.* **2014**, *39*, 510–554.
5. Chalal, N.; Bouhali, H.; Hamaizi, H.; Lebeau, B.; Bengueddach, A. *Microporous Mesoporous Mater.* **2015**, *210*, 32-38.
6. Riachy, P.; Stébé, M. -J.; Lebeau, B.; Pasc, A.; Vidal, L.; Blin, J. -L. *Microporous Mesoporous Mater.* **2016**, *221*, 228-237.
7. Seo, M.; Hillmyer, M. A. *Science* **2012**, *336*, 1422–1425.
8. Saba, S. A.; Mousavi, M. P. S.; Bühlmann, P.; Hillmyer, M. A. *J. Am. Chem. Soc.* **2015**, *137*, 8896–8899.
9. Thomas, A.; Goettmann, F.; Antonietti, M. *Chem. Mater.* **2008**, *20*, 738–755.
10. Cagnon, B.; Py, X.; Guillot, A.; Stoeckli, F. *Microporous Mesoporous*

Mater. **2003**, *57*, 273–282.

11. Zhao, C.; Wang, W.; Yu, Z.; Zhang, H.; Wang, A.; Yang, Y. *J. Mater. Chem.* **2010**, *20*, 976.
12. He, X.; Zhao, N.; Qiu, J.; Xiao, N.; Yu, M.; Yu, C.; Zhang, X.; Zheng, M. *J. Mater. Chem. A* **2013**, *1*, 9440-9448.
13. Yang, X.; Tan, L.; Xia, L.; Wood, C. D.; Tan, B. *Macromol. Rapid Commun.* **2015**, *36*, 1553–1558.
14. He, Y.; Zhu, X.; Li, Y.; Peng, C.; Hu, J.; Liu, H. *Microporous Mesoporous Mater.* **2015**, *214*, 181-187.
15. Xu, Y.; Jin, S.; Xu, H.; Nagai, A.; Jiang, D. *Chem. Soc. Rev.* **2013**, *42*, 8012–8031.
16. Lim, Y.; Cha, M. C.; Chang, J. Y. *Sci. Rep.* **2015**, *5*, 15957.
17. Li, A.; Sun, H. -X.; Tan, D. -Z.; Fan, W. -J.; Wen, S. -H.; Qing, X. -J.; Li, G. -X.; Li, S. -Y.; Deng, W. -Q. *Energy Environ. Sci.* **2011**, *4*, 2062-2065.
18. Yang, R. -X.; Wang, T. -T.; Deng, W. -Q. *Sci. Rep.* **2015**, *5*, 10155.
19. Fan, W.; Liu, X.; Zhang, Z.; Zhang, Q.; Ma, W.; Tan, D.; Li, A. *Microporous Mesoporous Mater.* **2014**, *196*, 335–340.
20. Jiang, J. X.; Su, F.; Trewin, A.; Wood, C. D.; Niu, H.; Jones, J. T. A.; Khimyak, Y. Z.; Cooper, A. I. *J. Am. Chem. Soc.* **2008**, *130*, 7710–7720.

21. Moreland, J. C.; Wilkes, G. L.; Moreland, C. G.; Sankar, S. S.; Stejskal, E. O.; Turner, R. B. *J. Appl. Polym. Sci.* **1994**, *52*, 1175–1180.

22. Yang, Y.; Shi, E.; Li, P.; Wu, D.; Wu, S.; Shang, Y.; Xu, W.; Cao, A.; Yuan, Q. *Nanoscale* **2014**, *6*, 3585–3592.

23. Wang, L.; Wang, H.; Liu, F.; Zheng, A.; Zhang, J.; Sun, Q.; Lewis, J. P.; Zhu, L.; Meng, X.; Xiao, F. S. *ChemSusChem* **2014**, *7*, 402–406.

24. Shevchenko, L. L. *Russ. Chem. Rev.* **1963**, *32*, 201–207.

25. Van Kuringen, H. P. C.; Eikelboom, G. M.; Shishmanova, I. K.; Broer, D. J.; Schenning, A. P. H. J. *Adv. Funct. Mater.* **2014**, *24*, 5045–5051.

Chapter V.

Pd Nanoparticles Encapsulated and Hierarchically Porous Polymer Sponge for Semi-Continuous Reaction

V-1. Introduction

Microporous organic polymers (MOPs) have been successfully used as heterogeneous catalyst supports due to its various advantages such as high surface area, physicochemical stability, controllable chemical composition, and insolubility in reaction media enabling the catalysts to be easily recycled.[1-6] However, the mass transfer of the reagents and products can be inhibited due to limited space in MOPs, which reduces the reaction rate.[7]

For improving the mass transfer, 3-dimensional highly interconnected porous structures are desirable. A commercially available sponge is a promising basis for constructing 3-dimensional porous network structure. A number of studies used the sponges as a scaffold or a sacrificial scaffold for the various heterogeneous catalysts such as TiO_2 nanoparticles embedded in rGO,[8] metal nanosheets,[9] and nanowires.[10] The open macropore system of the sponge facilitates the passage of reactants to the catalyst surface.[10]

A number of studies have nicely demonstrated the concept of tea-bag-like catalysts.[11-14] Tea-bag-like catalysts are designed to be loaded into a reaction mixture like a tea bag. After being used, the catalysts could be removed easily from the system and reused in the next cycle.[11] Gaab group immobilized the dendritic catalysts in dialysis membrane bags.[12] Greiner group reported

poly(p-xylene) based immobilization of dendrimer[13] or Au NPs.[14] But the mass transfer is still one of problems to overcome.

The sponges which have highly porous interconnected network structures and the monolithic properties could be used in the same manner as a tea bag. In addition, the compressibility of sponge can improve the mass transfer problem because the simple compression and release process enhances the fluid exchange.[15,16] In this work, a Pd NPs encapsulated microporous organic polymer/polyurethane sponge composite (S-M-Pd) was prepared by carrying out the Sonogashira-Hagihara coupling reaction of an aryl halide and an alkyne whitin a polyurethane sponge. After the reaction, the Pd catalysts dispersed over the microporous organic polymer were used as a precursor for Pd NPs. The catalytic performance of the catalyst composite for the 4-nitrophenol reduction reaction and the Suzuki-Miyaura coupling was investigated. The catalyst composite was fitted into a syringe, and used for methylene blue reduction reaction, showing its application possibility for a semi-continuous flow reaction.

V-2. Experimental

Materials. 1,3,5-Triethynylbenzne, 1,4-diiodobenzene and sodium borohydride ($NaBH_4$) were purchased from TCI. 2,5-Diiodobenzoic acid, bis(triphenylphospine)palladium(II) dichloride and copper iodide were purchased from Sigma-Aldrich. Toluene and triethylamine (TEA) were purchased from Junsei. Sodium hydroxide was purchased from Daejung Chemical & Metals Co. All chemicals were used without any further purification. Urethane sponge was purchased from 3M and washed with ethanol and acetone before using. All other solvents and reagents were in chemically pure grade and used as purchased.

Preparation of S-M-Pd, S-M, and M. S-M-Pd: 1,3,5-Triethynyl benzene (150 mg, 1 mmol), 1,4-diiodobenzne (264 mg, 0.8 mmol) and 2,5-diiodobenzoic acid (75 mg, 0.2 mmol) were dissolved in toluene and TEA (9 mL, 2:1, v/v) and the solution was transferred to a 20 mL vial. After adding $PdCl_2(PPh_3)_2$ (210 mg, 0.3 mmol) to the solution, a cylindrical polyurethane sponge (diameter - 2 cm, height - 2 cm, 90 mg) was placed in the vial. A solution of CuI (19 mg, 0.1 mmol) in toluene and TEA (1 mL, 2:1, v/v) was added to the mixture quickly. The reaction was carried out at room temperature for 12 h without stirring. After filtration, the polymer composite was heated up

to 60 °C in a 0.1 M NaOH solution in ethanol, water and N,N-dimethylformamide (50 mL, 1:1:1, v/v/v) for 24 h. The resulting polymer composite was filtered, washed with water, ethanol, tetrahydrofuran and Soxhlet extracted with methanol. The polymer was dried in vacuo at 90 °C for 48 h. S-M-Pd was obtained as dark brownish sponge (190 mg). FT-IR (KBr, cm^{-1}): 3300, 3050, 2957, 2921, 2850, 2205, 1784, 1681, 1582, 1506, 1455, 1406, 1376, 1102, 1014, 878, 834, 679, 603, 546.

S-M (polyurethane sponge with the microporous polymer): S-M was prepared by the same procedure for synthesis of S-M-Pd but the reduction of palladium catalysts was omitted. S-M was obtained as brownish sponge (170 mg). FT-IR (KBr, cm^{-1}): 3369, 3289, 3050, 2982, 2208, 1796, 1718, 1580, 1508, 1438, 1406, 1359, 1094, 1012, 958, 875, 836, 680, 540.

M (Microporous polymer): M was prepared by the same procedure for synthesis of S-M without the polyurethane sponge. M was obtained as brittle brownish monolith. FT-IR (KBr, cm^{-1}): 3417, 3295, 3050, 2976, 2202, 1792, 1714, 1580, 1508, 1438, 1406, 1359, 1094, 1012, 958, 875, 836, 680, 540.

4-Nitrophenol reduction reaction. To an aqueous ethanol solution (10 mL,

1:1, v/v) of 4-nitrophenol (0.1 mM) and sodium borohydride (0.1 M), 20 mg of S-M-Pd was added. The reaction carried out with or without compression and release of S-M-Pd at a rate of 3 s per cycle.

The Suzuki-Miyaura reaction. Bromobenzene (0.053 mL, 0.5 mmol), phenylboronic acid (91.4 mg, 0.75 mmol) and K_2CO_3 (138 mg, 1 mmol) were added in 4 mL of aqueous ethanol (1:1, v/v). The reaction was carried out at 60 ^oC, and S-M-Pd was compressed and released at a rate of 3 s per cycle.

Methylene blue reduction reaction using S-M-Pd as a semi-continuous flow reactor. A cylindrical S-M-Pd was fitted into a 10 mL of syringe. A aqueous ethanol solution (10 mL, 1:1, v/v) of methylene blue (0.2 mM) with sodium borohydride (0.1 M) was transferred to the syringe.

Instrumental Characterization. ^1H NMR spectra were recorded on a Bruker Avance 300 spectrometer (300 MHz). Solid-state ^{13}C NMR spectra were recorded on a Bruker Avance 400WB spectrometer (100 MHz) equipped with a CP-MAS probe. TGA measurements were performed on a TA modulated TGA2050 with a heating rate of 10 $^oC\ min^{-1}$ under nitrogen. Fourier transform infrared (FT-IR) measurements were made on a PERKIN ELMER Spectrum GX I using KBr pellets. N_2 uptake amounts were measured by using a Belsorp-Max (BEL Japan, Inc.) apparatus. UV-Vis spectra were obtained with the use of

a Sinco S-3150 spectrometer. SEM images were obtained by using a JEOL JSM-6330F microscope. Energy-dispersive X-ray spectroscopy (EDS) elemental maps were obtained using Oxford instrument X-Max^N detector and analyzed with AZtecEnergy EDS analysis. Transmission electron microscopy images were obtained by using a JEOL JEM-2010 microscope at 200 keV. The compression test was performed on KES-FB3 autometic compression tester. ICP (Inductively Coupled Plasma) emission spectrometer was measured using VARIAN 730ES. GC-MS measurements were performed on a ISQ LT. X-ray photoelectron spectroscopy (XPS) measurements were performed on a KRATOA AXIS-His spectrometer equipped with a Mg K_α X-ray source.

V-3. Results and Discussion

V-3-1. Synthesis and Characterization

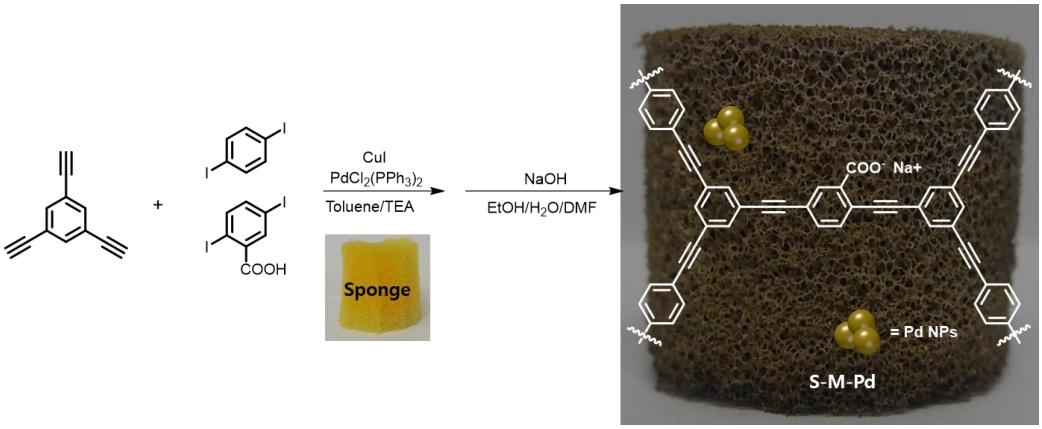

Scheme V-1. Synthesis of S-M-Pd.

Scheme V-1 shows the synthetic method for the S-M-Pd. For the synthesis of the S-M-Pd, a polyurethane sponge (S) was soaked in a solution of 1,3,5-triethynyl benzene, 1,4-diiodobenzne and 2,5-diiodobenzodic acid in toluene/TEA (2:1, v/v) and the Sonogashira-Hagihara coupling reaction was carried out at room temperature without stirring. 1,4-Diiodobenzene was used as a major halide and 2,5-diiodobenzoic acid was used to provide carboxyl functionality, which could adjust wettability to aqueous environment.[17,18] The palladium catalysts which were used for the Sonogashira-Hagihara coupling reaction would be remained and wholly dispersed over the polymers. They were used as precursors for Pd NPs. Combining the reduction of palladium complex

with in situ catalyzed polymerization enables confinement of Pd NPs in the polymer network.[2,19,20] Pd NPs were prepared by soaking the composite into 0.1 M NaOH solution in ethanol, water and N,N-dimethylformamide (50 mL, 1:1:1, v/v/v) at 60 ^{o}C for 24 h. Hydroxide ions were responsible for the reduction of Pd(II).[21,22] While carrying out this procedure, the carboxylic acid groups were transformed to the carboxylate anions, which enhance the wettability to aqueous environment.

The polymer structures were characterized by solid state ^{13}C cross-polarization/magic angle spinning NMR (CP/MAS NMR) spectroscopy (Figure V-1a). The peaks at 136, 131 and 123 ppm were observed, which corresponded to the aromatic carbons bonded to carboxylic carbon, hydrogen and acetylene carbon, respectively. The peak at 90 ppm was assigned to acetylene carbons. The peaks at 157, 75 and 17 ppm were derived from the polyurethane sponge.[23] In the case of TGA thermogram, the composite polymer degradation ranging from 250 ^{o}C to 350 ^{o}C was mainly originated from the polyurethane sponge (Figure V-1b). The degradation over 350 ^{o}C was mainly due to the microporous polymers. Compared with TGA thermogram of S-M, the Pd content of S-M-Pd was estimated to about 10 wt% (Figure V-2). This result was consistent with the ICP analysis. In the case of FT-IR spectrum, all of the bands from the polyurethane sponge and microporous polymers were shown including

the peak at 3300 cm^{-1} from C-H stretching vibration of the terminal alkynes and the peak at 2205 cm^{-1} from -C≡C- stretching vibration (Figure V-1c). The peaks appeared at 1510 ~ 1650 cm^{-1} and ~1400 cm^{-1} were originated from the CO_2^- asymmetric and symmetric stretching vibration, respectively, which confirmed the existence of the carboxylate anions in the S-M-Pd.[24] The XRD pattern showed amorphous characters of microporous polymers and the most representative reflections of Pd(0), which indexed fcc structure. The reflection peaks at 40.1°, 46.5° and 68.1° were corresponded to the indexed planes of the crystals of Pd(0) (111), (200) and (220), respectively.[25]

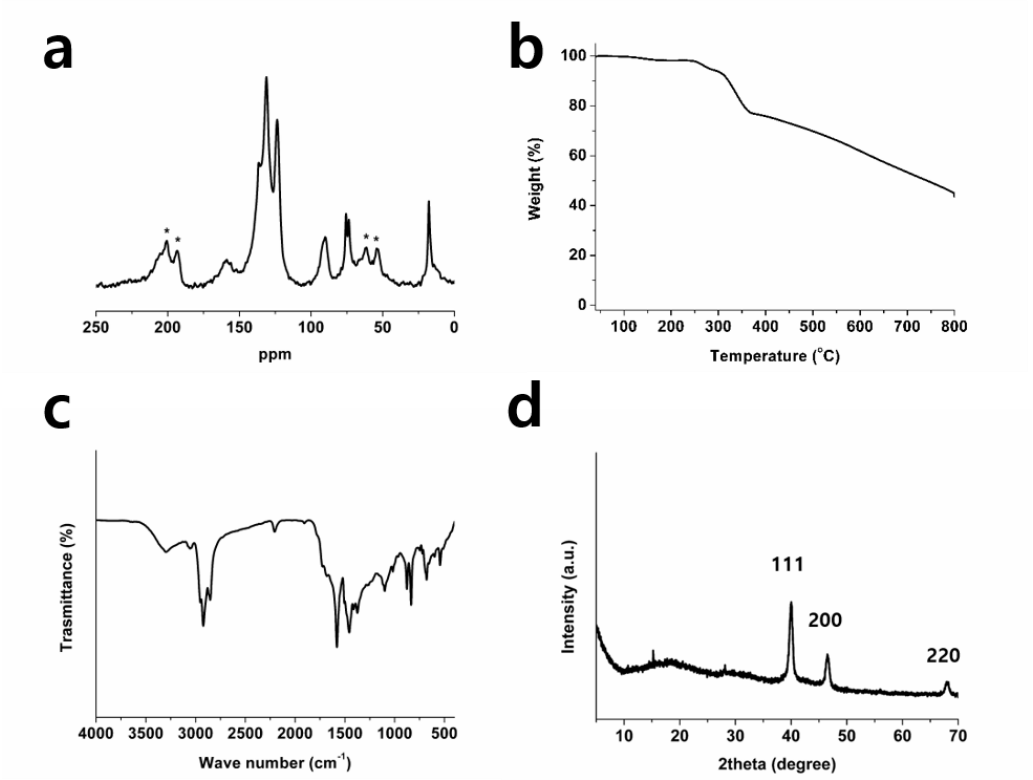

Figure V-1. (a) ^{13}C CP/MAS solid NMR spectrum, (b) TGA thermogram, (c) FT-IR spectrum, and (d) XRD pattern of S-M-Pd.

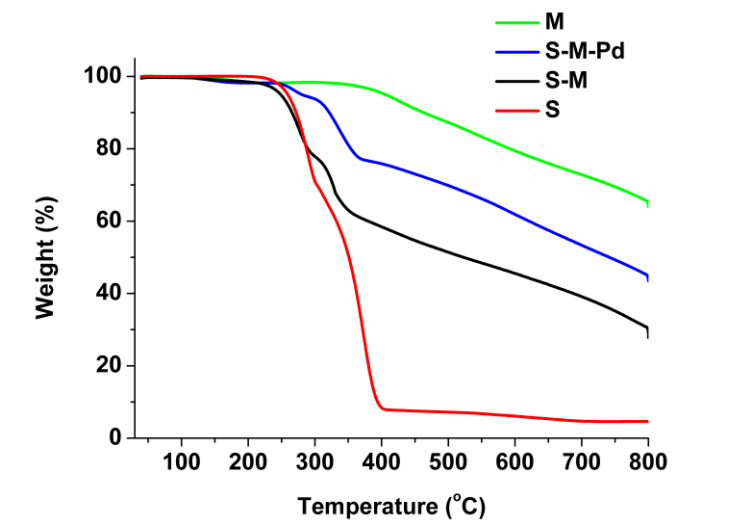

Figure V-2. TGA thermograms of M, S-M-Pd, S-M, and S.

Figure V-3 shows the microstructures of S-M-Pd observed by SEM. The polyurethane sponge indicated by white arrow was shown in the Figure V-3a. The microstructures of the microporous polymers were fibrous structures with spherical particles. The fibers were micrometer scale in length and the spherical particles were micrometer scales in diameter. The fibers had open ends, indicating tube-like structures, which was often observed in the structural analogues like the conjugated microporous polymers series (Figure V-3c).[16,26] Pd NPs were not discernable in SEM images, but could be observed in TEM images. Pd NPs with size in the range of 5 – 30 nm were wholly distributed over the spherical particles and tubes (Figure V-4). The EDS mapping of Pd also supported the results (Figure V-5). XPS analysis revealed two broad peaks

at 335.74 eV from Pd(0) $3d_{5/2}$ and 337.19 eV from Pd(II) $3d_{5/2}$, suggesting the existence of Pd(0) and Pd(II) (Figure V-6).[1,4,5]

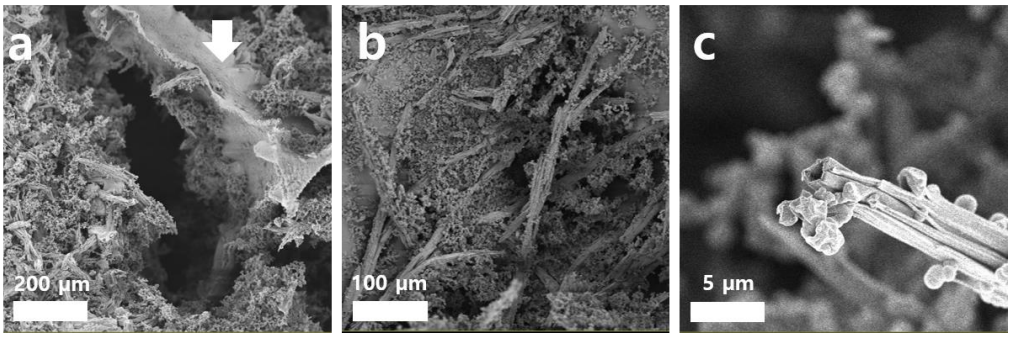

Figure V-3. SEM images of S-M-Pd (a white arrow indicates the polyurethane sponge).

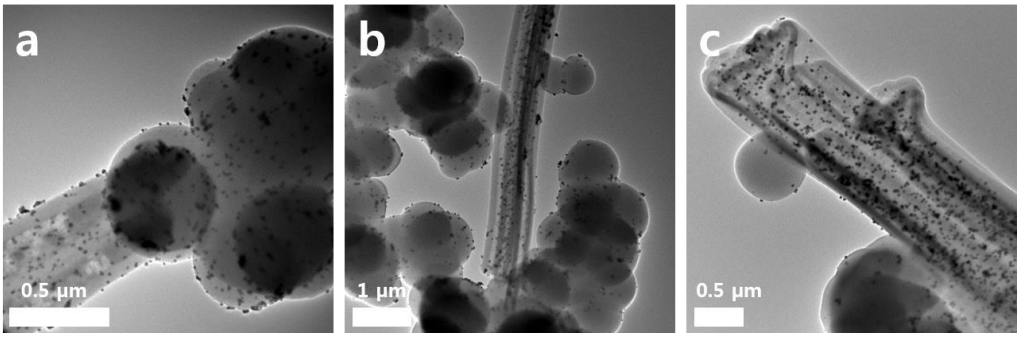

Figure V-4. TEM images of S-M-Pd.

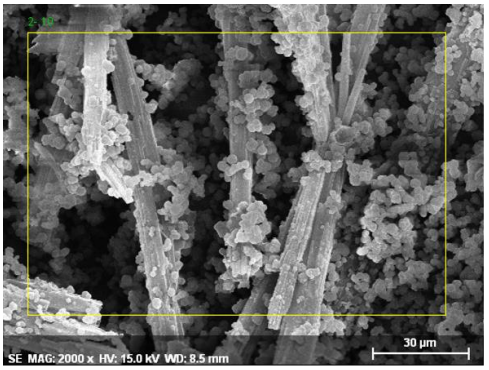

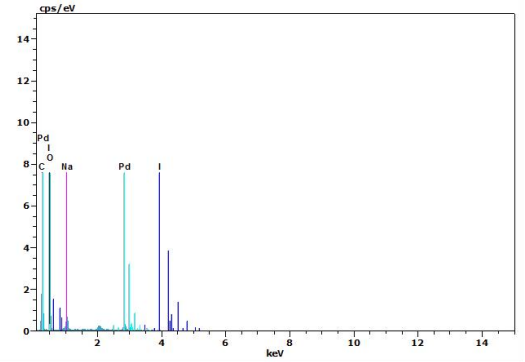

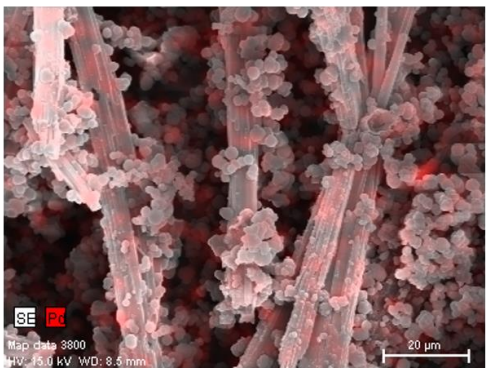

Element	C	O	Pd	Na	I
wt (%)	69.79	18.17	6.84	4.86	0.34
at (%)	80.43	15.72	0.89	2.92	0.04

Figure V-5. EDS mapping of S-M-Pd for Pd.

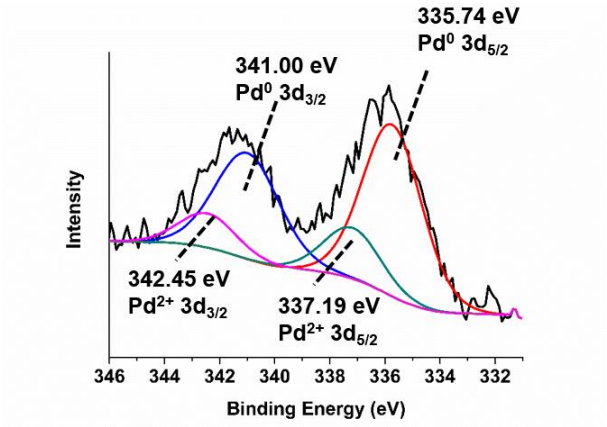

Figure V-6. Pd 3d XPS spectrum of S-M-Pd.

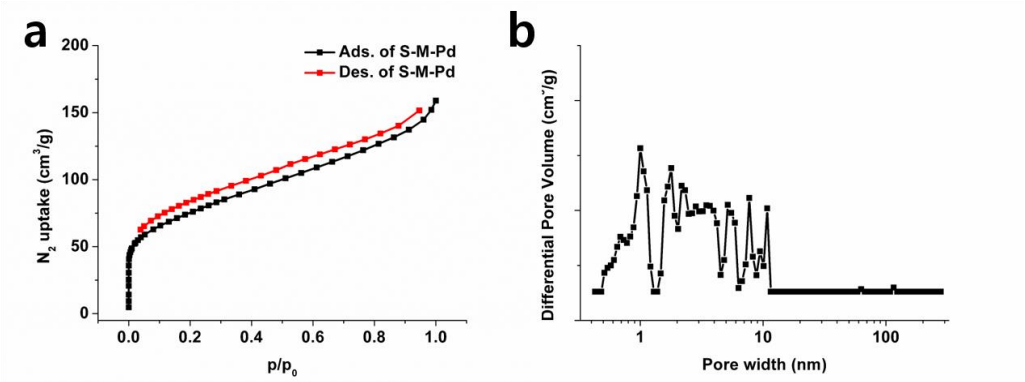

Figure V-7. (a) N_2 adsorption-desorption isotherms measured at 77 K and (b) NL-DFT pore size distribution of S-M-Pd.

The N_2 adsorption-desorption isotherms and pore size distributions are shown in Figure V-7. The Brunauer-Emmett-Teller (BET) surface area of S-M-Pd calculated from the N_2 adsorption isotherms was 270 m^2g^{-1}. The microporous polymer (M) and microporous polymer with sponge (S-M) showed 340 m^2g^{-1} and 306 m^2g^{-1}, respectively (Figure V-8). In the case of the pore size distributions from the Nonlocal density functional theory (NL-DFT) showed that the polymer had micro-, meso- and macropores. These results supported that S-M-Pd has hierarchical pore structures.

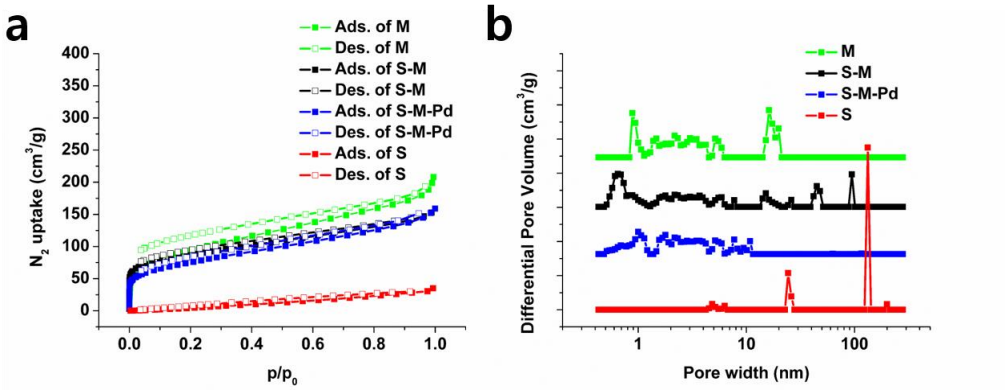

Figure V-8. (a) N_2 adsorption-desorption isotherms and (b) NL-DFT pore size distributions of M, S-M, S-M-Pd, and S.

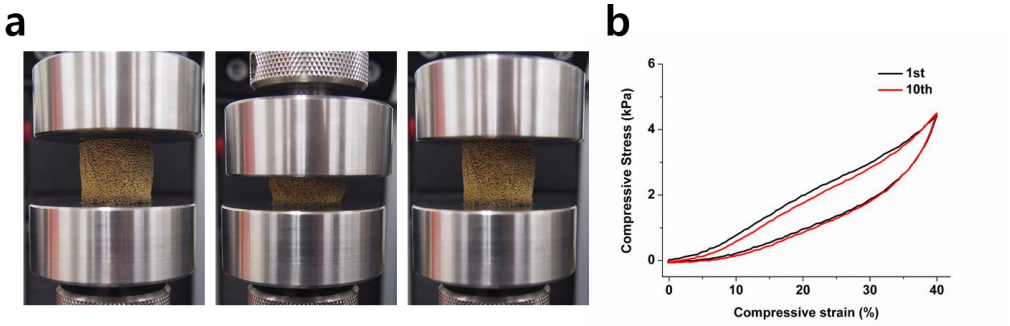

Figure V-9. (a) Sequential images of S-M-Pd in as-prepared, compressed, and released state and (b) compressive stress-strain curves of S-M-Pd for the 1st and 10th cycles.

The S-M-Pd had reversible compressibility. It recovered its initial shape after the removal of the external force (Figure V-9a). The compression test of S-

M-Pd shows no significant change in the stress-strain behavior during 10 cycles of compression and release, indicating a high mechanical stability of the polymer against the compressive force.

V-3-2. 4-Nitrophenol Reduction Reaction and the Suzuki-Miyaura Coupling Reaction

Taking advantages of hierarchical porous structures and mechanical stability against compressible stress, S-M-Pd was utilized as a tea-bag-like catalyst. The 4-nitrophenol reduction reaction was monitored by the UV-Vis absorption spectroscopy. A cube of S-M-Pd (20 mg) obtained by cutting with knife was immersed in an aqueous ethanol solution (10 mL) of 4-nitrophenol (0.1 mM) with the sodium borohydride (0.1 M). The absorption peak at 400 nm, which was attributed to 4-nitrophenolate ion, was gradually decreased with increasing the reaction time. When S-M-Pd was compressed and released at a rate of 3 s per cycle, the reaction was completed in 5 min. On the other hands, it took 30 min in the static condition without the compression and release. It seemed that while the S-M-Pd was compressed and released repeatedly, the fluid exchange took place vigorously, and thereby the mass transfer of reactants was enhanced. The reaction with compression and release cycles was 6 times

faster than in the static condition. To recycle the S-M-Pd, the centrifugation or filtration was not needed. Only after being removed out of the solution and washing with organic solvents, it could be used for the next reaction. During the successive 5 reactions, there was no significant decrease in catalytic ability.

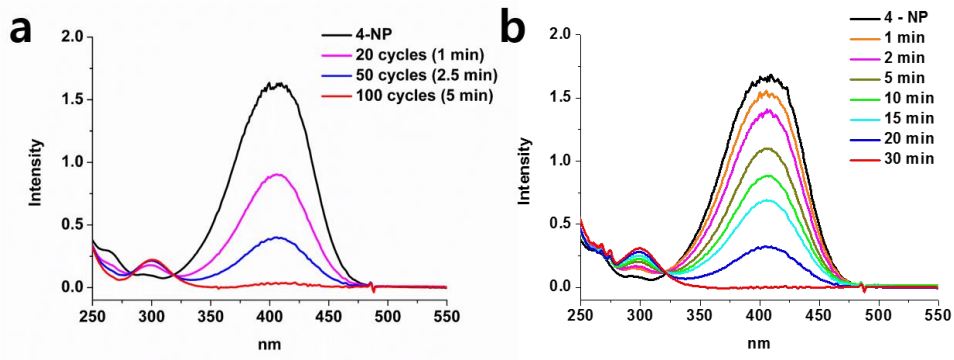

Figure V-10. UV-Vis absorption spectra measured during the 4-nitrophenol reduction reaction with S-M-Pd under (a) compression and release, and (b) static conditions.

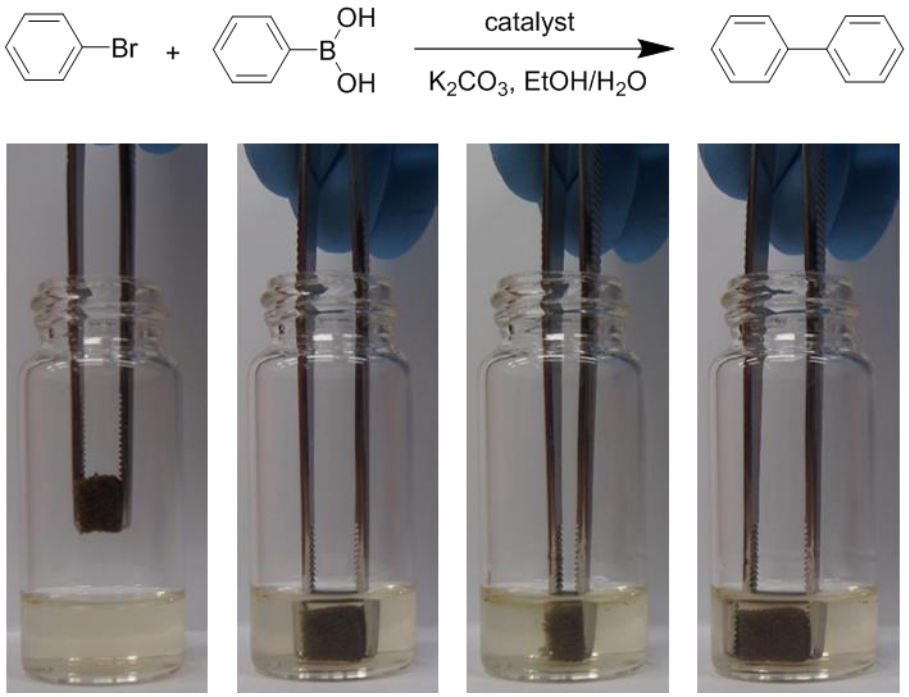

Figure V-11. Suzuki-Miyaura coupling reaction using S-M-Pd. Sequential photographs taken during the compressed and release process.

The Suzuki-Miyaura coupling reaction was also carried out under aerobic condition (Figure V-11). To a solution of bromobenzene (0.5 mmol), phenylboronic acid (0.75 mmol) and K_2CO_3 (1 mmol) in 4 mL of aqueous ethanol (1:1, v/v), a cube of S-M-Pd (20 mg) was immersed. The compression and release of S-M-Pd were performed at a rate of 3 s per cycles in the reaction mixture. The reaction proceeded in about 80 % after 30 min and was completed after 1 h when checked by GC-MS and ^{1}H-NMR spectroscopy (Figure V-12).

The recycled S-M-Pd could be used for the Suzuki-Miyaura coupling reaction at least 5 times without significant loss of catalytic activity. The ICP analysis of the reaction mixture showed almost no Pd species leaching (< 0.3 %) during 5 cycles of the reaction.[27]

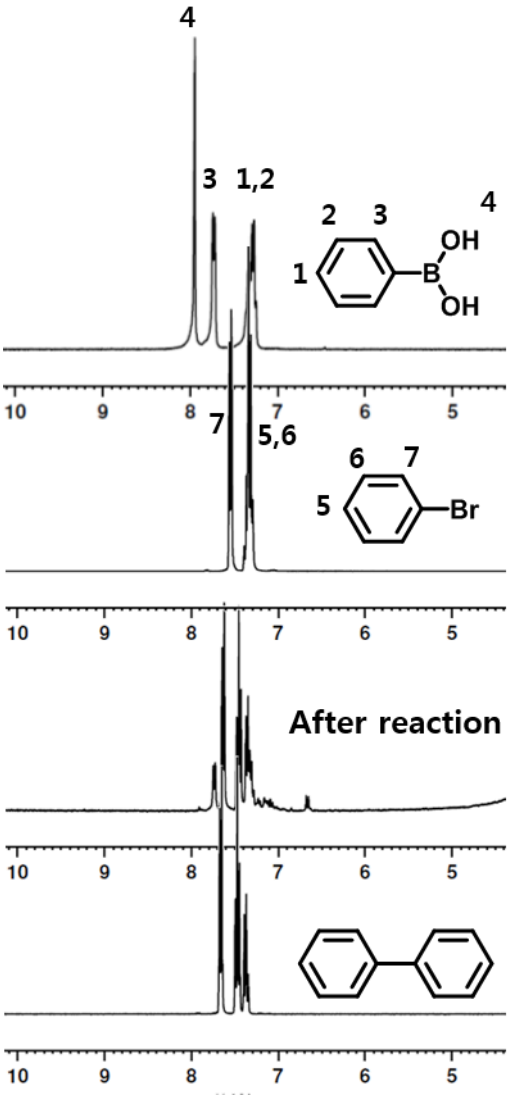

Figure V-12. ^{1}H-NMR spectra of phenylboronic acid, bromobenzene, reaction mixture after 1 h, and biphenyl in DMSO-d_6.

V-3-3. Semi-Continuous Flow Reactor for Methylene Blue Reduction Reaction

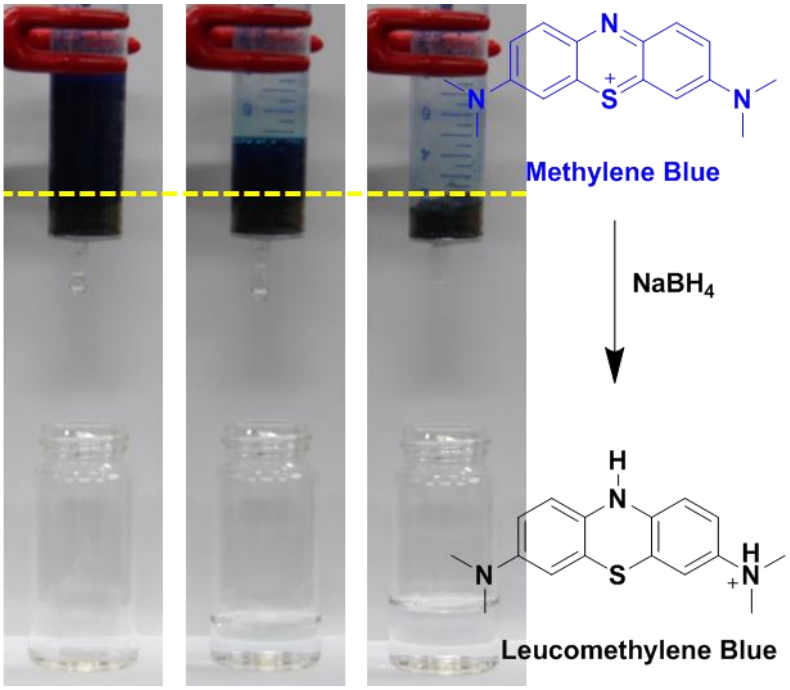

Figure V-13. Sequential photographs taken during the methylene blue reduction reaction using a S-M-Pd as a semi-continuous flow reactor. The yellow line indicates S-M-Pd.

S-M-Pd could be prepared in various shapes by cutting with a knife. A cylindrical S-M-Pd was prepared to fit into a syringe (10 mL) and used for a semi-continuous flow reaction. In the continuous flow reaction system, the catalyst is typically placed in a packed-bed reactor and the reaction mixture is

flown through the reactor using appropriate pumping system.[28-30] Similarly, the reaction mixture was put into the syringe and passed throguth S-M-Pd for the reaction. The methylene blue reduction reaction was chosen as an exemplary application. An aqueous ethanol solution (5 mL, 1:1, v/v) of methylene blue (0.2 mM) with sodium borohydride (0.1 M) was transferred to the syringe reactor. The reaction proceeded while passing through S-M-Pd to yield colorless leucomethylene blue (Figure V-13). The flow rate was about $1mLmin^{-1}$, and no undesirable leakage was observed due to the tight fitting of S-M-Pd. The UV-Vis spectrum of the solution coming out of the syringe showed no absorption peak of methylene blue, indicating its complete consumption (Figure V-14). There was a possible chance of absorption of methylene blue molecules in the S-M-Pd due to the large surface area, micro pores and the anionic charge character on the surface of the polymer.[16,31] When a methylene blue solution containing no sodium borohydride was used, the blue colored solution came out of the syringe (Figure V-15). However, the intensity of UV-Vis absorption spectra of methylene blue decreased after passing through the S-M-Pd, indicating some dye molecules were adsorbed on S-M-Pd (Figure V-16). The amount of absorbed dye molecules was estimated to be about 0.21 μmol (20 %) by UV-Vis spectroscopy (an extinction coefficient of methylene blue: 54447 $M^{-1}cm^{-1}$). The adsorbed molecules in S-

M-Pd came out by washing with ethanol and the reactor could be used for several more successive reactions without further purification.

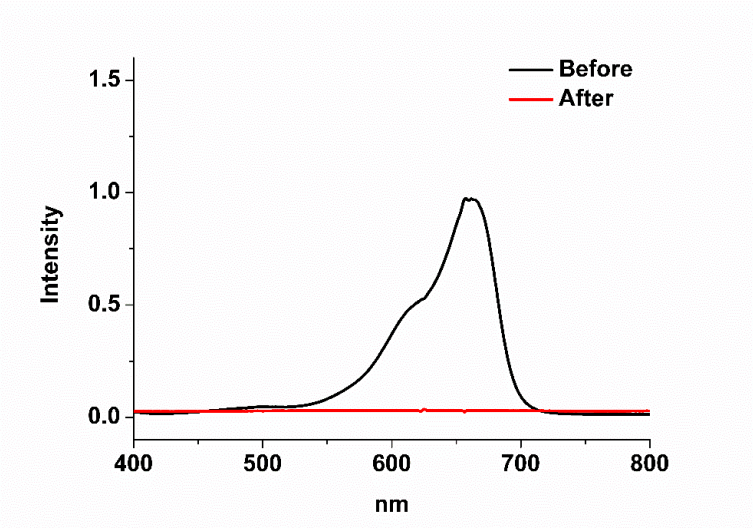

Figure V-14. UV-Vis absorption spectra of methylene blue with $NaBH_4$ before and after passing through the S-M-Pd. The original methylene blue solution was diluted 10 times (0.02 mM).

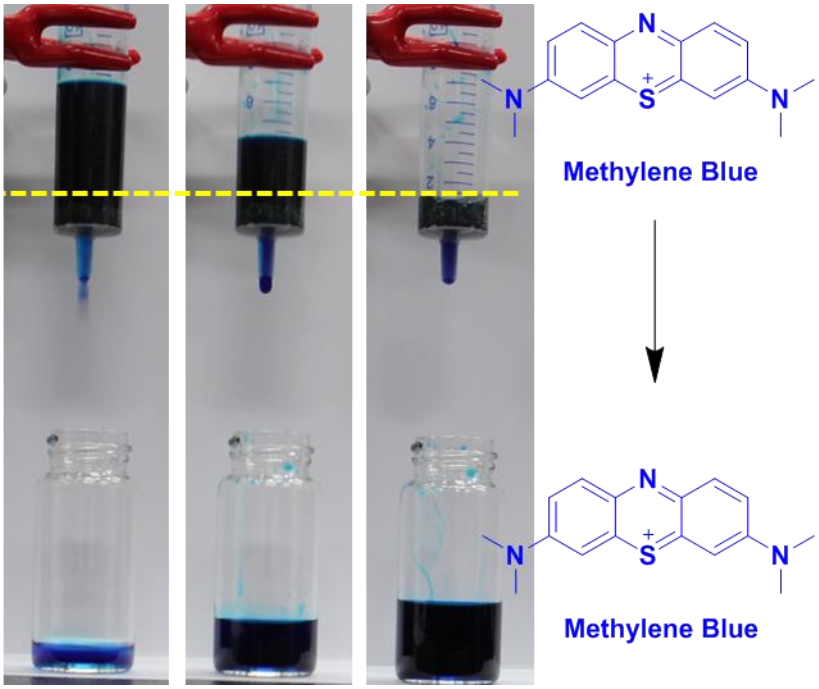

Figure V-15. Sequential photographs taken during a methylene blue solution (0.2 mM) without $NaBH_4$ passed through a semi-continuous flow reactor.

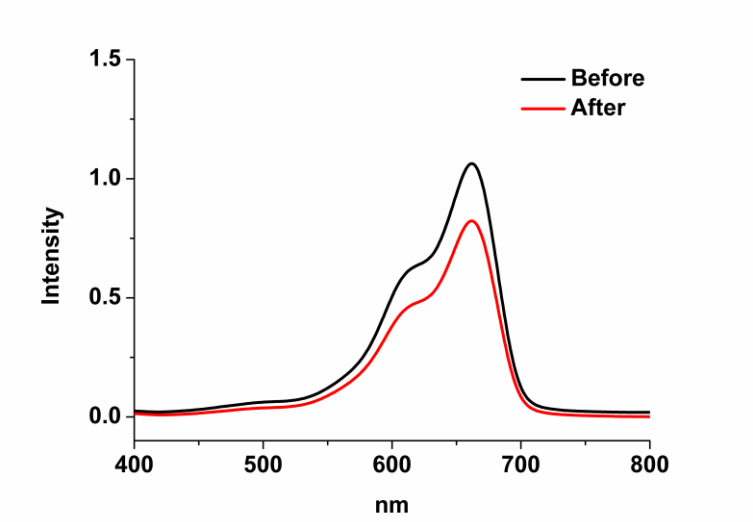

Figure V-16. UV-Vis absorption spectra of methylene blue without $NaBH_4$ before and after passing through the S-M-Pd. The methylene blue solution before and after passing through the S-M-Pd were diluted 10 times.

V-4. Conclusion

A compressible heterogeneous catalyst (S-M-Pd) was prepared, which consisted of the polyurethane sponge and the Pd NPs encapsulated microporous polymer. The monolithic S-M-Pd has highly interconnected porous structure and mechanical stability against compressive stress. These properties allow the S-M-Pd to being used as a tea-bag-like catalyst for the 4-nitrophenol reduction reaction and the Suzuki-Miyaura coupling reaction. The compression and release process in the reaction mixtures enhanced the mass transfer of the reactants to the catalyst surface, resulting in the considerable increase of the reaction rate. S-M-Pd was easily recycled and reused without significant loss of catalytic activity. After being fitted into syringe, S-M-Pd was successfully used for the semi-continuous reduction reaction of methylene blue with sodium borohydride. The heterogeneous catalysts with a hierarchical porous structure , compressible and monolithic properties are expected to find applications in a variety of batch and continuous reactions.

V-5. References

1. Li, L.; Chen, Z.; Zhong, H.; Wang, R. *Chem. Eur. J.* **2014**, *20*, 3050–3060.
2. Jiang, X.; Zhao, W.; Wang, W.; Zhang, F.; Zhuang, X.; Han, S.; Feng, X. *Polym. Chem.* **2015**, *6*, 6351–6357.
3. Rangel, E. R.; Maya, E. M.; Sánchez, F.; de la Campa, J. G.; Iglesias, M. *Green Chem.* **2015**, *17*, 466–473.
4. Li, L.; Zhou, C.; Zhao, H.; Wang, R. *Nano Res.* **2015**, *8*, 709–721.
5. Li, L.; Zhao, H.; Wang, R. *ACS Catal.* **2015**, *5*, 948–955.
6. Sun, Q.; Dai, Z.; Meng, X.; Wang, L.; Xiao, F. -S. *ACS Catal.* **2015**, *5*, 4556–4567.
7. Wang, Z.; Chen, W.; Han, Z.; Zhu, J.; Lu, N.; Yang, Y.; Ma, D.; Chen, Y.; Huang, S. *Nano Res.* **2014**, *7*, 1254–1262.
8. Jing, L.; Tan, H. L.; Amal, R.; Ng, Y. H.; Sun, K. -N. *J. Mater. Chem. A* **2015**, *3*, 15675–15682.
9. Ye, K.; Zhang, D.; Zhang, H.; Cheng, K.; Wang, G.; Cao, D. *Electrochim. Acta* **2015**, *178*, 270–279.
10. Ge, J.; Wang, X.; Yao, H. -B.; Zhu, H. -W.; Peng, Y. -C.; Yu, S. -H. *Mater. Horiz.* **2015**, *2*, 509–513.

11. Fan, L.; Yi, R.; Yu, L.; Wu, Y.; Chen, T.; Guo, R. *Catal. Sci. Technol.* **2012**, *2*, 1136–1139.

12. Gaab, M.; Bellemin-Laponnaz, S.; Gade, L. H. *Chem. Eur. J.* **2009**, *15*, 5450–5462.

13. Lindner, J. -P.; Röben, C.; Studer, A.; Stasiak, M.; Ronge, R.; Greiner, A.; Wendorff, H. -J. *Angew. Chem. Int. Ed.* **2009**, *48*, 8874–8877.

14. Mitschang, F.; Schmalz, H.; Agarwal, S.; Greiner, A. *Angew. Chem. Int. Ed.* **2014**, *53*, 4972–4975.

15. Yang, Y.; Shi, E.; Li, P.; Wu, D.; Wu, S.; Shang, Y.; Xu, W.; Cao, A.; Yuan, Q. *Nanoscale* **2014**, *6*, 3585–3592.

16. Lim, Y.; Cha, M. C.; Chang, J. Y. *Sci. Rep.* **2015**, *5*, 15957.

17. Liu, F.; Wang, L.; Sun, Q.; Zhu, L.; Meng, X.; Xiao, F. -S. *J. Am. Chem. Soc.* **2012**, *134*, 16948–16950.

18. Wang, L.; Wang, H.; Liu, F.; Zheng, A.; Zhang, J.; Sun, Q.; Lewis, J. P.; Zhu, L.; Meng, X.; Xiao, F. -S. *ChemSusChem* **2014**, *7*, 402–406.

19. Wang, F.; Mielby, J.; Richter, F. H.; Wang, G.; Prieto, G.; Kasama, T.; Weidenthaler, C.; Bongard, H. -J.; Kegnæs, S.; Fürstner, A.; Schüth, F. *Angew. Chem. Int. Ed.* **2014**, *53*, 8645–8648.

20. Ishida, T.; Onuma, Y.; Kinjo, K.; Hamasaki, A.; Ohashi, H.; Honma, T.; Akita, T.; Yokoyama, T.; Tokunaga, M.; Haruta, M. *Tetrahedron* **2014**,

70, 6150–6155.

21. Grushin, V. V.; Alper, H. *Organometallics* **1993**, *12*, 1890–1901.
22. Amatore, C.; Kaïm, L. E.; Grimaud, L.; Jutand, A.; Meignié, A.; Romanov, G. *Eur. J. Org. Chem.* **2014**, ***22***, 4709–4713.
23. Moreland, J. C.; Wilkes, G. L.; Moreland, C. G.; Sankar, S. S.; Stejskal, E. O.; Turner, R. B.; *J. Appl. Polym. Sci.* **1994**, *52*, 1175–1180.
24. Shevchenko, L. L. *Russ. Chem. Rev.* **1963**, ***32***, 201–207.
25. Wu, Z.; Jiang, H. *RSC Adv.* **2015**, ***5***, 34622–34629.
26. Tan, D.; Xiong, W.; Sun, H.; Zhang, Z.; Ma, W.; Meng, C.; Fan, W.; Li, A. *Microporous Mesoporous Mater.* **2013**, *176*, 25–30.
27. Qian, H.; He, Q.; Zheng, J.; Li, S.; Zhang, S. *Polymer* **2014**, *55*, 550–555.
28. Jas, G.; Kirschning, A. *Chem. Eur. J.* **2003**, *9*, 5708–5723.
29. Frost, C. G.; Mutton, L. *Green Chem.* **2010**, *12*, 1687–1703.
30. Cantillo, D.; Kappe, C. O. *ChemCatChem* **2014**, *6*, 3286–3305.
31. van Kuringen, H. P. C.; Eikelboom, G. M.; Shishmanova, I. K.; Broer, D. J.; Schenning, A. P. H. J. *Adv. Funct. Mater.* **2014**, *24*, 5045-5051.

국문요약

유기젤은 물리적 혹은 화학적인 가교결합으로 이루어진 3차원적인 네트워크 구조와 많은 양의 유기용매로 구성되어있다. 작은 분자의 자기조립 현상은 물리적인 가교구조를 이루는 반면 두 개, 세 개 내지 여러 개의 중합기를 가진 단위체의 중합반응은 화학적인 가교구조를 이룬다. 본 연구에서는 반응성 유기젤을 이용하여 기능성 고분자 재료를 합성하고 재료의 특성과 응용 가능성을 조사하였다.

먼저 물리적 가교결합을 이루는 중합이가능한 유기젤로부터 열변색성 고분자 나노콤포지트 필름을 제조하였다. 유기젤화제 (**1**) 은 3,4,5-tris(ω-decenyl)benzamide 그룹이 quarterthiophene 코어에 아마이드 결합으로 연결된 구조를 가지며 유기젤화제 (**2**) 는 전체적으로는 (**1**)과 같은 구조이나 tris(ω-decenyl) 이 tris(ω-decanyl)로 치환된 구조이다. MMA 하에서 형성된 유기젤을 광중합을 통해 PMMA 나노콤포지트 필름을 제조하였다. PMMA – **1** (0.5 wt%)은 가역적인 열변색성을 보였다. 365 nm 빛 하에서 발광특성이 120 ºC까지 열을 가함에 따라 주황색에서 밝은 초록색으로 변하였고, 상온으로 식혔을 때 다시 주황색으로 돌아왔다. 반면 유기젤화제 **2**로부터 제조한 PMMA 나노콤포지

트 필름은 가역적인 열변색성을 보이지 않았다. PMMA - **1** 의 가역적 열변색성은 PMMA 매트릭스 내에 공유결합으로 연결되어 있는 올리고싸이오펜 그룹의 열가역적인 conformational 변화서 기인한 것으로 추정하였다.

두 번째로, 1,4-diiodobenzene과 1,3,5-triethynylbenzene의 소노가시라-하기하라 반응을 별도의 스터링 없이 보낼 시 화학적인 가교결합을 이루는 유기젤을 형성함을 이용하여 압축성이 있고 산과 염기 그룹이 각각 도입된 위계적 기공성 고분자를 제조하였다. 먼저 1,4-diiodobenzene과 1,3,5-triethynylbenzene의 소노가시라-하기하라 반응일 이용하여 고분자 (HM) 를 제조하고, 각각 sulfonation 반응과 추가적인 소노가시라 반응을 통해 산과 염기 그룹을 도입하였다. SO_3H 그룹이 부여된 고분자 (HM-A) 와 방향족 $–NH_2$ 그룹이 부여된 고분자 (HM-B) 모두 압축성이 있는 단일체로 제조 되었고 위계적 기공성을 보였다. HM-A와 HM-B를 잘라 차례로 주사기에 넣고 semi-continuous flow reactor로 사용하였다. 산성 촉매를 사용하는 반응인 benzaldehyde dimethyl acetal의 deacetalization 반응 후 염기성 촉매를 사용하는 반응인 maloronitrile과의 knoevenagel condensation 반응을 순차적으로 보낸 결과, 반응이 성공적으로 이루어졌고 일반적인 배치에서 반응시키는

것보다 용매의 사용량과 시간이 훨씬 적게 소모되었다. 제조된 고분자 촉매는 촉매의 활성이 크게 감소하지 않고 재사용이 용이하였다.

세 번째로, 폴리우레탄스폰지 (PUS) 안에서 1,3,5-triethynyl benzene, 1.4-diiodobenzene 그리고 2,5-diiodobenzoic acid 의 소노가시라-하기하라 반응을 통해 PUS와 함께 화학적 가교결합을 이루는 유기젤을 형성시킨 후 압축성이 있는 위계적 기공성 고분자 (PUS-MOP-A)를 제조하였다. 기공표면에 산성 기능기를 부여하기위해 2,5-diiodobenzoic acid를 공단위체로 사용하였다. 1,4-Diiodobenzene을 주요 단위체로 사용하였을 때 생성되는 미세기공성고분자가 파이버 형태를 지녔고, PUS-MOP-A의 경우 1,4-diiodobenzene과 2,5-diiodobenzoic acid를 4:1 의 비율로 사용하였다. 306 m^2g^{-1}의 BET 넓은 비표면적을 지닌 PUS-MOP-A를 KOH에 담가 표면의 carboxyl 그룹을 carboxylate 음이온으로 바꾸었다. 이렇게 제조된 PUS-MOP-Aa는 0 도의 물 접촉각을 보이며 빠르게 물을 흡수하였다. PUS-MOP-Aa의 물 속 화학물질 제거 능력을 양이온 염료인 Methylene Blue (MB)와 음이온 염료인 Methylene Orange (MO)를 대표 화학물질로 사용하여 비교하였다. PUS-MOP-Aa의 가역적 압축성을 이용하여 MB 용액 하에서 반복적인 압축을 수행하였을 때 MB에 대해 빠른 제거 능력을 보였다. 한편 PUS-MOP-Aa는 표면이 음이온

특성을 지니기 때문에 MB와 MO가 섞여 있는 용액의 경우 양이온 특성이 있는 MB를 선택적으로 더 잘 제거함을 보였고, 간단한 산 처리와 세척으로 염료를 제거한 후 재사용할 수 있었다.

마지막으로, 팔라듐 나노파티클이 도입된 위계적 기공성 고분자 (S-M-Pd) 를 제조하였다. PUS-MOP-A와 마찬가지로 폴리우레탄스폰지 안에서 1,3,5-triethynyl benzene, 1,4-diiodobenzene 그리고 2,5-diiodobenzoic acid의 소노가시라-하기하라 반응을 통하여 화학적 가교결합을 이루는 유기젤을 형성 시킨 후, 소노가시라-하기하라 반응 시 이용되었던 팔라듐 촉매를 이용하여 팔라듐 나노파티클을 제조하였다. 제조된 S-M-Pd는 가역적 압축성을 지니고 위계적 기공성을 가지며 270 m^2g^{-1}의 BET 비표면적을 가졌다. S-M-Pd는 4-nitrophenol 의 환원 반응과 스즈키커플링 반응에 티백과 같은 방식으로 이용되었다. 4-nitrophenol 환원 반응 시 반응용기 내에서 S-M-Pd의 반복적으로 가역적 압축을 수행하였을 때 가만히 담가 두었을 때보다 6배 빠른 반응 속도를 보였다. 이는 반복적인 압축이 물질 전달을 더 용이하게 하였기 때문으로 보인다. 한편, S-M-Pd를 실린더모양으로 칼로 자른 뒤 주사기에 넣어 semi-continuous reactor 로 이용하였다. MB 환원 반응을 성공적으로 수행하였고, 별도의 정제 없이 몇 번의 연속적인 반응 또

한 성공적이었다.

주요어: 유기젤, 열변색성, 위계적 기공성 고분자, 스폰지, 촉매.

학번: 2010-20642